Functional Nanostructured Materials: Synthetic Aspects & Properties Evaluation

Kumulative Dissertation

zur

Elangung des Doktorgrades

der Naturwissenschaften

(Dr. rer. nat.)

dem

Fachbereich Chemie der Philipps-Universität Marburg

Vorgelegt von

M. Sc. Chem. Fei Chen

aus

Jiangxi / China

Marburg an der Lahn 2011

Vom Fachbereich Chemie der Philipps-Universität Marburg am

_____ als Dissertation angenommen.

Erstgutachterin: Prof. Dr. Seema Agarwal

Zweitgutachter: Prof. Dr. Andreas Greiner

Tag der mündlichen Prüfung: _____

Hochschulkennziffer: 1180

"To study without thinking is useless, to think without studying is idle."

-- Confucius

Table of Contents

List of symbols and abbreviations

AA	Acrylic acid
AC	4,4'-Di(methacryloylamino) azobenzene
AM	Acrylamide
BPDA	3,3′,4,4′-biphenyltetracarboxylic dianhydride
BTDA	Benzophenone-3,3′,4,4′-tetracarboxylic dianhydride
CMC	Critical micelle concentration
DABCO	1,4-Diazabicyclo[2.2.2]octane
DCM	Dichloromethane
d_6-DMSO	Deuterated dimethylsulfoxide
DEMA	Diethanol-*N*-methylamine
DLS	Dynamic light scattering
DMF	Dimethylformamide
DMTA	Dynamic mechanical thermal analysis
DSC	Differential scanning calorimetry
6FDA	4,4′-(Hexafluoroisopropylidene)diphthalic anhydride
FTIR	Fourier transform infrared spectroscopy
GPC	Gel permeation chromatography
HMBC	Heteronuclear multiple bond correlation

HMQC	Heteronuclear multiple quantum correlation
MBC	Minimum bactericidal concentration
mg	Milligram
MIC	Minimum inhibition concentration
ml	Milliliter
M_n	Number average molecular weight
M_w	Weight average molecular weight
MWDs	Molecular weight distributions
nm	Nanometer
NRs	Nanorods
PA6	Polyamide 6
PAA	Poly(amic acid)
PDI	Polydispersity
PBS	Phosphate buffered saline
PCL	Poly(ε-caprolactone)
PEG	Polyethylene glycol
PEO	Polyethylene oxide
PHA-b-PEO	Poly(hexamethylene adipate)-Polyethylene oxide block copolymers
PI	Polyimide
PMDA	Benzene-1,2,4,5-tetracarboxylic dianhydride

Polyester-5, 7	Poly(pentylene heptanoate)
PPA	Polyphosphoric acid
P2VP	Poly(2-vinylpyridine)
PSAPs	Photochromic Superabsorbent Polymers
QD	Quantum dots
SAP	Superabsorbent polymers
SEM	Scanning Electron Microscopy
SILAR	Successive ionic layer adsorption and reaction
Span 60	Sorbitan monostearate
T	Temperature (°C)
TDI	2,4-toluenediisocyanate
TE	Tissue engineering
TEM	Transmission electron microscopy
T_g	Glass transition temperature
TGA	Thermal gravimetric analysis
THF	Tetrahydrofuran
THz-TDS	Terahertz time-domain spectroscopy
$Ti(OBu)_4$	Titanium(IV) butoxide
T_m	Melting temperature
TMS	Tetramethylsilane

TPU	Thermoplastic polyurethane
UCST	Upper critical solution temperature
μ	Micrometer
λ	Wavelength
UV/Vis	Ultraviolet-visible spectroscopy
WAXD	Wide angle X-ray diffraction
ΔH_m	Heat of fusion
ΔH_c	Heat of crystallization
$\Delta H_m°$	Heat of fusion with 100% crystallinity

1. Introduction

1.1 Motivation

Functional nanomaterials with size less than 1μm have received extensive scientific as well as technological attention due to their potential applications in microelectronics, biomedical, and optical materials. This is because new and unexpected properties are less likely to develop with micron-scale bulk materials. There are many methods to prepare functional nanomaterials including phase separation, block copolymer self-assembly, electrospinning and heterophase polymerization etc. Divided by morphology and shape, functional nanomaterials comprise nanofibers, nanoparticles, naorods, nanowires etc. Among these nanomaterials, nanofibers and nanoparticles have received increasing attention due to their potential applications in biomedical and microelectronics fields.

Electrospinning is the state-of-the-art method for the preparation and production of continuous nanofiber nonwovens, which has been highlighted in recent years. Due to the small size, high surface to volume ratio and other unique properties, a wealth of chemistry as well as new methods have been applied to modify the electrospun nanofibers to impart new functionalities. On the other hand, heterophase polymerization provides chemists a direct way to form functional nanomaterials (mainly nanoparticles), whose properties and morphologies can be controlled by polymerization methods and conditions.

This work aims to prepare some functional nanomaterials including stimuli-responsive nanofibers and nanoparticles, biodegradable nanofibers and low dielectric constant nanofibers for biomedical and microelectronic applications.

1.2 Theoretical background and prior research

1.2.1 Smart nano-objects by self-assembly of block copolymers in solution

The strategies to synthesize functional nanomaterials (mainly polymer materials) contain a broad range of methodology, such as phase separation[1,2], heterogeneous polymerization to form nano (micro) particles[3,4], electrospinning of polymer

solutions to form nanofibers[5-9] and nano-objects by self-assembly of block copolymers in solution[10]. Among these different methods, block copolymers occupy a huge area of research, because they offer a vast range of possibilities for architecture, size, and chemical composition. Advances in polymer chemistry[11], such as anionic polymerization and most recently living radical polymerization[12], have enabled a large amount of block copolymers to be synthesized with great control over their architecture, molecular weight, chemical composition and functionality. Their intrinsic properties allow the combination of different polymers and therefore the design of novel materials potentially comprising several different properties (e.g. thermoplastic, rubber, electrical conductivity etc.).

Amphiphilic molecules in water are the most studied examples of self-assembling molecules in selective solvents. The block copolymers undergo two basic processes in solvent media: micellization and gelation. Micellization occurs when the block copolymer is dissolved in a large amount of a selective solvent for one of the blocks. Under these circumstances, the polymer chains tend to organize themselves in a variety of structures from micelles or vesicles to cylinders. The soluble block will be oriented towards the continuous solvent medium and become the "corona" of the micelle formed, whereas the insoluble part will be shielded from the solvent in the "core" of the structure (see Figure 1**)**. In contrast to micellization, gelation occurs from the semidilute to the high concentration regime of block copolymer solutions and results from an arrangement of ordered micelles.

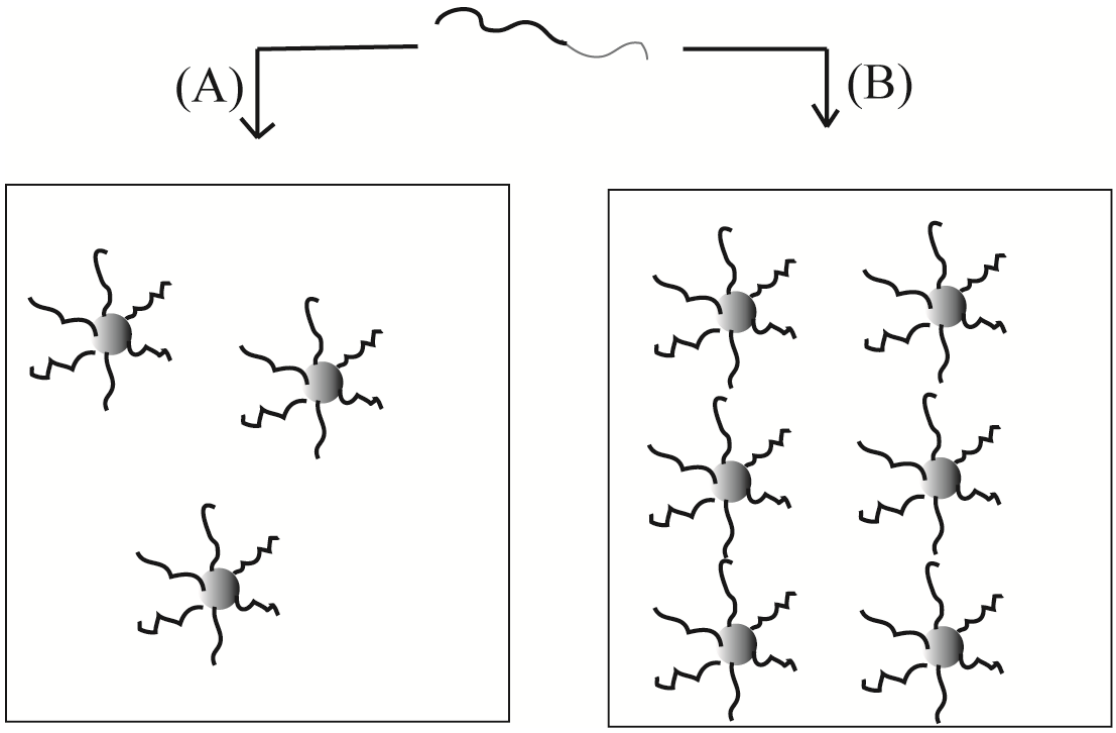

Figure 1. Different geometries formed by block copolymers in selective solvent conditions: (A) micellization at the critical micelle concentration and (B) gelation at high concentration from diblock copolymers.

Thanks for the development of polymerization methods, a variety of monomers were chosen to form amphiphilic block copolymer micelles, in which stimulus responsive nano-assemblies attracted great attention these years. By design the specific hydrophobic polymers to external stimulus such as pH[13], temperature[14], and hydrolytic degradation[15], block copolymers micelles and vesicles, therefore find applications for the delivery of anticancer drugs[16] and as contrast agents for medical imaging[17] and so on. Lecommandoux and co-workers employed stimuli-responsive blocks to encapsulate various hydrophilic and /or hydrophobic species, such as drugs, in these vesicles and used them as efficient carriers that can deliver their contents at the right place and moment by activation of magnetic or pH triggers[18].

In brief, by controlling the architecture of individual molecules, amphiphilic block copolymers can generate nanostructures either in an undiluted melt or in solution.

Their synthetic nature allows the design of interfaces with different chemical functional groups and geometrical properties which will undoubtedly find a wide range of applications in the scientific as well as technical community. Still it has some drawbacks, such as complexity of choosing proper solvent and determining the critical micelle concentration (CMC) for micelle formation. Research on block copolymer nanoparticles and nanostructures is a relatively new area and there is still a great deal left to explore.

1.2.2 Functional nanoparticles by heterophase polymerization method

Compared with self-assembly method utilizing resultant amphiphilic block copolymers to form nanomaterials in aqueous solution, heterophase polymerization is a direct way to form nanoparticles or other nanostructured materials in water during heterophase polymerization process[19]. As one of the most important techniques to prepare polymer latices which play an essential role in our daily life such as cosmetics, detergents, newspapers, or paints, the development of new heterophase polymerization techniques, the adoption of new polymerization mechanism to the particular conditions, the synthesis of block copolymers and hybrid nanoparticulate structures were given special emphasis in recent years.

Among all the heterophase polymerization methods, emulsion polymerization is the most relevant, but also special cases, as the particles are newly built up by nucleation processes and monomer transport via the continuous phase. The monomer can be fed continuously into the reactor either as neat monomer or as an emulsion. For large scale production in industry, the monomer to water ratio is adjusted in such a way that a solids content typically between 40- 60 % or even higher is obtained.

In the cases of suspension, miniemulsion and microemulsion polymerization, the monomer must be only slightly water soluble as it has to form a separate phase in the shape of spherical droplets where size is controlled by a proper choice of the dispersing technique (stirring, ultrasonic treatment, homogenization) in combination with the stabilizing system. The droplet size decreases in the order suspension>

microsuspension> miniemulsion> microemulsion polymerization. The polymerization recipes are designed in such a way (for instance oil soluble instead of water soluble initiators) that the polymerization takes place mainly inside the preformed monomer droplets. In these techniques selected and specific stabilizers have to support the emulsification process and the stabilization of the monomer droplets. The comparison of different heterophase polymerization processes and mechanisms were well summarized in a previous review by Antonietti[3].

As a promising synthetic way to synthesize nanostructured functional materias, the controlled radical polymerization (CRP) has become one of the most rapidly growing topics in the field of polymer research[20]. Thus enabled by the adaptation of controlled radical polymerization processes to heterophase polymerization processes, it is straightforward to synthesize well defined polymers and also block copolymers under aqueous heterophase conditions.[21] This is an important step towards a broad commercial applications of controlled radical polymerization as all the benefits of both heterophase polymerization process and CRP can be combined.

In summary, both from an application point of view as well as scientific perspective, heterophase polymerization provides chemists and material scientists a powerful and challenging technique to prepare nanostructured functional materials. Many novel well-controlled morphology and chemical composition with new properties or functions (micro) nanoparticles will be brought by such promising polymerization method.

1.2.3 Composite nanomaterials: synthesis by electrospinning and their applications

As discussed in previous chapters, self-assembly and heterophase polymerization provide material chemists huge opportunities to fabricate functional nanostructures with well defined morphology and chemical composition. One limitation for these two methods in common is that the nanostructured materials can only be produced in aqueous/organic phase and morphology is mainly micro (nano) particles. Some

methods such as phase separation can also prepare one dimensional (1D) nanostructured materials like nanorods, nanowires, but among these methods, electrospinning seems to be the simplest and most versatile technique capable of generating 1D nanostructures (mainly nanofibers, other types of 1D nanostructures, such as nanobelts or nanorods can be prepared by special methods[22]) from a variety of polymers and composite materials[6, 7, 23]. The simplicity to control the fiber diameter, the high surface to volume ratio, and pore size and wide variety in usable polymers, make electrospinning attractive for a wide range of biomedical applications such as tissue engineering, wound dressing, drug delivery[9] and some other application in filters[24], catalysis[25], nanofiber reinforcement[26]and so on.

1.2.3.1 Electrospinning process

The typical setup for electrospinning generally consists of a high voltage power supply, a spinneret, and an electrically conductive collector (like a piece of aluminum foil) (Figure 2). During electrospinning, due to the surface tension, a droplet of polymer solution is formed at the tip of the needle, the applied voltage make the polymer solution highly electrified and the induced charges are evenly distributed over the surface. Once the strength of the electric field overcomes the surface tension of the liquid, a liquid jet forms and moves towards the counter electrode[27]. During the movement of the jet in the air, the remaining solvent evaporates and solid fibers with certain diameters are deposited on the collector. A variety of parameters such as polymer concentration, applied voltage, solution conductivity, solvent, temperature and humidity etc. will influence the resultant fibers[28], there are no universal parameters applicable to every polymer, but by adjusting some key parameters such as polymer concentration, applied voltage and humidity, a vast range of nanostructured materials (mainly nanofiber) can be formed with different diameters, shape and morphology.

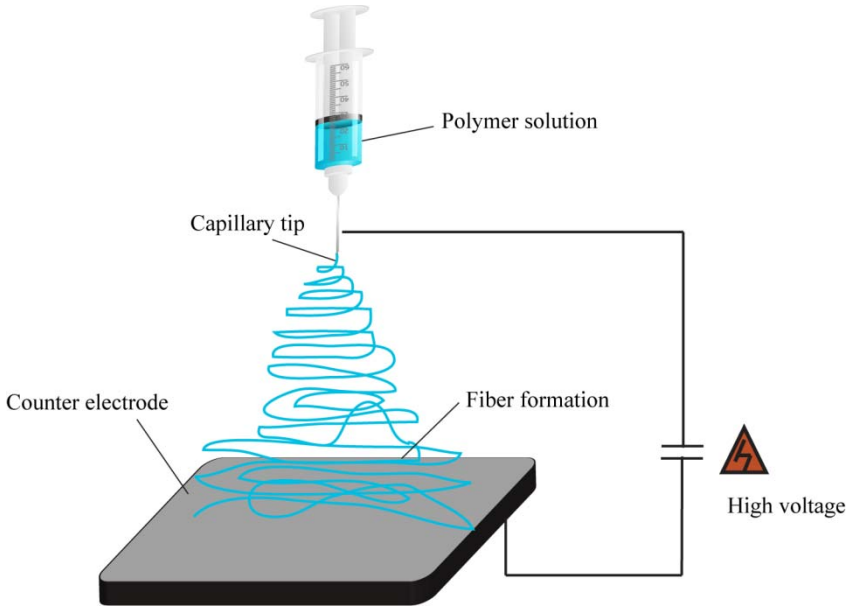

Figure 2. Schematic setup for electrospinning.

1.2.3.2 Methodology for fabrication of composite nanomaterials

Emulsion electrospinning

As a versatile and convenient technique, conventional electrospinning has already proved to be a promising technique to form nanofibers for future biomedical applications, especially controlled drug delivery. By directly electrospinning of mixtures of drugs and polymer, hydrophobic drugs could be encapsulated into hydrophobic nanofibers (like PLLA nanofiber) but showed nearly zero-oder kinetics of drug release[29]. On the other hand, water soluble drugs could be electrospun into a water-soluble polymer but such composite fibers are not suitable for in vitro drug release as they can quickly dissolve in blood or tissue fluid[30]. Thus, the emulsion electrospinning method was proposed to overcome these limitations. The major steps of emulsion electrospinning comprises emulsification to form a water/oil (W/O) emulsion, dissolution of a fiber forming polymer, and electrospinning of the emulsion, the schematic illustration of emulsion electrospinning was nicely shown by Qi and co-workers.(Figure 3)[31]. As an example, Li and co-workers have shown that successful encapsulation of proteinase K as a model protein into poly(ethylene glycol)-b-poly(L-lactide) (PELA) fibers by emulsion electrospinning comprises a

sustained release of proteinase K after an initial burst release. Furthermore no decrease in the proteins activity was observed[31]. Jing and co-workers also have made use of this technique for the encapsulation of doxorubicin hydrochloride (Dox) in amphiphilic PELA diblock copolymers[32]. Clearly, emulsion electrospinning offers many advantages. Besides various combinations of hydrophilic and hydrophobic systems, in particular for drug encapsulation and modification of drug release, emulsion electrospinning will undoubtedly extend the application of conventional electrospinning in biomedical fields.

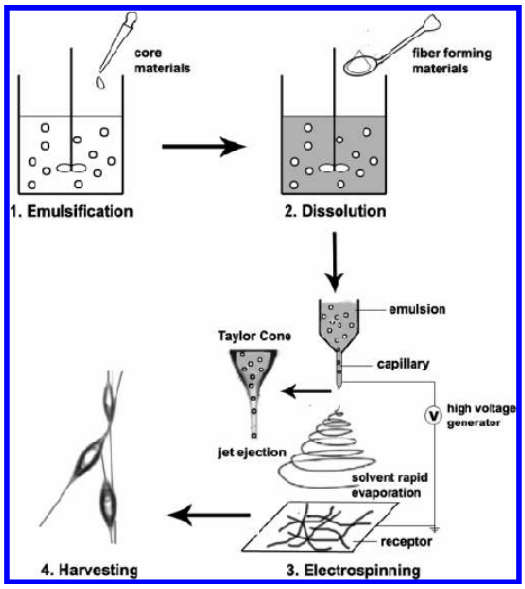

Figure 3. Schematic illustration of emulsion electrospinning (reproduced with permission from year 2006 American Chemical Society[31]).

Suspension electrospinning

Although emulsion electrospinning provides more possibilities in biomedical applications, its concept still make use of toxic and/or flammable organic solvents either as a continuous phase (W/O emulsion) or a separated phase (O/W emulsion) which could hinder the actual in vivo medical applications and the development for large scale productions and applications in agriculture. This demands a need for further solutions regarding electrospinning of polymers only from water which termed as “green electrospinning”. An alternative to this could be electrospinning of polymer

suspensions from water as continuous phase. Suspension electrospinning comprises two strategies: electrospinning of primary latex and secondary latex suspensions. The primary latex suspension can be obtained directly by emulsion or miniemulsion polymerization which are well established with a large technical scale, but are available only for a limited number of polymers. Often they require surfactants, which would be hazardous for biomedical or agricultural applications. In previous work in our group, successful electrospinning of polystyrene suspensions was achieved by combination of a small amount of fiber forming water-soluble polymer[33], which acts as a kind of template polymer as schematically shown in Figure 4[34]. By removing the water-soluble polymer, "corn-type" polystyrene nanofibers were obtained, whose stability depends significantly on the size of the latex particles. Smaller latex particles, form more stable hexagonal arrangement along the fiber main axis. Although the concept of electrospinning of primary polystyrene particles was successful, the latex fibers formed were too brittle after removal of the template polymer and therefore were of no use for any applications. By applying lower T_g latex particles, inter and intra-latex particle cross-linking was proved a useful method to improve the mechanical stability[35, 36].

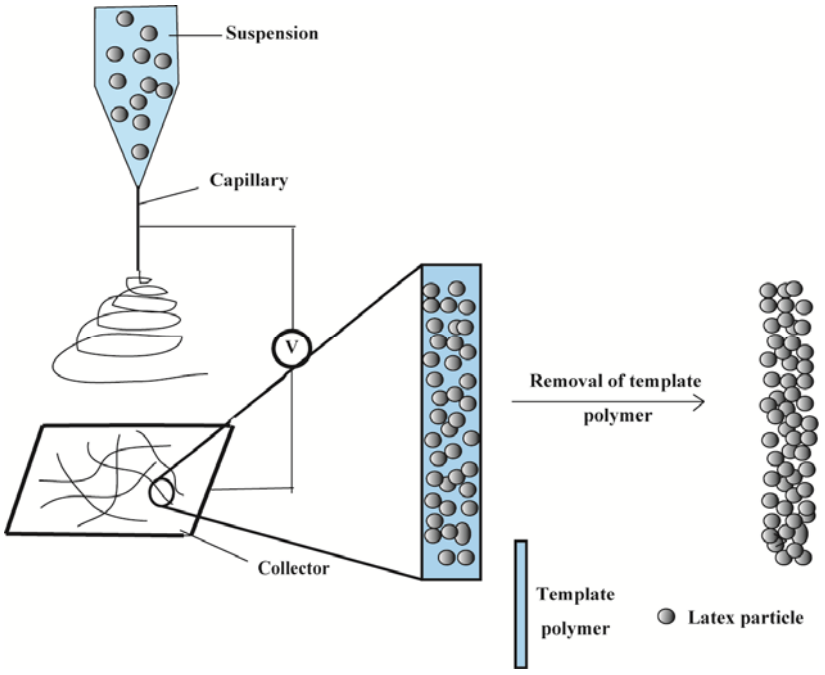

Figure 4. Schematic description of suspension electrospinning primary lattices.

Electrospinning of secondary latex suspensions-water stable nanofibers from water phase

Electrospinning of water-based secondary lattices could be a new field leading to a wealth of novel electrospun systems and green electrospinning which is free of surfactants and harmful organic solvents. One example is the preparation of amphiphilic biodegradable copolyesters which were processed to high solid content of secondary suspensions by dialysis. Electrospinning of this system in the presence of a small amount of water soluble polymer resulted in smooth electrospun fibers. The whole electrospinning process is free of organic solvents and surfactants which are paving the way for more promising applications of the feasible method of electrospinning of useful nanofiber nonwovens, the details about the electrospining of secondary latex suspensions is described in the main part of this thesis.

1.2.3.3 Applications of electrospun functional nanomaterials

As electrospinning is a remarkably simple and powerful technique for generating 1D composite nanomaterials, it has received increasing attention during last decades. Because of the multifunctional properties of the composite materials, they have already been applied in many areas such as biomedical fields[37, 38], nano-electronic and optical devices, chemical and biological sensors[39, 40], environment and energy fields[41]. Here only few of successful applications from biomedical, stimuli-responsive sensors and energy sector were emphasized.

Biomedical applications

The biomedical field might be one of the most important application areas utilizing the electrospinning technique. Due to the facile production of very thin fibers of few nanometers in diameters and therefore with large surface areas, ease of functionalization and processing, the applications of electrospinning mainly consists of tissue engineering, drug release, would dressing, enzyme immobilization etc. In the tissue engineering application, among the essential properties for scaffolds besides biocompatibility, biodegradability and mechanical properties, the scaffold architecture

is very important for transportation of nutrients and waste during cells proliferation and differentiation as well as it affects cell binding[42]. Electrospinning provides possibilities to generate loosely connected three dimensional (3D) mats with high porosity, interconnected pores and high surface area which can mimic extra cellular matrix (ECM) structure and thus makes itself an ideal candidate for use in tissue engineering. Stevens and co-workers[42] demonstrated that the cells binding to nanoscale architectures, which have bigger surface area, absorb proteins and present more binding sites to cell membrane receptors, while on microscale architecture, the cells spread as if cultured on flat surfaces (Figure 5).

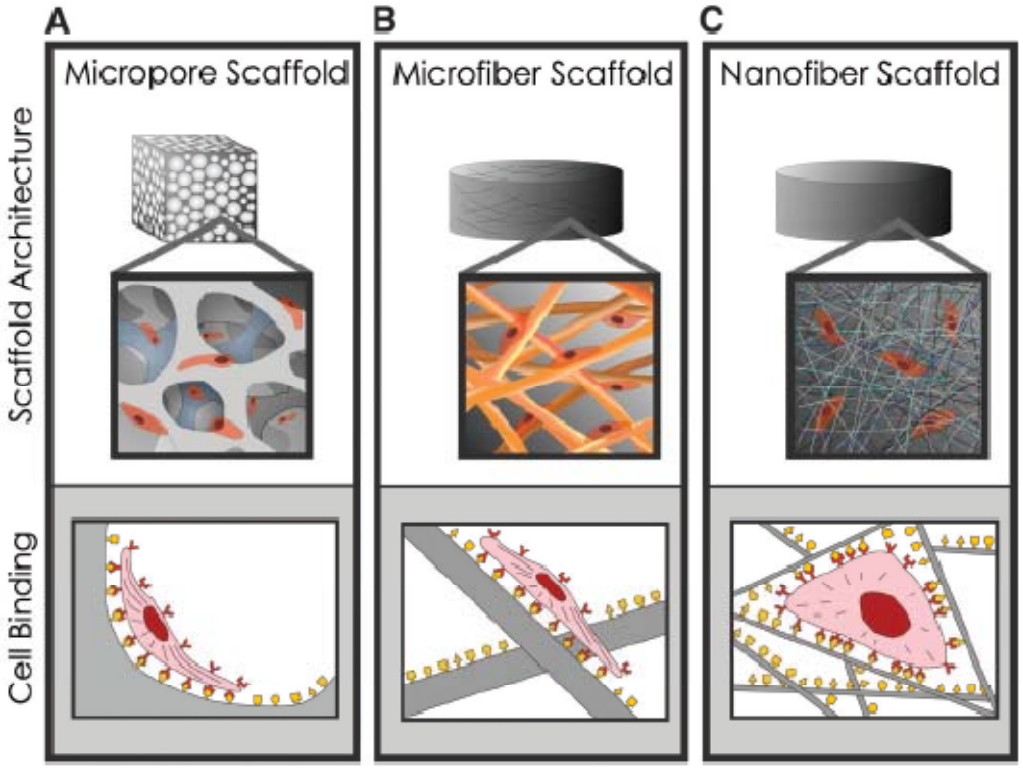

Figure 5. Scaffold architecture affects cell binding and spreading(Copyright © 2005, American Association for the Advancement of Science[42]).

Besides utilized as powerful tools to prepare 3D scaffolds in tissue engineering, another interesing example to show the potential of electrospun nanoifber in the biomedical field is the preparation of attolitre-volume reactors. As shown in Figure 6, Anzenbacher and co-workers utilize 100-300 nm polymer nanofiber as nanocarriers

for reagents to initiate a micro-reaction[43]. Polymer nanofibers doped with reagents are overlaid to form a rectangular grid-like mat. Fusing the nanofibres at their intersections leads to mixing of their contents in the junctions to create an attoreactor containing zeptomole amounts of reagents and products. This novel attolitre-volume reactor might be potentially important for a number of disciplines, including molecular electronics and molecular biology, as well as circumvent potential problems associated with reagent and product toxicity.

Another promising direction for electrospun nanofiber in biomedical application is to encapsulate drugs inside the polymer nanofibers and thus easily control the release profile of drugs in vitro or in vivo conditions. Greiner and co-workers prepared bovine serum albumin (BSA)-loaded PVA nanofiber by electrospinning[44]. By coating a layer of poly(p-xylylene) (PPX) using the chemical vapor deposition (CVD) method, the composite fibers posses a controlled retarded release of BSA depending on the thickness of the coated PPX.

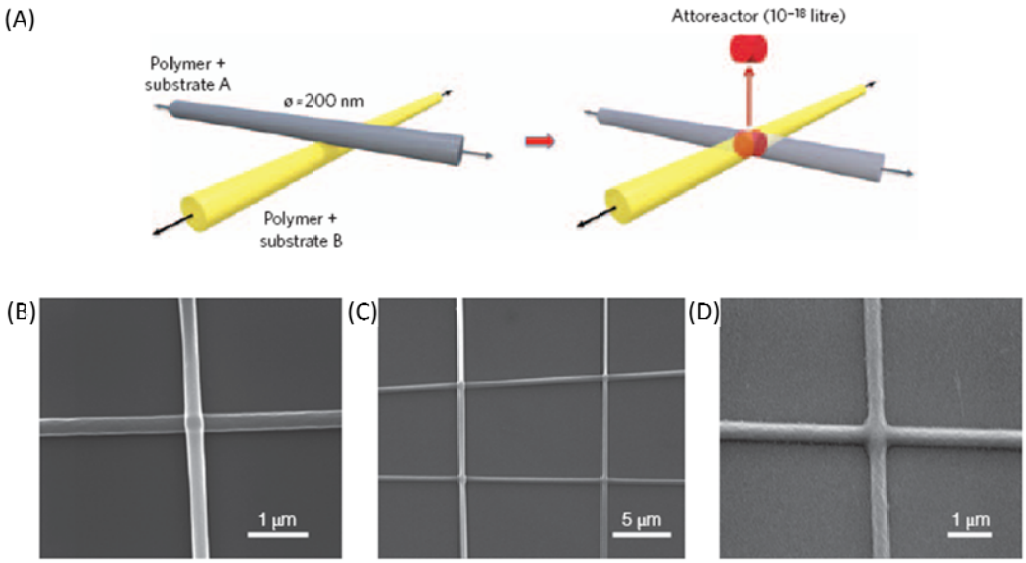

Figure 6. (A) Schematic representation of the principle. (B, C) Scanning electron microscope (SEM) images of electrospun polyurethane nanofibers overlaid in a rectangular grid. (D) SEM image of the fused fibers.(Copyright©2009, nature Publishing Group[43])

Stimuli and biological sensors

Stimuli responsive sensors are widely applied in our daily life and high technology devices. Based on the stimulus source, the sensors can be divided into temperature, pH, photo and humidity responsive sensors etc. As an example, Okuzaki and co-workers[45] showed the successful preparation of thermo-responsive nanofibers by electrospinning poly(N-iso-propylacrylamide-co-stearyl acrylate). The resultant fiber had an average diameter of 207 nm, and due to the large surface area and high porosity of the fibers, the swelling rate of the nanofiber mats was found to be one order of magnitude higher than the corresponding bulk gels. Figure 7 shows the swelling behavior in pure water between 25 to 40°C. Other stimuli-responsive nanofibers also posses similar fast response rates and have been found to have a variety of applications.

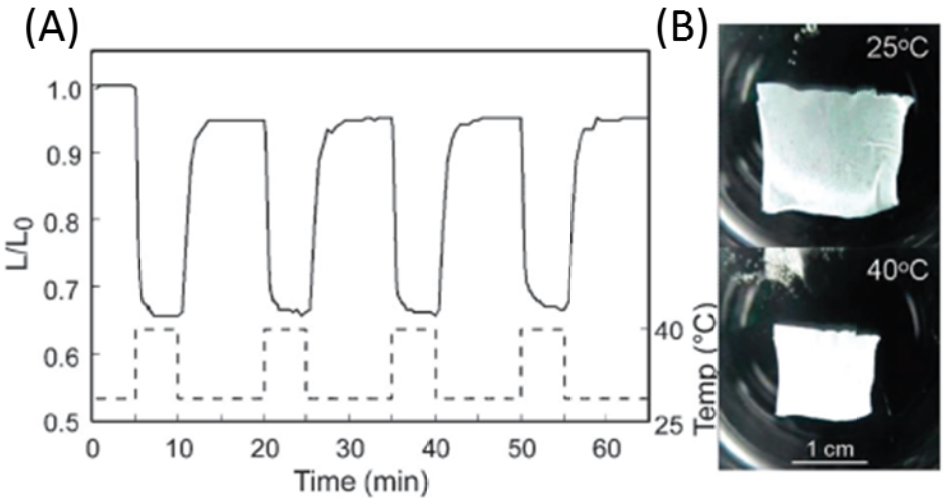

Figure 7. (A) Temperature-dependent deswelling and swelling of poly- (NIPA-co-SA) nanofiber mats (2 cm× 2 cm× 20 mm) in pure water (between 25 and 40 °C; L/L_0 is the length of the fiber mat expressed as relative to the original length at 25 °C); (B) shows representative photomicrographs of the fibers at 25 °C (top) and 40 °C (bottom).(Copyright (2009) American Chemical Society[45])

Composite electrospun nanofibers can also act as biosensors and convert a biological signal into an electrical output. For instance, Wei and co-workers have demonstrated

that various enzymes could be encapsulated in nanoporous silica nanofibers by the electrospinning method, which act as excellent biosensors.[46]

Environmental and Energy applications

The electrospun nanofiber mats are a potential candidate as an environment-cleaning material due to its large surface area, porous structure, and cost-effective preparation. As an example, Ramakrishna and co-workers have fabricated 1D composite nanomaterias containing poly(vinylchloride) polymer and a catalyst for the detoxification of nerve agents, which have been prepared from *β*-cyclodextrin and *o*-iodosobenzoic acid.[47]

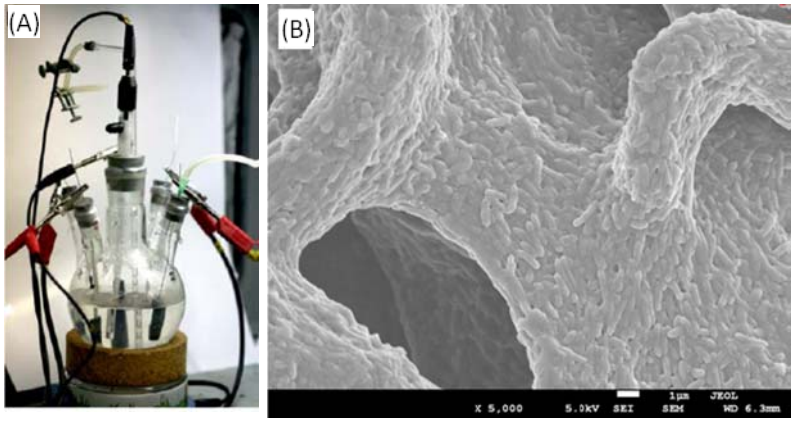

Figure 8. (A) Electrochemical cell for the simultaneous study of different electrode materials. (B) SEM images of biofilms in the porous 3D-ECFM after electricity generation. (Copyright (2011) Royal Society of Chemistry [51])

Besides environmental protection, electrospun nanofibers were also applied in advanced technology and devices for highly efficient and clean energy generators[48, 49]. Ramakrishna and co-workers reported for the first time a simple method of fabricating TiO_2@CdS nanorods (NRs) by combining electrospinning and successive ionic layer adsorption and reaction (SILAR) techniques sequentially. The photovoltaic application was explored by assembling this nanostructure into quantum dots (QD) sensitized solar cells which gave a best efficiency of over 0.5 %[50]. Chen and co-workers showed the successful synthesis of three-dimensional carbon fiber

electrodes prepared by electrospinning and solution blowing. The novel electrodes were shown to be excellent electrode materials for bioelectrochemical systems such as microbial fuel cells or microbial electrolysis cells. The bioelectrocatalytic anode current density is shown to reach values of up to 30 $A \cdot m^{-2}$, which represents the highest reported values for electroactive microbial biofilms (Figure 8)[51]. All of these contributions indicate a bright future for searching ideal materials for production of clean and renewable energy.

1.3 Aim and concept of this work

The fundamental objective of this work is the formulation of new functional nanostructured materials including stimuli responsive nanocomposites, nanoparticles and biodegradable nanofibers as well as the investigation of their properties. Special attention is placed on the preparation of nanocomposites with water absorption/ desorption controlled by photo-irradiation, thermo-responsive and antibacterial nanodispersions and fast biodegradable (co)polyester nanofibers for potential biomedical applications.

The concept of this work is the formulation of nanofibers and nanoparticles utilizing functional polymers, which include photo-responsive superabsorbent polymers, antibacterial and thermo-responsive quaternized polyurethanes and biodegradable (co)polyesters. The methods for preparing the functional nanomaterials are mainly based on electrospinning and heterophase polymerization. The scheme below describes the sequence and connection between chapters in the whole dissertation.

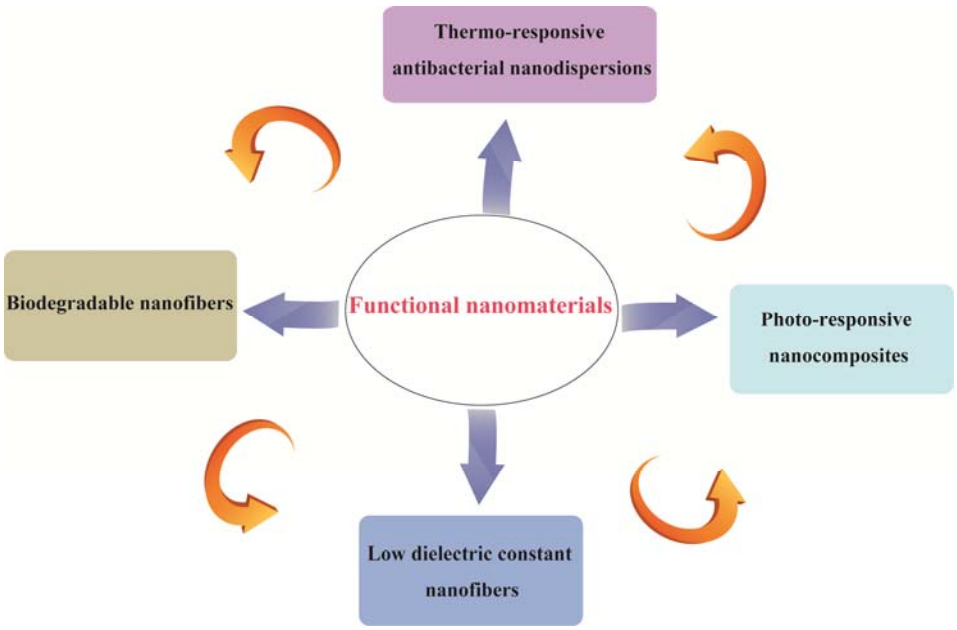

For stimuli responsive systems, functional nanocomposites were prepared by combination of photoresponsive superabsorbent particles with hydrophilic elastic polyurethane nanofibers by the electrospinning technique. The concept was that the

elastic fiber could serve as a substrate to hold the particles and such nanocomposites were expected to possess good water absorption/desorption capacity controlled by photo irradiation, good mechanical strength, and therefore have a big potential in biosensor and drug release applications. Further we utilized cationic segmented block copolyurethane to form antibacterial and thermo-responsive dispersions. Such nano-dispersions with upper critical solution temperature (UCST) behavior have a big potential to be used for drug encapsulation and controlled release for various therapeutic applications.

As an extension of nanostructured materials in biomedical applications, fast biodegradable odd-odd polyester and nanofiber of poly (hexamethylene adipate)-PEO (PHA-b-PEO) were synthesized. The concept of making odd-odd polyester was that odd number of carbon atoms in the main chain would hinder the molecular chains to crystallize and lead to a higher degradation rate. While for avoiding the use of harmful organic solvents during electrospinning, the “green electrospinning” concept was introduced by preparing high solid contents of amphiphilic PHA-b-PEO dispersion, and mixing the dispersion with a small amount of water soluble polymer and processing into nanofibers by electrospinning. Biodegradable fibers were finally produced by sacrificing water soluble template polymers.

In the final part of this dissertation, an idea of proper combination of fluorinated polyimides and electrospinning was attempted. The concept was that the large pores and surface roughness would decrease the dielectric constant of fluorinated polyimides. Such polyimides nanofibers would have better properties such as high hydrophobicity and good thermo-oxidative stability and could be of high use as insulating materials in dielectrics and filter industry.

2. Summary in German (Zusammenfassung)

Diese Dissertation hat die Synthese funktioneller, nanostrukturierter Materialien zum Gegenstand. Dies beinhaltet Stimuli-responsive Nanomatten-Komposite, Nanopartikel und bioabbaubare Polyesternanofasern, welche neuartige Eigenschaften wie eine kontrollierte Wasserabsorption bzw. –desorption aufweisen, über eine schnelle Temperatur-Responsivität verfügen und auf ihren potentiellen Einsatz in biomedizinischen sowie mikroelektronischen Anwendungen hin untersucht wurden.

Photoresponsive und superabsorbierende Nanomatten-Komposite wurden durch Kombination hydrophiler Polyurethan-Nanofasern mit vernetzten, photoresponsiven und superabsorbierenden Partikeln hergestellt. Die Eigenschaften der Nanokomposite wiesen dabei eine hohe Abhängigkeit vom Anteil der enthaltenen photochromen Superabsorberpartikel auf. Die Komposit-Nanomatten verfügen über eine Wasseraufnahmekapazität von 40 g/g und erreichen ihr Absorptionsmaximum bereits innerhalb von 2 Minuten, was sie gegenüber konventionellen Superabsorbern auszeichnet, die dazu üblicherweise länger benötigen. Das elastische Polyurethan dient in diesem Fall als Matrix zur Fixierung der Partikel und verleiht dem Nanokomposit darüber hinaus gute mechanische Eigenschaften. Dieses Komposit-Material bietet sich zum Einsatz im Rahmen einer kontrollierten Wirkstofffreisetzung an oder auch zur Anwendung im Bereich der Sensorik. Als weiteres Stimuli-responsives System wurden antibakterielle, stabile, kationische, segmentierte Urethan-Blockcopolymer-Nanopartikel mit einer oberen kritischen Lösungstemperatur (upper critical solution temperature, UCST) durch eine zweistufige Polykondensation von 2,4-Toluoldiisocyanat, Diethanol-*N*-methylamin und Polyethylenglycol (PEG) hergestellt. Aus dem Polymer wurde durch einfaches Erhitzen auf 90 °C und anschließendes Abkühlen auf Raumtemperatur eine stabile Dispersion erhalten. Die Einführung von PEG-Segmenten wirkte sich positiv auf die Ausbildung der Dispersion aus ohne dabei die antibakterielle Aktivität einzubüßen; zudem lassen sich Partikelgröße sowie UCST durch den PEG-Gehalt und die Konzentration der Dispersion einstellen. Auf diesem Weg wurde eine neuartige,

antibakterielle sowie thermoresponsive Dispersion erhalten, welche ein großes Potential zur Anwendung im Bereich der Wirkstoffverkapselung und kontrollierten Freisetzung zu verschiedenen therapeutischen Zwecken birgt.

Der Arbeit an funktionellen, Stimuli-responsiven, nanostrukturierten Materialien folgt die Einführung von Bioabbaubarkeit in den Kapiteln 3 und 4 als weiterer Funktionalität. Kapitel 3 behandelt die Synthese schnell abbaubarer, zweifach ungeradzahliger (*odd-odd*) Polyester sowie deren Abbauverhalten mit und ohne Einsatz von Enzymen. Die *odd-odd*-Struktur der Kettenrückgrats führt dazu, dass der 5,7-Polyester eine relativ geringe Kristallinität aufweist und dadurch im Vergleich zu kommerziellem Poly-ε-caprolacton (PCL) über eine schnellere Abbaurate verfügt. Durch Rasterelektonenmikroskopie sowie optische Polarisationsmikroskopie wurde ermittelt, dass der Abbau dabei sowohl in den amorphen Domänen als auch an der Oberfläche beginnt, was mit einer Veränderung der Oberflächenmorphologie einhergeht. Damit wurde der Klasse der bioabbaubaren Polyester ein weiterer Vertreter hinzugefügt, der über ein eigenes Profil zum Einsatz in mannigfaltigen biomedizinischen Anwendungen verfügt. Basierend darauf wurden Polyhexamethylenadipat-Polyethylenoxid (PHA-b-PEO) Blockcopolymere synthetisiert und zu wässrigen Suspensionen von hohem Feststoffgehalt weiterverarbeitet. Diese Suspensionen wurden mit einem geringen Anteil an hochmolekularem Polyethylenoxid versetzt und zu den entsprechenden Nanofasern elektroversponnen; nach Extraktion mit Wasser wurden stabile PHA-b-PEO Nanofasern erhalten. Dieses Konzept des Elektrospinnens von Biopolymeren aus wässrigen Suspensionen mit Verzicht auf gesundheitsschädliche, organische Lösungsmittel wird als „Grünes Elektrospinnen“ (*green electrospinning*) nahe gelegt und bietet neuartige Perspektiven für Anwendungen in den Bereichen Medizin, Pharmazie und Landwirtschaft.

Der letzte Teil dieser Dissertation beschäftig sich damit, die Charakteristika elektrogesponnener Nanofasern, wie zum Beispiel ein hohes Oberfläche zu

Volumen-Verhältnis, miteinander verbundene Poren und eine raue Oberflächenstruktur, mit denen fluorierter Polyimide zu verknüpfen. Dazu wurden diese durch Elektrospinnen zu Nanomatten verarbeitet, welche über eine niedrige Dielektrizitätskonstante, eine hohe thermo-oxidative Stabilität sowie Hydrophobizität verfügen. Neben ihrer Eignung für die Filter- und Kompositindustrie könnten diese von hohem Nutzen als Isolator in Verbundzwischenschicht-Dielektrika sein.

3. Summary

In this dissertation, the synthesis of functional nanostructured materials including stimuli responsive nanomat composites, nanoparticles and biodegradable polyester nanofibers are presented. Further the novel properties such as controlled water absorption/desorption, fast thermo responsive properties and potential applications in biomedical and microelectronic fields were investigated.

In chapter 4.1, photoresponsive superabsorbent nanomat composites were prepared by combination of hydrophilic polyurethane nanofibers with crosslinked photoresponsive superabsorbent particles, the properties of nanocomposites were highly dependent upon the amount of the superabsorbent photochromic particles added. The composite nanomats had a high water absorption capacity of 40 g/g and reached to the maximum absorption in two minutes which was faster than the conventional superabsorbers. The elastic polyurethane served as a substrate to capture most of the particles and provided good mechanical properties for the nanocomposties. Such nanocomposites could be of utility for drug release and sensor applications. Also stimulus responsive antibacterial cationic segmented block copolyurethane nanoparticles with upper critical solution temperature (UCST) behavior was synthesized in chapter 4.2 by polyaddition of 2,4-toluene diisocyanate, diethanol-*N*-methylamine and polyethylene glycol (PEG) in two steps. Stable dispersions were prepared by facile heating up to 90 °C and cooled down to room temperature. The introduction of PEG segments was found to favor the formation of stable dispersion and keep the antibacterial activity, the particle size and UCST could be adjusted by the PEG contents and concentration of the dispersions. Such novel antibacterial dispersion had a big potential to be used for drug encapsulation and controlled release for various therapeutic application.

Followed the previous research on functional stimuli responsive nanostructured materials, biodegradability functionality was introduced and investigated in the following two chapters. Chapter 4.3 describes a fast degrading odd-odd aliphatic polyester synthesis and degradation behavior with and without enzyme. Due to the

odd-odd structure of the main chain, the polyester-5,7 had a relative low crystallinity and possessed a faster degradation rate compared to commercial poly(ε-caprolactone) (PCL). The degradation was started in the amorphous region and on the surface with change in surface morphology which was confirmed by SEM and optical polarized microscopy. It would be an addition to the class of biodegradable aliphatic polyesters having its own profile for different biomedical applications. Based on this study, poly(hexamethylene adipate)-PEO (PHA-b-PEO) block copolymers were synthesized and processed to aqueous suspensions with high solid contents. This suspension was mixed with a small amount of high molecular weight PEO and electrospun into corresponding nanofibers. The stable nanofibers of PHA-b-PEO were obtained after extraction by water. Such concepts of utilizing electrospinning of biopolymers from aqueous suspensions avoiding harmful organic solvents are suggested to be "green electrospinning" and offer novel perspectives for application in actual medicine, pharmacy and agriculture.

In the last part of this dissertation, utilizing the characteristics of electrospun nanofibers (e.g. high surface to volume ratio and rough surface structures), fluorinated polyimides were processed into nanomats by electrospinning techniques. The corresponding nanofibers have a low dielectric constant, high thermo-oxidative stability and hydrophobicity which could be of high use as insulating material in interlayer dielectrics besides their use in filter and composite industry.

4. Cumulative part of dissertation

4.1 Stimuli-Responsive Elastic Polyurethane-Based Superabsorber Nanomat Composites

The manuscript about the content of this chapter has already been published.

Fei Chen, Andreas Greiner, Seema Agarwal*, Stimuli Responsive Elastic Polyurethane based Superabsorber Nanomat Composites, *Macromolecular Materials and Engineering*, **2011**, 296, 517–523

4.1.1 Summary and discussion

This work shows the success of making photoresponsive superabsorber nanomats. They are made by the combination of a porous hydrophilic polyurethane nanofiber matrix with photoresponsive superabsorbent particles. The resulting nanocomposites have very high loading (up to 50 wt%), good water absorption capacity (4000 %) and relatively good tensile strength (3 MPa). Such nanocomposites could be of utility not only for house hold cleaning purposes but could be applied in drug release and sensors.

The trans-to-cis isomerization is well known to change the distance between the 4 and 4’ carbons of the aromatic rings and thereby causes a macroscopic volume change in the polymer on photo irradiation. In this work, the photoresponsive superabsorber particles containing a crosslinked hydrophilic core and a hydrophobic azobenzene containing shell was synthesized by the known procedure. [Soft Matter, 2008, 4, 768-774]. The chemical structure of the particles and illustration of water removal from swollen photoresponsive absorbent polymer by light irradiation is given in Schemes 1 and 2. This novel superabsorbent and photochromic particles were prepared via inverse suspension polymerization, the hydrophilic crosslinker *N*,*N’*-methylene bisacrylamide (BIS) and photochromic crosslinker

bis(methacryloylamino)azobenzene (AC) was used respectively to generate the core and shell of the particles.

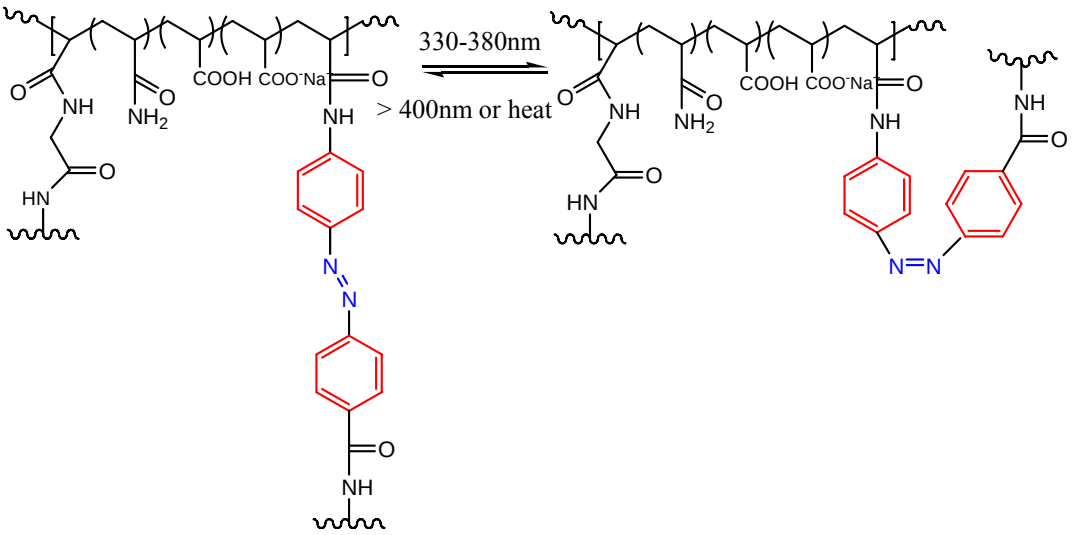

Scheme 1. Chemical structure of the photoresponsive superabsorber particles used for making superabsorber nanocomposites.

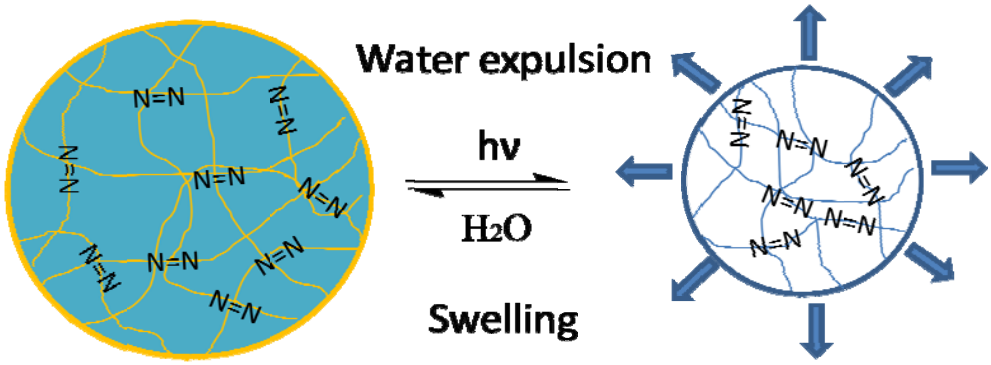

Scheme 2. Water removal of swollen photoresponsive superabsorbent polymer by light irradiation.

The synthesized particles have diameters of around 50-100 μm and were immobilized onto the hydrophilic TPU nanofibers by the process of electrospinning. The TPU nanofiber served as a substrate for holding the particles and provided strength and elasticity to the hydrogel particles. The typical morphology of composite nanomats with 50 wt% of the PSAPs was depicted in Figure 1. It was clearly shown that the particles were captured and stabilized by the elastic TPU nanofibers. This morphology

of particles trapped between the nanofibers could be one of the most important reasons account for avoiding “gel effect”, a disadvantage in the conventional hydrogel particles.

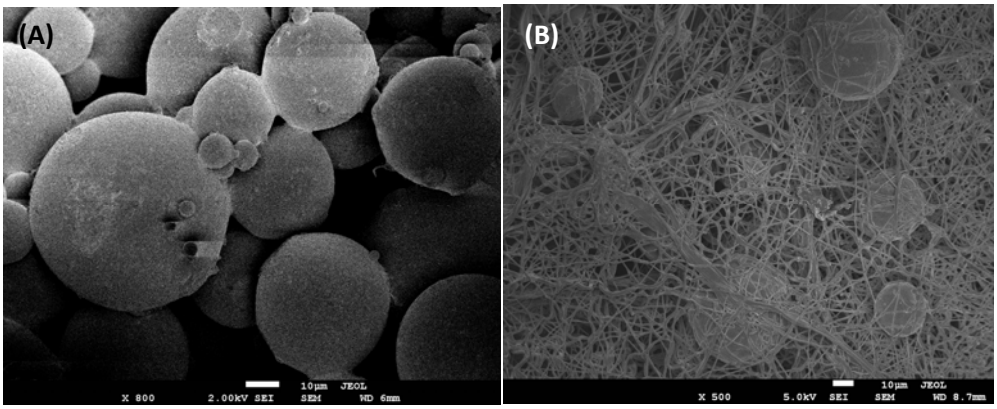

Figure 1. SEM pictures of (A) PSAP particles and (B) 50 wt% PSAP particles in TPU nanofibers.

The absorbency tests of nanomats were performed using water. Figure 2(A) shows a graph of the equilibrium absorbency of water containing 0-50 wt% PSAP particles at room temperature. The absorbency capacity increased with an increase in the amount of particles in the composite. The maximum absorbency capacity of water was 45 g/g for composites with 50 wt% particles. Also, the composite superabsorbent nanomat had a much faster absorbency rate (60 s) to reach to equilibrium compared to the normal absorbent hydrogel particles (at least 5-10 min). Figure 2 shows the exceptional elastic properties of these nanocomposites.

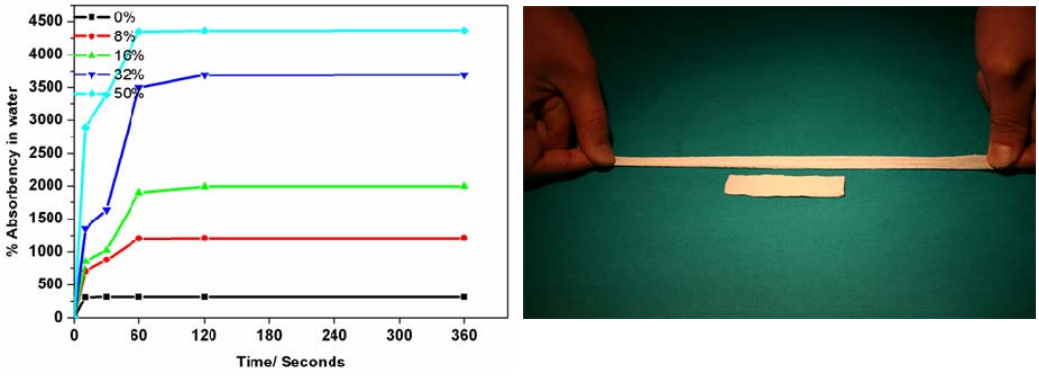

Figure 2. Rate of absorption of composite nanofiber with different contents of absorbent PSAP particles at room temperature (left) and pictures to show the good elastic properties of nanocomposites (right).

For studying the photoresponsivity of the composite nanomats, the weight loss of the equilibrated composites with water on irradiation at 350 nm was determined at 30 min time intervals (Figure 3). Two samples were prepared for the weight loss test. The results showed that TPU/PSAPs composite fibers showed higher weight loss than the sample without irradiation.

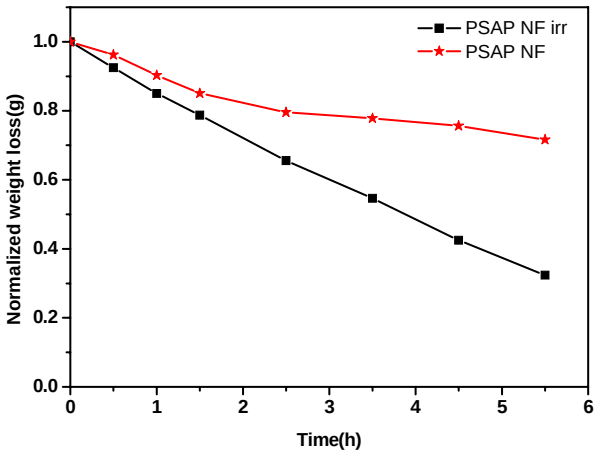

Figure 3. Weight loss of TPU/PSAP composite nanofiber with 32 % of PSAPs particles on irradiation. "irr" means irradiation.

The details of this work are published in *Macromolecular Materials and Engineering*, **2011**, 296, 517–523 and attached in Appendix 8.1.

4.1.2 Declaration of my contribution

The preparation of composite polymeric nanomats and characterization was carried out by me. The draft of the manuscript was written by me. Prof. Dr. Andreas Greiner proposed many useful suggestions for this project. Prof. Dr. Seema Agarwal gave the total support and main correction for the manuscript.

4.2 Multifunctional Polyurethane Aqueous Dispersions showing Thermo Responsivity with UCST and Antibacterial Properties

The manuscript about the content of this chapter was already submitted.

Fei Chen, Judith Hehl, Yu Su, Claudia Mattheis, Seema Agarwal*, Multifunctional Polyurethane Aqueous Dispersions showing Thermo Responsivity with UCST and Antibacterial Properties, *Journal of Colloid and Interface Science*. **2011**, Submitted.

4.2.1 Summary and discussion

In the chapter 4.1, superabsorbent and photo-responsive particles were synthesized and combined with nanofibers to form nanomat composites. These functional nanocomposites have a big potential for house hold cleaning, drug release and sensor applications. For household cleaning applications, besides absorbency and desorbing capability, a growing public awareness of hygiene and the pathogenic effects, stain and malodor formation resulting from microbial contamination has caused a quickly increasing use of biocides in personal care. Therefore, in this work, with an aim to synthesize an antibacterial stable dispersion with facile way for personal care, segmented block co-polyurethane nanoparticles with upper critical solution temperature (UCST) behavior are studied.

Polymers with quaternary ammonium groups are a kind of important antibacterial polymers. Their mechanism of antibacterial action is primarily the targeting and disruption of the bacterial cell membrane. Due to this very general mode of action, these compounds can be used to destroy a wide range of bacteria and the activity can potentially be recovered by removal of dead cell material from the polymer surface.

Firstly, the segmented block copolyurethane base polymer P(TDI-DEMA-PEG) was synthesized by a standard polyaddition procedure using 2,4-toluenediisocyanate (TDI), diethanol-*N*-methylamine (DEMA) and PEG (M_n 2000) as monomers according to Scheme 3. The chemical structure was confirmed by nuclear magnetic resonance

(NMR) spectroscopy, an obvious peak at 3.51 ppm which is assigned to the CH_2 group from PEG confirmed that PEG was successfully introduced into the copolymer. By calculating the integration of signals from CH_2 groups of PEG (3.51 ppm) with $-NCH_3$ groups (2.3 ppm) from DEMA, it was found that the composition of PEG in copolymers fits very well with the feeding ratio; furthermore no signs of urea linkages, but only urethane linkages were observed in the copolymers (data shown in appendix 8.2). In the following discussion, base homo-polyurethane and quaternized polyurethane are denoted as PU-0 and QPU-0, co-polyurethane and quaternized co-polyurethane are named as PU-X and QPU-X, with X referring to the molar ratio of PEG2000 in the copolymers.

The procedure to prepare the dispersions is very simple; the polymers were directly dissolved in hot water (98 °C), after cooling to room temperature, opaque dispersions were formed which showed obvious UCST behavior. The dispersion stability and particle size analysis revealed that by incorporation of PEG segments into the copolymers, the solid content of the dispersion can be increased but the stability did not decrease accordingly. The results are summarized in Table 1.

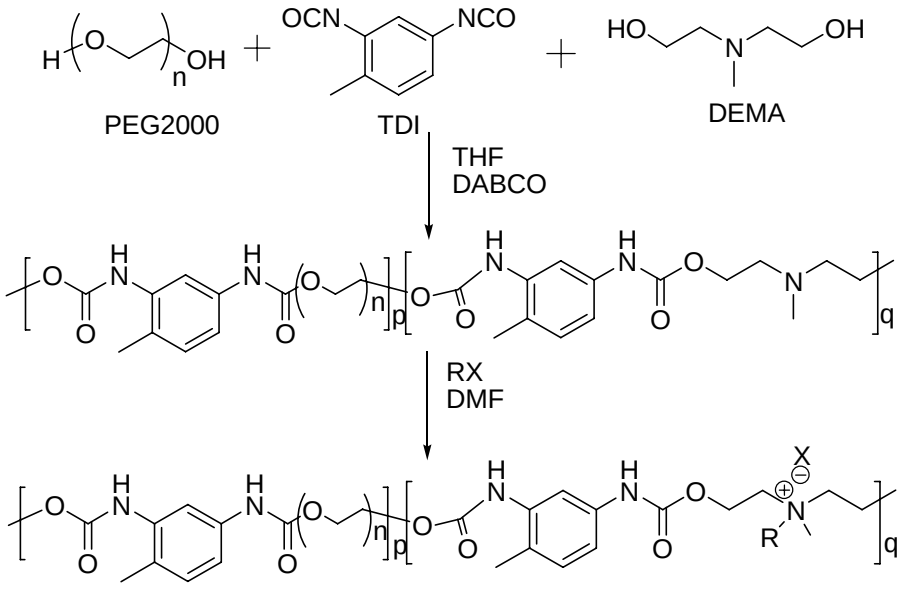

Scheme 3. Synthetic route of the base polymer PU-0 and quaternized QPU-0 from 2,4-toluene diisocyanate (TDI) and diethanol-*N*-methylamine (DEMA).

Table 1. Dispersion experiments of the cationic polyurethanes.

+: soluble -: insoluble *: dispersion & gel like precipitate

QPU-X	**C(PU) /% wt/wt**	**Solubility**	**Dispersion**
QPU-0	≤5	+	*
	10	-	
QPU-1	>1≤8	+	*
QPU-3	>1≤10	+	*
QPU-5	>1≤12	+	*[a]
QPU-10	>1≤20	+	solution

a: quaternized co-polyurethane(QPU-5) polymers can form a dispersion only above 5wt%.

Particle sizes were determined by DLS for different concentrations of the aqueous dispersion of QPU-1. A summary of the results for all measurements is shown in Table 2. An obvious increasing particle size was observed with increasing dispersion concentration, the particle size increased from 70 nm at 1 wt% to around 1000 nm at 8 wt% for QPU-1. The particle size measurement by DLS was also done for the same concentration of copolyurethane with different PEG ratios. There is no big difference of particle size among all the samples, the only change can be observed is that by increasing the PEG content in the copolymer, the particle size distribution decreased but the particle size kept constant around 80 nm.

Table 2. Particle size of quaternized PU dispersions.

QPU	Diameter /nm	QPU	Diameter /nm
1% QPU-0	128±97	1% QPU-1	71±26
1% QPU-1	71±26	2% QPU-1	167±53
1% QPU-3	100±35	3% QPU-1	369±164
1% QPU-5	136±58	4% QPU-1	358±94
		5% QPU-1	563±28
		6% QPU-1	1054±122
		8% QPU-1	863±93

The UCST behavior of the QPU dispersions was investigated using turbidity photometric measurements. The quaternized polyurethane dispersions with the same concentration but with different contents of PEG in the composition were studied. It was expected that the UCST would decrease with increasing content of PEG in the copolymers, but the results were reverse with our expectation. Figure 4 shows the UCST increased with increasing PEG content in the first stage but later decreased again when the PEG content reached to 5 mol%. Surprisingly the 5 wt% dispersion of QPU-1 also showed LCST behavior around 37.7°C (data not shown here). This complex UCST phenomenon was probably due to the contribution of PEG segments and further investigation needs to be done to fully understand it.

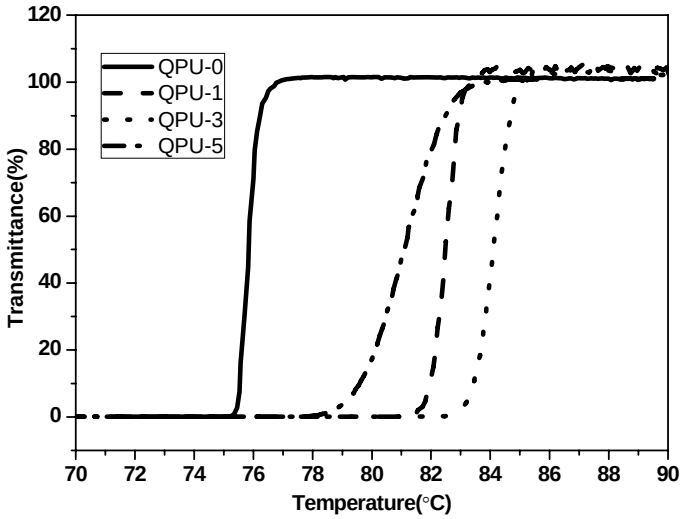

Figure 4. Turbidity measurements of 5 wt% quaternized PU with different PEG contents to investigate the influence of PEG on the UCST behavior of copolymers (first cooling cycle).

The antibacterial properties of the dispersions were investigated by several standard methods. All dispersions proved to be active against *E. coli*; the determined MIC and MBC values do not differ among the tested dispersions (see Table 3) and are with concentrations of 78 µg/ml as MIC (minimum inhibition concentration) and 156 µg/ml as MBC (minimum bactericidal concentration) in a good range. When the focus comes to the speed of antibacterial action, the homo cationic polyurethane dispersion showed to be the best. Already after 10 minutes of contact, the dilution with a concentration of 2.5 mg/ml and all higher concentrated samples killed > 99.9% of the cells, as shown in Figure 5. After a longer contact time of 120 minutes also the other dispersions showed a total reduction of bacteria growth at concentrations of ≥ 625 µg/ml or even ≥ 313 µg/ml as depicted in Figure 5.

Table 3. Minimum inhibition concentration (MIC) and minimum bactericidal concentration (MBC) of the dispersions towards a 10^5 cfu/ml suspension of *E. coli*.

Sample	MIC / μg ml^{-1}	MBC / μg ml^{-1}
QPU-0	78	156
QPU-1	78	156
QPU-3	78	156
QPU-5	78	156

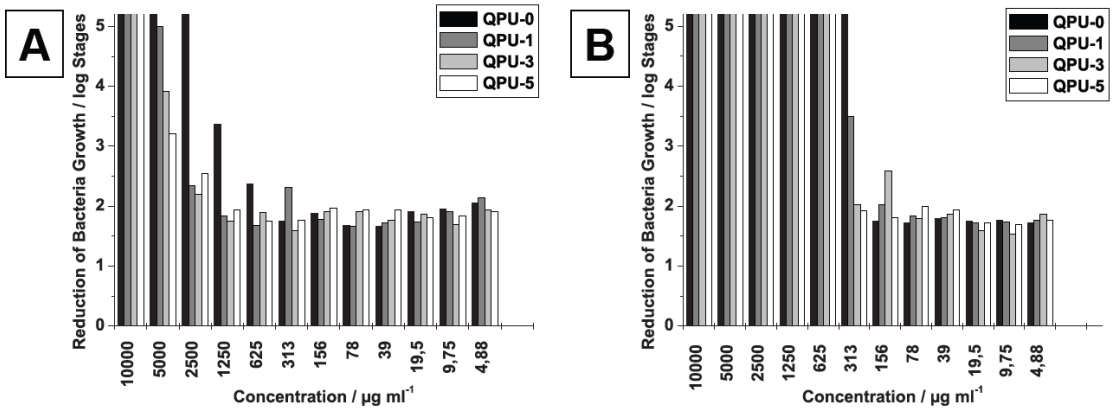

Figure 5. Reduction of bacteria growth for different dilution stages of the dispersions after (A) 10 minutes and (B) 120 minutes contact to *E. coli* (10^5 cfu/ml).

The details of this work was already submitted to *Journal of Colloid and Interface Science* and attached in Appendix 8.2.

4.2.2 Declaration of my contribution

The plan and execution of synthesis of co-polyurethane and the manuscript was done by me. Yu Su made research practical with me on this topic and helped in synthesis and characterization. Claudia Mattheis performed the antibacterial tests. Prof. Dr. Seema Agarwal gave the total support and main correction for the manuscript.

4.3 A Fast Degrading Odd-Odd Aliphatic Polyester-5,7 made by Condensation Polymerization for Biomedical Applications

The manuscript about the content of this chapter was already accepted.

Fei Chen, Jan Martin Nölle, Steffen Wietzke, Marco Reuter, Sangam Chatterjee, Martin Koch, Seema Agarwal*, A Fast Degrading Odd-Odd Aliphatic Polyester-5,7 made by Condensation Polymerization for Biomedical Applications, *Journal of Biomaterials Science: Polymer Edition*. **2011**, Accepted.

4.3.1 Summary and discussion

Previous two chapters have shown the preparation and characterization of functional stimuli-responsive nanostructured materials. For different applications includes tissue engineering and drug release, biodegradability functionality is of great importance.

Aliphatic polyesters received continued attention as it is an important kind of environmental friendly and degradable polymers for medical and non-medical applications. The degradability rate depends upon the type of chemical linkage, molecular weight, hydrophobicity, crystallinity, flexibility etc. Among all these parameters crystallinity has a key influence on biodegradation behavior, thus in this work a novel polyester with odd carbon atoms in the main chain was synthesized starting from pentanediol and 1,7-heptanedioicacid by polycondensation reaction in the presence of titanium tetrabutoxide (TBT) as catalyst. The reaction was carried out in two steps and polyphopsphoric acid was used as heat stabilizer (Scheme 4).

The structural characterization of the resulting polymer was confirmed by 1D and 2D NMR spectroscopy. The molecular weight, thermal stability etc. were investigated by using gel permeation chromatography (GPC), differential scanning calorimetry (DSC) and wide angle X-ray diffraction (WAXD). A single melting peak was seen at about 43 °C but no clear glass transition could be seen in the DSC. In an attempt to observe the glass transition temperature, a new tool for determining the glass transition

temperature was employed: non-contact, non-destructive terahertz time-domain spectroscopy (THz TDS).

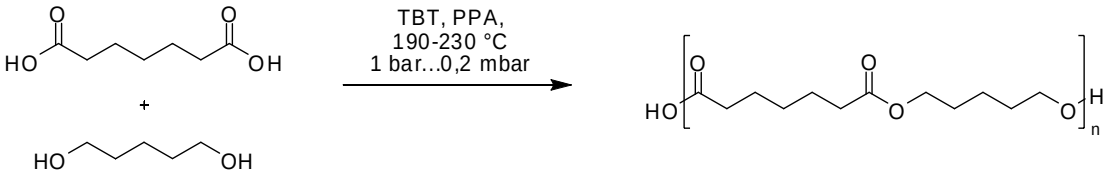

Scheme 4. Synthetic scheme for the formation of polyester-5,7 by polycondensation of 1,7-heptanedioic acid and 1,5-pentanediol.

Temperature-dependent THz TDS measurements reveal the glass transition by a change in the thermal gradient of the THz refractive index. This step marks the beginning of the translational motion of backbone chain segments in the amorphous domains. Due to the model of the free volume, there is a decrease in density with increasing temperature that is higher at temperatures above the glass transition than below. This two regime behavior is reflected by the refractive index according to the Lorentz-Lorenz law. Figure 6 depicts the temperature-dependent refractive index of the biodegradable polyester-5,7 at 1.0 THz (33 cm^{-1}). Both temperature regimes can be fitted by a linear regression. The intersection yields the glass transition temperature T_g in the vicinity of -53 °C.

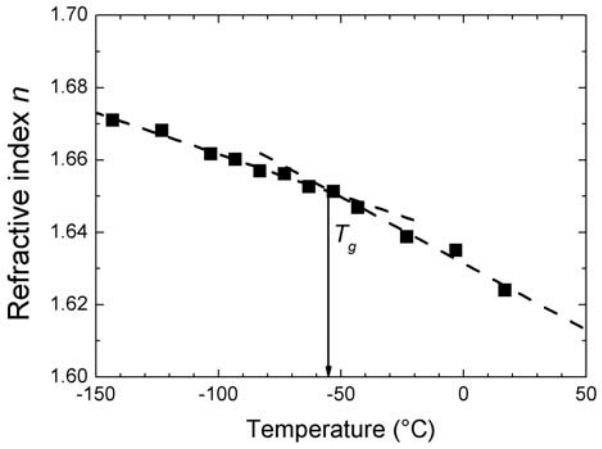

Figure 6. THz refractometry reveals the glass transition temperature at the intersection of two linear fits representing the two temperature regimes of the refractive index at 1.0 THz (33 cm^{-1}).

The enzymatic degradability of the polyester-5,7 was evaluated using lipase from *P. Cepacia* at 37 °C. A comparison of degradation rate was done with commercial standard polycaprolactone (PCL) with similar chemical structure in the main chain. The weight loss profile of polyester-5,7 and PCL at different time intervals in presence of the lipase enzyme is shown in the Figure 7. A very fast degradation of polyester-5,7 can be seen from the curve in comparison to PCL; after 8 h in 0.2 mg/ml *pseudomonas lipase* buffer solution, the weight loss was already about 53 %, after 22 h more than 90 wt% of the samples degraded to water soluble products, which were further analyzed by ^{1}H NMR and GPC. The degradation products of polyester in water after 8 h of degradation was monitored by ^{1}H NMR spectroscopy, the results showed the degradation products mainly consist of 1,5-pentanediol, 1,7-heptanoic acid and oligomers (data not shown here).

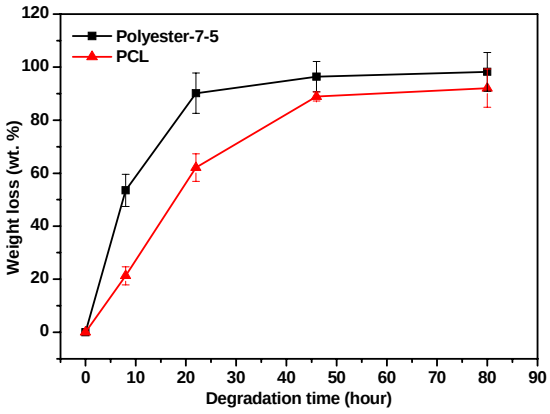

Figure 7. Weight loss profiles of polyester-5, 7 and PCL; degradation in phosphate buffer (pH 7.0) in presence of *Pseudomonas lipase* (0.2mg/ml).

To further understand the reason of the fast enzymatic degradation of polyester-5,7, optical polarized microscopy and SEM were employed to investigate the crystalline spherulites and surface morphology during degradation. Polyester-5,7 before degradation was semicrystalline with about 50 % crystallinity, calculated based on the heat of fusion observed in the first heating cycle from DSC (data not shown here), and the bigger spherulites as observed by optical polarized microscope. The percentual

crystallinity calculated for PCL was about 60% (melting enthalpy of 136 J/g for 100% crystalline PCL is taken from the literature) and smaller spherulites formed (Figure 8). After degradation for about 8h, the percentual crystallinity increased in the left over samples of polyester-5,7 and PCL to about 67-68% but with smaller spherulites for PCL. This could be due to the degradation in the amorphous region thereby increasing the relative crystallinity of the degraded sample.

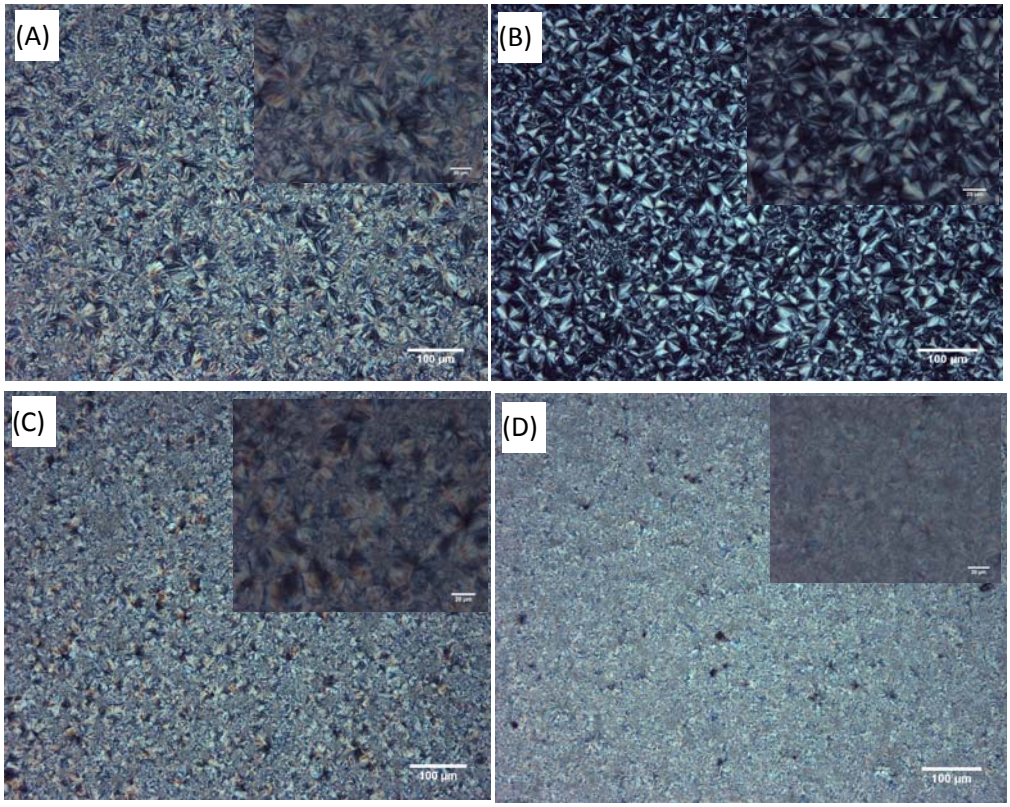

Figure 8. Optical microscope pictures of polyester-5,7 (A) before degradation (B) after degradation (8 h) (C) polycaprolactone (PCL) before degradation and (D) PCL after degradation (8 h).

SEM was used to investigate the surface morphological changes during degradation. The scanning electron micrographs of polyester before and after degradation are shown in the Figure 9. Degradation led to surface erosion; fibrillar and sponge like structures were observed. The SEM characterization of the cross section of the polyester film before and after 22 h degradation in lipase was also done. The

morphology after 22 h degradation remained the same as before degradation, which showed degradation was probably due to surface erosion. The degradation behavior observed for polyesters was almost the same as observed for the known degradable polycaprolactone except its fast rate of degradation.

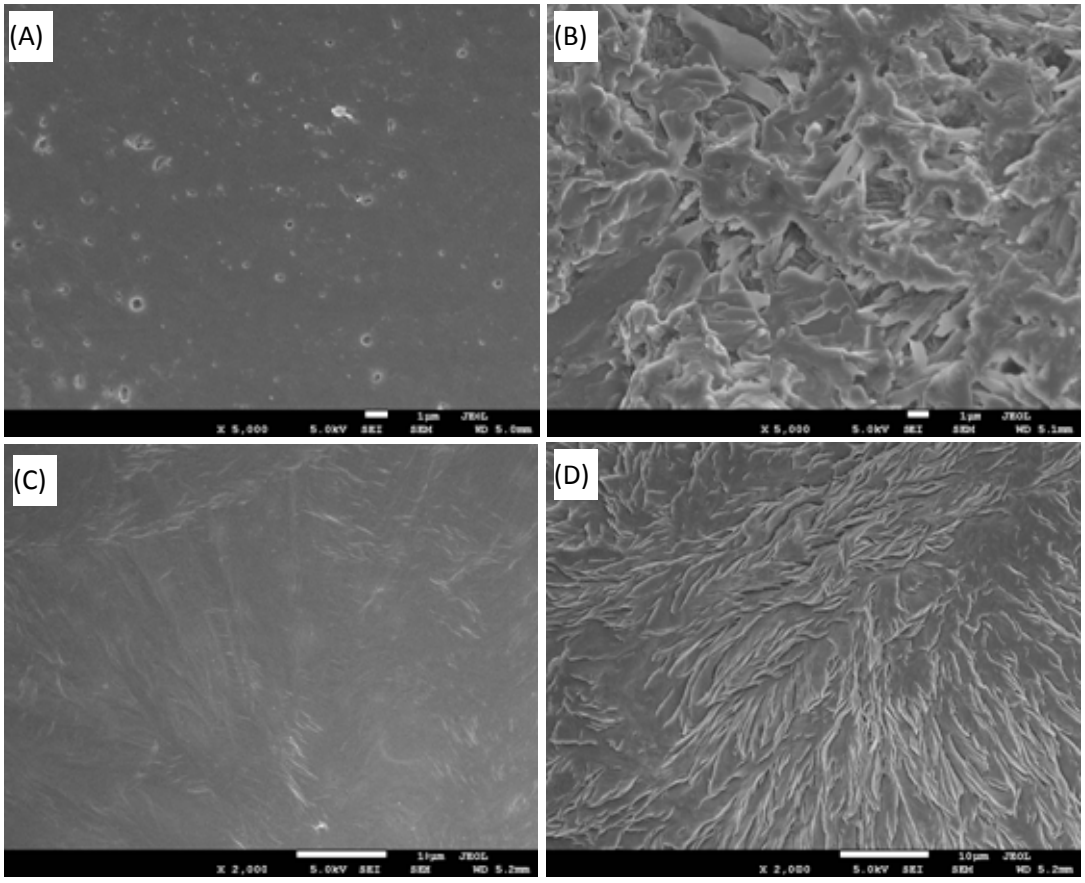

Figure 9. SEM pictures of polyester-5,7 and PCL films during degradation; (A) Polyester-5,7 before degradation (B) after 22 h of degradation; (C) PCL before degradation (D) after 22 h of degradation.

The details of this work was already accepted by *Journal of Biomaterials Science: Polymer Edition* and attached in Appendix 8.3.

4.3.2 Declaration of my contribution

The synthesis work of polyester-5,7 was done by Jan Martin Nölle. The structural characterization, enzymatic degradation and all other tests were carried out by me. The Terahertz time-domain spectroscopy (THz TDS) was done by the research group of Prof. Martin Koch (group members of Steffen Wietzke, Marco Reuter and Sangam Chatterjee). The draft of manuscript was written by me and Prof. Dr. Seema Agarwal gave the total support and main correction for the manuscript.

4.4 Nanofibers by Green Electrospinning of Aqueous Suspensions of Biodegradable BlockCopolyesters for Applications in Medicine, Pharmacy and Agriculture

The manuscript about the content of this chapter has already been published.

Jinyuan Sun, Kathrin Bubel, ***Fei Chen***, Thomas Kissel, Seema Agarwal, Andreas Greiner*, Nanofibers by Green Electrospinning of Aqueous Suspensions of Biodegradable Block Copolyesters for Applications in Medicine, Pharmacy and Agriculture, *Macromol. Rapid Commun*. 2010, 31, 2077–2083.

4.4.1 Summary and discussion

In Chapter 4.3, a fast enzymatic degradable polyester-5,7 with odd carbon atoms in the main chain was successfully synthesized by polycondensation in melt. This novel polyester could be processed into nanofibers by electrospinning and utilized in regenerative scaffolds for tissue engineering. Like all other polyesters, these polymers have the property in common only to dissolve in harmful organic solvents, thereby limiting their utility for actual biomedical and agricultural applications. One feasible method to solve this limitation is to make aqueous suspensions by solvent displacement methods or emulsions etc. from these biodegradable polyesters. With a small amount of matrix polymer, like high molecular weight PEO, they can be processed into stable nanofibers by extraction of the template polymer. This novel concept to prepare biodegradable nanofibers avoiding organic solvent is claimed here as “green electrospinning” (Figure 10). This requires the development of a high solid content polyester suspension in water where the melting point of the polyester blocks should be relatively low.

Generally the secondary suspensions of homo-polyesters have a very low solid content due to its high hydrophobicity in water. Thus in this chapter, with the aim to develop a high solid content of polyester dispersion in water, biodegradable poly(hexylene adipate)-block-(methoxypolyethylene oxide) copolymers (PHA-PEO)

were synthesized and processed to high solid content dispersions. This suspension next was mixed with a small amount of high molecular weight PEO as well as polyoxyethylene-20-stearyl ether (Brij78) and electrospun into the corresponding nanofibers. After extraction with water, nanofibers of PHA-PEO were obtained.

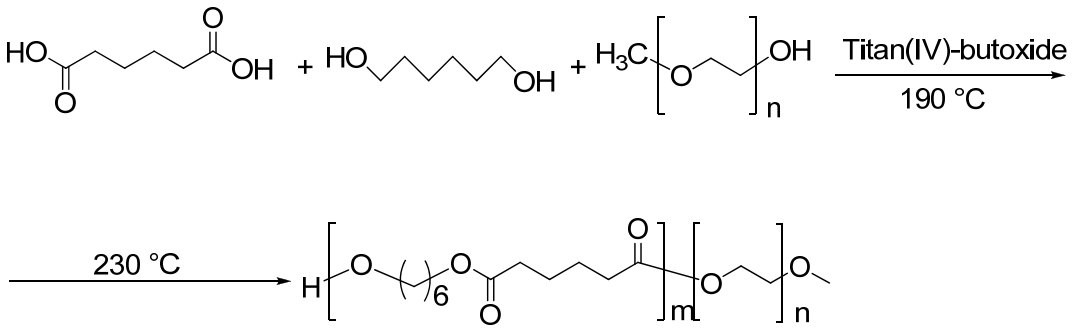

Scheme 5. Synthesis of poly(hexylene adipate)-block-(methoxypolyethylene oxide) (PHA-b-PEO)

The synthesis of the diblock copolyesters was performed by melt polycondensation, as shown in Scheme 5. The expected chemical structure of PHA-b-PEO was confirmed by ^{1}H NMR, ^{13}C NMR and IR spectroscopy. (Details can be seen in the appendix publication 8.4).

PHA-b-PEO was dissolved in acetone, after addition of a solution of water and Brij78, ultrasound was applied. Finally, acetone was removed by slow evaporation at room temperature and milky aqueous suspensions without any precipitation were obtained with contents of 2.94 wt%. Analysis of the particle diameter by dynamic light scattering showed average particle diameters of 177 nm. Although the suspensions were stable at room temperature for at least 10 d, the suspensions were of too low a solid content to be useful for nanofibers preparation by suspension electrospinning. For achieving higher concentrated suspensions, dialysis method with PVA (15 wt% in water) was selected as outer media and 2.5 wt% aqueous suspension with Brij 78 was kept in dialysis membrane(MWCO 10 000). Due to the osmotic pressure difference, a constant weight loss of the original suspension in the dialysis tubes was measured with 100 h, resulting in a corresponding aqueous suspension of 16 wt% PHA-b-PEO.

This milky suspension did not show visible precipitation and displayed an average particle diameter of 108 nm by dynamic light scattering.

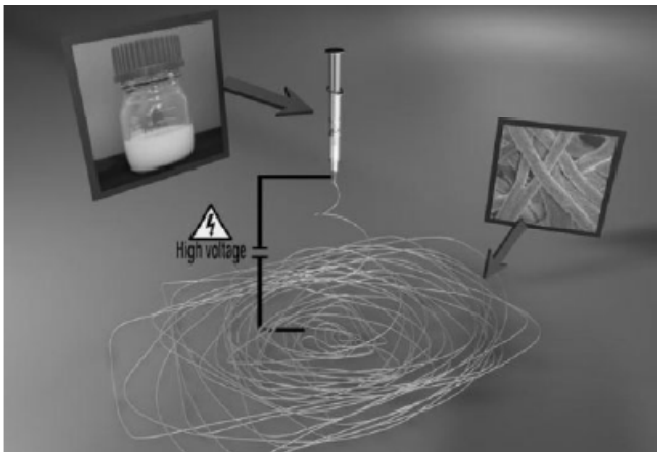

Figure 10. The schematic diagram of "green electrospinning" to form biodegradable nanofibers.

As mentioned previously, water soluble polymers are required as template polymers for "green electrospinning". Therefore, electrospinning of PHA-b-PEO was completed with different amounts of PEO relative to PHA-b-PEO. After electrospinning, the composite fibers were treated with water in order to test the water stability of the fibers. Fiber diameters of the as spun fibers ranged from 350 to 550 nm (Figure 11). After treatment with water at 20 °C for 24 h, the fibers showed no sign swelling or disintegration. The fiber surfaces of the as spun fibers appeared to be somewhat smoother that the corresponding fibers after water treatment.

As spun fibers and water treated fibers were also analyzed with ^{1}H NMR spectroscopy (Data no shown here), no traces of PEO and Brij78 were found in the water treated fibers, thereby showing the complete removal of PEO and the surfactant. This also proved the success of the concept of making stable biodegradable nanofiber non-wovens from secondary water suspensions free of harmful organic solvents.

In sum, biodegradable PHA-b-PEO diblock copolyesters were successfully synthesized and processed by dialysis method to aqueous secondary suspensions of 16 wt%. With the template polymer PEO, water stable biodegradable PHA-b-PEO

nanofiber non-wovens were formed by extraction of PEO. The method developed in this chapter will open up many perspectives for water based electrospinning and expand the biodegradable nanofibers in actual biomedical and agricultural applications.

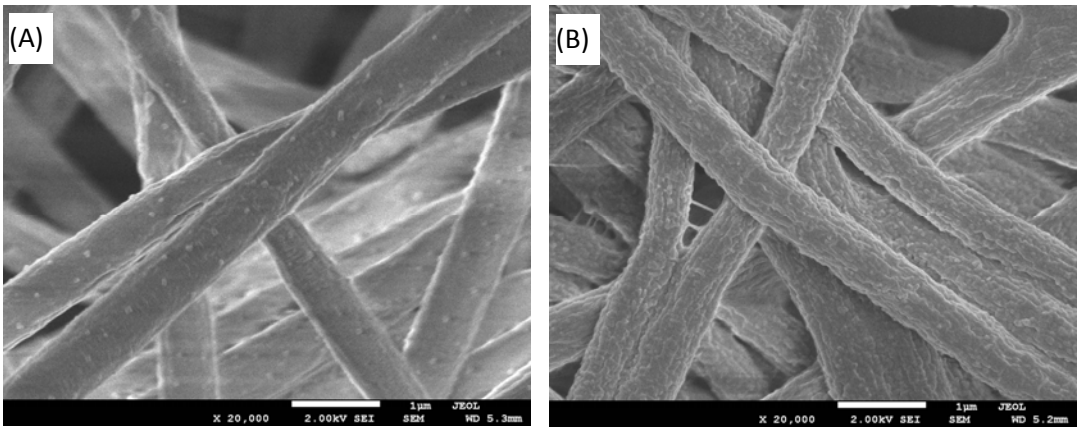

Figure 11. SEM of electrospun fibers of PHA-PEO-2b with 4% PEO, (A) before and (B) after water treatment for 2 d at 25 °C at higher magnification.

The details of this work have already been published in *Macromol. Rapid Commun*. 2010, 31, 2077–2083 and attached in Appendix 8.4.

4.4.2 Declaration of my contribution

The synthesis of PHA-b-PEO and secondary dispersion was done by Jinyuan Sun. The initial electrospinning of dispersions with PEO template and SEM characterization was done by me, the chemical structure confirmation before and after water treatment for the as spun fiber was done by Kathrin Bubel. Prof. Dr. Andreas Greiner gave the total support and main writing the manuscript and Prof. Dr. Seema Agarwal contributed for the correction of the manuscript and useful discussion.

4.5 Low Dielectric Constant Polyimide Nanomats by Electrospinning

The manuscript about the content of this chapter has already been published.

Fei Chen, Debaditya Bera, Susanta Banerjee*, Seema Agarwal*, Low Dielectric Constant Polyimide Nanomats by Electrospinning, *Polymers for Advanced Technologies*, **2011**, early view online.

4.5.1 Summary and discussion

The previous four chapters described the potential application of responsive and biodegradable nanofibers in house hold cleaning, medicine, pharmacy and agriculture. The assumption of this chapter was the combination of proper materials (fluorinated polyimides) with the electrospinning technique could produce low dielectric constant materials used as insulating material in interlayer dielectrics due to the large pores in electrospun nanofibers and the high surface to volume ratio.

With an aim to provide low dielectric constant polyimide membranes with good processability, high thermal stability and low water absorption, we choose fluorinated polyimides and use electrospinning to form nanomats. The polyimides in this work were based on 4,4-Bis[3'-trifluoromethyl-4'-(4'-amino benzoxy)benzyl] biphenyl (Q) and virous fluorinated and non-fluorinated dianhydrides. The detailed characterization in terms of thermal stability, dielectric constant and hydrophobicity was also reported.

The synthesis of poly(ether imides) were carried out by two steps via poly(amic acid) intermediate (scheme 6), the highly viscous poly(amic acid) solutions were diluted to different solid contents and electrospun (Figure 12). The nanofibers were collected on a rotating drum shaped roller with high rotating speed to form aligned nanofiber belts.

The fiber morphology and dimensions of the nanofibers mats was investigated using SEM. It was observed that the nanofibers were aligned longitudinally and the average diameter varies from 100-200 nm.

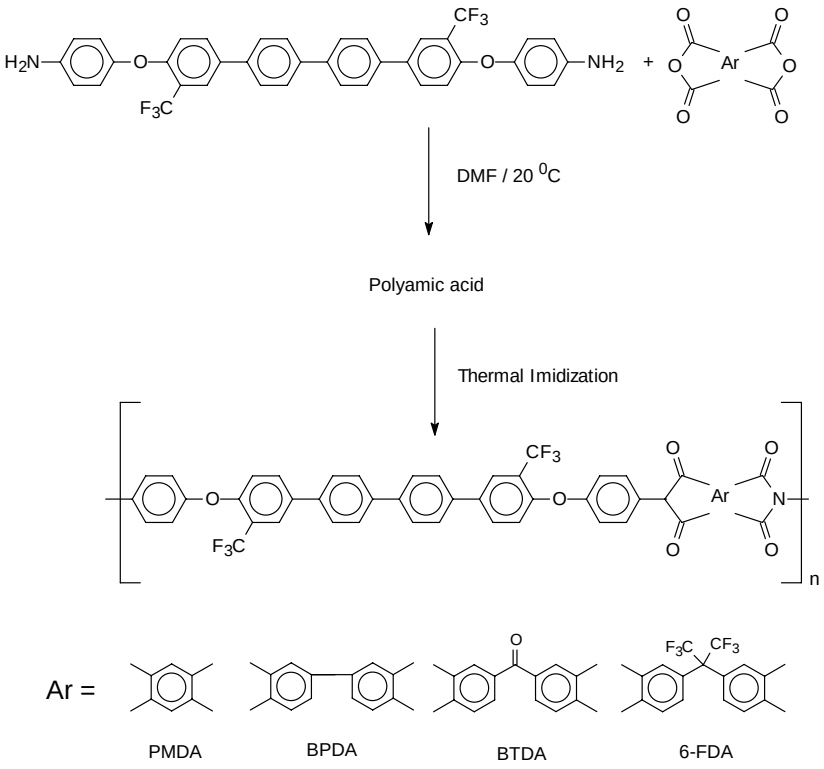

Scheme 6. Reaction scheme for the synthesis of poly(ether imide)s.

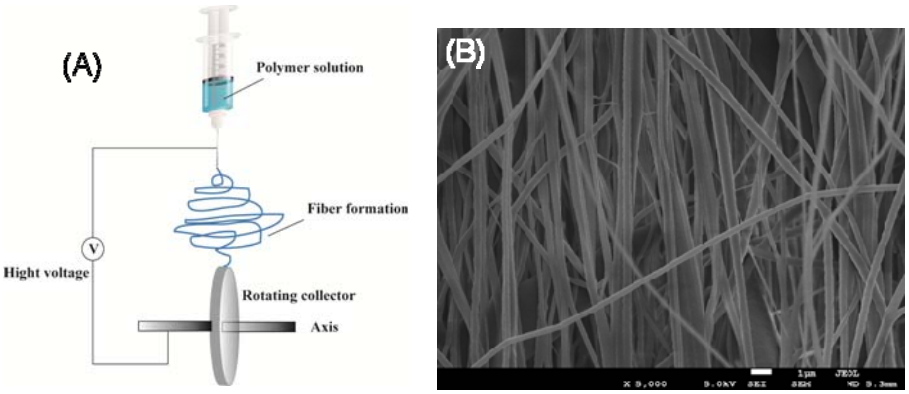

Figure 12. (A) Schematic illustration of electrospinning setup for collecting the aligned PPA nanofiber and (B) SEM images of aligned Q-6FDA-i nanofiber.

Further, electrospun polyimides mats were evaluated for their mechanical properties (Figure 13). The polyimide mat prepared from BPDA showed the highest tensile strength at break. The value is much higher than the polyimide film prepared from BPDA. The results also showed the importance of rod-like structure of polyimide in getting thigh strength and high modulus fibers as Q-FDA and Q-BTDA nanofiber

mats have relatively lower mechanical strength compared to their correspondent films.

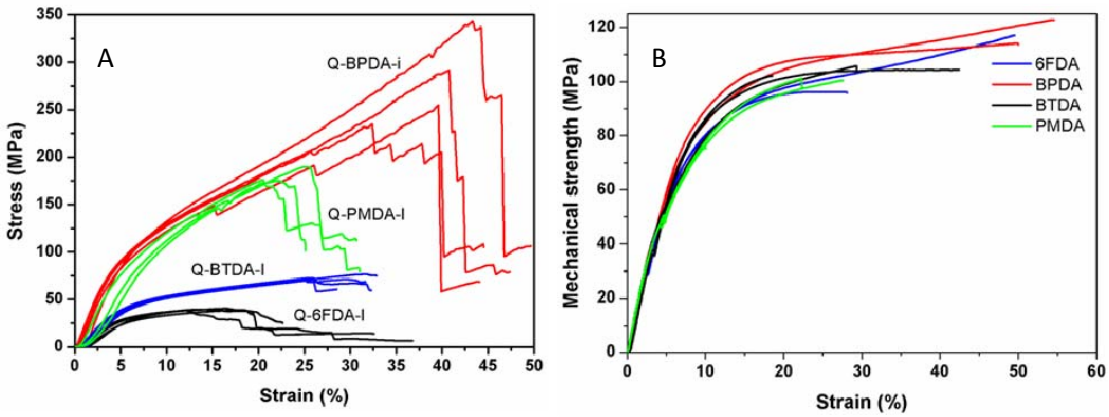

Figure 13. Stress-strain curves of (A) polyimide mats and (B) films.

The dielectric constant of the polyimide mats and the films were calculated from their corresponding capacitance values at 1 MHz. The dielectric constant values are summarized in Table 4. It was observed that the dielectric constant of the aligned nanofiber mats were considerably lower than their analogous film samples. The values are much lower than the commercially available polyetherimide ULTEM 1000 and polyimide Kapton H at 1 kHz. The lower dielectric constant of these polyimide nanofiber mats was probably due to the large pores and high surface to volume ratio between the nanofibers.

For microelectrics industry, low moisture absorption and hydrophobic surface is also a key consideration, thus the hydrophobic behavior of polyimide films and polyimide nanomats were evaluated by water contact angle test. Figure 14 showed all polyimide mats have hydrophobic nature with highest value of contact angle about 125° for fluorinated polyimide mat Q-6 FDA-i. Another obvious observation is that all the electrospun mats have higher contact angles compared to the corresponding films, this can be attributed the porous rough nano structures surface generated by electrospinning enhances the hydrophobicity.

Table 4. Water contact angle and dielectric constant of the imidized aligned nano fiber mats and the polyimide films.

Sample	Aligned polyimide mats		Polyimide films	
	Contact angle(°)	Dielectric constant at 1 MHz	Contact angle(°)	Dielectric constant at 1 MHz
Q-PMDA-i	114±5	1.739	84±5	2.901
Q-BPDA-i	118±4	1.607	77±2	2.861
Q-BTDA-i	120±3	1.765	75±2	2.957
Q-6FDA-i	125±4	1.430	83±3	2.787

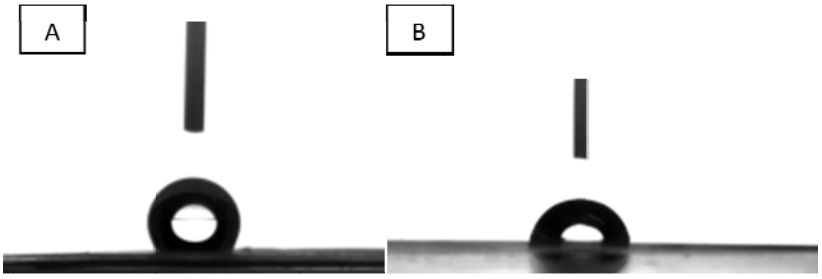

Figure 14. Different wetting behaviors of (A) polyimide Q-6FDA-i polyimide mat (contact angle 125±4^{o}) (B) Q-6FDA-i film (contact angle 83±3^{o}).

In sum, polyimide nanofiber mats and films have been prepared by the reaction of a fluorinated diamine monomer 4,4-Bis[3'-trifluoromethyl-4'-(4'-amino benzoxy)benzyl] biphenyl (Q) with different commercially available fluorinated and non-fluorinated dianhydrides in two steps. The amorphous poly(ether imide)s containing bis-trifluoromethyl groups (Q-6FDA) exhibited not only low dielectric constants-lower than those of the commercially available poly(ether imide) ULTEM 1000 and PI Kapton H at 1 kHz-but also excellent long term thermo-oxidative stability and enhanced hydrophobicity relative to non-fluorinated dianhydride-based

polyimides. Such materials could be of high use as insulating material in interlayer dielectrics besides their use in filter and composite industry.

The details of this work has already been published in *Polymers for Advanced Technologies* and attached in Appendix 8.5.

4.5.2 Declaration of my contribution

The synthesis of monomer 4,4-Bis[3'-trifluoromethyl-4'-(4'-amino benzoxy)benzyl] biphenyl and dielectric constant test was done in Prof. Dr. Susanta Banerjee's group by Debaditya Bera. Prof. Dr. Seema Agarwal supported the whole project, proposed many useful suggestions and helped in writing the introduction part of the manuscript. The preparation of electrospun nanofibers and characterization, writing the draft of manuscript were done by me.

5. Outlook

Stimuli responsive materials and biodegradable polymers have been received increasing interest in the scientific as well as the technical community as they have big potential applications in biosensors, tissue engineering, drug delivery and many more fields. By proper choice of processing technique such as electrospinning, it is possible to produce nanostructured materials from these functional polymers. Due to novel characteristics in the nanosized dimension, the functional materials possess some new unique properties which surely will pave the way for more promising applications in biomedical fields. Thus the study in this work emphasized on the preparation and characterization of some functional nanomaterials by electrospinning and heterophase polymerization. The fundamental work presented here provides some concepts for making novel functional nanostructured materials and surely a large number of possible research directions could be developed based on this work.

For stimuli responsive superabsorbent nanomats, the water absorption / desorption was controlled by photo irradiation due to photo responsivity of the embedded particles; the influence of particle size on photo-responsive rate should be further investigated. For a real biosensor application, the desorption rate of these nanocomposites should be optimized and other hydrophilic biodegradable elastomers could be a good choice as substrate. For the antibacterial segmented block copolyurethane nanoparticles with UCST behavior, the full understanding of UCST behavior influenced by the degree of quaternization and the pH should be further investigated. For smart drug encapsulation and release, a proper hydrophilic drug needs to be chosen to investigate the drug release profile in vitro. As a choice, PCL segments could be introduced into the copolymer to impart the biodegradability of this particle system for further biomedical applications.

In the second main part of this dissertation, novel odd-odd polyester and PHA-b-PEO copolyesters were synthesized and enzymatic degradation results were shown. The polyester-5,7 showed a similar crystal structure and degradation mechanism with

commercial available PCL; the crystallization process and crystallization kinetics need to be investigated to determine the self-nucleation temperature. For a real biomedical application, the cytotoxicity test and in vivo degradation mechanism deserve further study. The PHA-b-PEO nanofiber by “green electrospinning” technique offers novel perspectives for application in medicine, pharmacy and agriculture, but still many work deserves further research including the biodegradation behavior of such “nanoparticles formed nanofiber”, the influence of molecular weight, PHA/PEO block ratio and block length should also be investigated to get a structure-property relationship for further applications.

The last part of this thesis showed successful preparation of low dielectric constant nanomats by proper combination of fluorinated polyimides with electrospinning processing technique. The mechanism needs to be proposed to explain the low dielectric constant, other fluorinated diamine monomers can be chosen for further investigation.

6. Acknowledgements

First and foremost, I would like to thank my direct supervisor prof. Dr. Seema Agarwal, for giving me this interesting research topic. I am deeply indebted to her guidance in my work. Without her continued support, I would not have been possible to achieve my goal during scheduled time. She showed me how to initiate and approach a research problem together with teaching me how to organize the results and the art of writing scientific paper.

I would also like to thank Prof. Dr. Andreas Greiner for his kindness and all the useful suggestions, his open mind and concern inspire me a lot during my entire PhD episode.

I want to give my gratitude to Prof. Dr. Haoqing Hou in the department of chemistry, Jiangxi Normal University, for his recommendation and continued concerning with my work.

Thanks also goes to the secretary of our group, Mrs. Edith Schmidt, for her numerous and patient help with the official work.

I want to thank all my former and present working group members for their kind help during my research and for making the group a wonderful work place. Firstly, I am very thankful to my lab mates: Claudia Mattheis, Christoph Luy and Qiao Jin for their friendly nature and kind help, the lab become an enjoyable work place because of all your participation. I gratefully acknowledge Claudia Mettheis, Ilka Elisabeth Paulus for their valuable assistance in reviewing my thesis so patiently. I owe my special thanks to Dr. Roland Dersch for his constructive advice and kind help. My thanks then go to Anna Bier and Martina Gerlach for their kind help in ordering chemicals for my work. Next, thanks go to Christoph Luy and Andreas Hedderich for helping me tackle all the computer related problems. Thanks then to Ilka Elisabeth Paulus, Yi Zhang, Christian Heel and Stefan Boken for showing me the MDSC technique and lots of GPC measurements. Thanks also go to Elisabeth Giebel for showing me the

mechanical tests, Jan Seuring for the DLS and polarized optical microscopy measurement. Thanks for Uwe Justus for his useful suggestions during my work.

I am grateful to Prof. Dr. Susanta Banerjee and his student Debaditya Bera in the materials science center, Indian Institue of Technology, Kharagpur, for their cooperation to finish the project “Low dielectric constant polyimide nanomats by electrospinning”, it was a wonderful experience cooperated with Prof. Dr. Susanta Banerjee.

Special thanks also go to the former group member Jan Martin Nölle, for his synthesis work of polyester-5, 7 for my enzymatic degradation investigation. I am also grateful to Prof. Dr. Martin Koch and his students Steffen Wietzke, Marco Reuter and Sangam Chatterjee for measuring the glass transition temperature by terahertz time-domain spectroscopy (THz TDS).

I am also grateful to Kathrin Bubel and former co-worker Jinyuan Sun for their cooperation to successfully finish the project “Nanofibers by green electrospinning of aqueous dispersions of biodegradable blockcopolyester for application in medicine, pharmacy and agriculture”.

Thanks my master practical student Yu Su for her passionate participation in part of my projects .

Thank Michael Hellwig and Dr. Andreas Schaper for helping me the electron microscope measurements.

I cannot forget to all my friends in Germany and China who always have been a source of inspiration. The valuable memories with their company, I will cherish throughout my life.

Finally, I want to thank my family: my parents for giving me life in the first place, for their unconditional support and affection never returned. I would also like to thank my elder brother and sister for their support my studies. My special thanks go to Yin Jian,

my girlfriend, for her love and support for my studies, without her encourage and understanding, I would have never concentrated on my work and finished my work in due time.

7. Literature

1. Heeger, A.J., J. Peet, and G.C. Bazan, "Plastic" Solar Cells: Self-Assembly of Bulk Heterojunction Nanomaterials by Spontaneous Phase Separation. Accounts of Chemical Research, 2009. **42**(11): p. 1700-1708.

2. Wong, N.B., et al., Nanomaterials separation by an ultrasonic-assisted phase transfer method. Chemical Physics Letters, 2008. **455**(4-6): p. 252-255.

3. Antonietti, M. and K. Landfester, Polyreactions in miniemulsions. Progress in Polymer Science, 2002. **27**(4): p. 689-757.

4. Yamazaki, S., S. Hattori, and Hamashim.M, Mechanism of Heterogeneous Polymerization of Vinyl Monomers in Aqueous Mediums .3. Relation between Monomer Concentration in Polymer Particles and Particle Size in Polymerization of Methyl Methacrylate. Chemistry of High Polymers, 1970. **27**(305): p. 600-&.

5. Lu, X.F., C. Wang, and Y. Wei, One-Dimensional Composite Nanomaterials: Synthesis by Electrospinning and Their Applications. Small, 2009. **5**(21): p. 2349-2370.

6. Huang, Z.M., et al., A review on polymer nanofibers by electrospinning and their applications in nanocomposites. Composites Science and Technology, 2003. **63**(15): p. 2223-2253.

7. Greiner, A. and J.H. Wendorff, Electrospinning: A fascinating method for the preparation of ultrathin fibres. Angewandte Chemie-International Edition, 2007. **46**(30): p. 5670-5703.

8. Reneker, D.H., et al., Electrospinning of nanofibers from polymer solutions and melts. Advances in Applied Mechanics, Vol 41, 2007. **41**: p. 43-195.

9. Agarwal, S., J.H. Wendorff, and A. Greiner, Use of electrospinning technique for biomedical applications. Polymer, 2008. **49**(26): p. 5603-5621.

10. Rodriguez-Hernandez, J., et al., Toward 'smart' nano-objects by self-assembly of block copolymers in solution. Progress in Polymer Science, 2005. **30**(7): p. 691-724.

11. Hawker, C.J. and K.L. Wooley, The convergence of synthetic organic and polymer chemistries. Science, 2005. **309**(5738): p. 1200-1205.

12. Matyjaszewski, K., Macromolecular engineering by controlled/living ionic and radical polymerization. Abstracts of Papers of the American Chemical Society, 2002. **223**: p. C106-C106.

13. Licciardi, M., et al., New folate-functionalized biocompatible block copolymer micelles as potential anti-cancer drug delivery systems. Polymer, 2006. **47**(9): p. 2946-2955.

14. Topp, M.D.C., et al., Thermosensitive micelle-forming block copolymers of poly(ethylene glycol) and poly(N-isopropylacrylamide). Macromolecules, 1997. **30**(26): p. 8518-8520.

15. Geng, Y., et al., Shape effects of filaments versus spherical particles in flow and drug delivery. Nature Nanotechnology, 2007. **2**(4): p. 249-255.

16. Ahmed, F. and D.E. Discher, Self-porating polymersomes of PEG-PLA and PEG-PCL: hydrolysis-triggered controlled release vesicles. Journal of Controlled Release, 2004. **96**(1): p. 37-53.

17. Torchilin, V.P., PEG-based micelles as carriers of contrast agents for different imaging modalities. Advanced Drug Delivery Reviews, 2002. **54**(2): p. 235-252.

18. Lecommandoux, S.B., et al., Magnetic nanocomposite micelles and vesicles. Advanced Materials, 2005. **17**(6): p. 712-+.

19. Antonietti, M. and K. Tauer, 90 years of polymer latexes and heterophase polymerization: More vital than ever. Macromolecular Chemistry and Physics, 2003. **204**(2): p. 207-219.

20. Matyjaszewski, K., Transformation of "living" carbocationic and other polymerizations to controlled "living" radical polymerization. Macromolecular Symposia, 1998. **132**: p. 85-101.

21. Qiu, J., B. Charleux, and K. Matyjaszewski, Controlled/living radical polymerization in aqueous media: homogeneous and heterogeneous systems. Progress in Polymer Science, 2001. **26**(10): p. 2083-2134.

22. Gilbert, R.G., ed. Emulsion polymerization: a mechanistic approach. 1995, Academic Press: London.

23. Kriha, O., et al., Connection of hippocampal neurons by magnetically controlled movement of short electrospun polymer fibers - A route to magnetic micromanipulators. Advanced Materials, 2007. **19**(18): p. 2483-+.

24. Li, D. and Y.N. Xia, Electrospinning of nanofibers: Reinventing the wheel? Advanced Materials, 2004. **16**(14): p. 1151-1170.

25. Kosmider, K. and J. Scott, Polymeric nanofibres exhibit an enhanced air filtration performance. Filtration & Separation, 2002. **39**(6): p. 20-22.

26. Dai, Y.Q., et al., Ceramic nanofibers fabricated by electrospinning and their applications in catalysis, environmental science, and energy technology. Polymers for Advanced Technologies, 2011. **22**(3): p. 326-338.

27. Chen, S.L., D.H. Han, and H.Q. Hou, High strength electrospun fibers. Polymers for Advanced Technologies, 2011. **22**(3): p. 295-303.

28. Reneker, D.H. and I. Chun, Nanometre diameter fibres of polymer, produced by electrospinning. Nanotechnology, 1996. **7**(3): p. 216-223.

29. Chase, G.G., et al., Effects of parameters on nanofiber diameter determined from electrospinning model. Polymer, 2007. **48**(23): p. 6913-6922.

30. Jing, Z., et al., Biodegradable electrospun fibers for drug delivery. Journal of Controlled Release, 2003. **92**(3): p. 227-231.

31. Zeng, J., et al., Influence of the drug compatibility with polymer solution on the release kinetics of electrospun fiber formulation. Journal of Controlled Release, 2005. **105**(1-2): p. 43-51.

32. Qi, H.X., et al., Encapsulation of drug reservoirs in fibers by emulsion electrospinning: Morphology characterization and preliminary release assessment. Biomacromolecules, 2006. **7**(8): p. 2327-2330.

33. Xu, X.L., et al., Ultrafine medicated fibers electrospun from W/O emulsions. Journal of Controlled Release, 2005. **108**(1): p. 33-42.

34. Greiner, A., et al., Preparation of water-stable submicron fibers from aqueous latex dispersion of water-insoluble polymers by electrospinning. Polymer, 2007. **48**(14): p. 3974-3981.

35. Stoiljkovic, A., et al., Preparation of water-stable submicron fibers from aqueous latex dispersion of water-insoluble polymers by electrospinning. Polymer, 2007. **48**(14): p. 3974-3981.

36. Stoiljkovic, A., et al., Poly(styrene-co-n-butyl acrylate) Nanofibers with Excellent Stability against Water by Electrospinning from Aqueous Colloidal Dispersions. Macromolecules, 2009. **42**(16): p. 6147-6151.

37. Klimov, E., et al., Designing Nanofibers via Electrospinning from Aqueous Colloidal Dispersions: Effect of Cross-Linking and Template Polymer. Macromolecules, 2010. **43**(14): p. 6152-6155.

38. Yoshimoto, H., et al., A biodegradable nanofiber scaffold by electrospinning and its potential for bone tissue engineering. Biomaterials, 2003. **24**(12): p. 2077-2082.

39. Lannutti, J., et al., Electrospinning for tissue engineering scaffolds. Materials Science & Engineering C-Biomimetic and Supramolecular Systems, 2007. **27**(3): p. 504-509.

40. Sukwattanasinitt, M., et al., Nanofibers Doped with Dendritic Fluorophores for Protein Detection. Acs Applied Materials & Interfaces, 2010. **2**(7): p. 1798-1803.

41. Xu, X.H., et al., Electrospun poly(vinyl alcohol)/glucose oxidase biocomposite membranes for biosensor applications. Reactive & Functional Polymers, 2006. **66**(12): p. 1559-1564.

42. Xia, Y.N., et al., Ceramic nanofibers fabricated by electrospinning and their applications in catalysis, environmental science, and energy technology. Polymers for Advanced Technologies, 2011. **22**(3): p. 326-338.

43. Stevens, M.M. and J.H. George, Exploring and engineering the cell surface interface. Science, 2005. **310**(5751): p. 1135-1138.

44. Anzenbacher, P. and M.A. Palacios, Polymer nanofibre junctions of attolitre volume serve as zeptomole-scale chemical reactors. Nature Chemistry, 2009. **1**(1): p. 80-86.

45. Zeng, J., et al., Poly(vinyl alcohol) nanofibers by electrospinning as a protein delivery system and the retardation of enzyme release by additional polymer coatings. Biomacromolecules, 2005. **6**(3): p. 1484-1488.

46. Okuzaki, H., K. Kobayashi, and H. Yan, Thermo-Responsive Nanofiber Mats. Macromolecules, 2009. **42**(16): p. 5916-5918.

47. Patel, A.C., et al., In situ encapsulation of horseradish peroxidase in electrospun porous silica fibers for potential biosensor applications. Nano Letters, 2006. **6**(5): p. 1042-1046.

48. Ramaseshan, R., et al., Functionalized polymer nanofibre membranes for protection from chemical warfare stimulants. Nanotechnology, 2006. **17**(12): p. 2947-2953.

49. Yang, S.Y., et al., Electrospun TiO(2) nanorods assembly sensitized by CdS quantum dots: a low-cost photovoltaic material. Energy & Environmental Science, 2010. **3**(12): p. 2010-2014.

50. Mukherjee, K., et al., Electron transport in electrospun TiO(2) nanofiber dye-sensitized solar cells. Applied Physics Letters, 2009. **95**(1).

51. Yang, S.Y., et al., Electrospun TiO2 nanorods assembly sensitized by CdS quantum dots: a low-cost photovoltaic material. Energy & Environmental Science, 2010. **3**(12): p. 2010-2014.

52. Chen, S.L., et al., Electrospun and solution blown three-dimensional carbon fiber nonwovens for application as electrodes in microbial fuel cells. Energy & Environmental Science, 2011. **4**(4): p. 1417-1421.

8. Appendix

8.1 Publication "Stimuli-Responsive Elastic Polyurethane-Based Superabsorber Nanomat Composites"

Fei Chen, Andreas Greiner, Seema Agarwal*, Stimuli-Responsive Elastic Polyurethane-Based Superabsorber Nanomat Composites, *Macromol. Mater. Eng.* 2011, 296, 517–523

Stimuli-Responsive Elastic Polyurethane-Based Superabsorber Nanomat Composites

Fei Chen, Andreas Greiner, Seema Agarwal*

Photoresponsive superabsorber particles containing a crosslinked hydrophilic core and a hydrophobic azobenzene-containing shell were used to prepare photoresponsive polymeric nanomats, thus combining photoresponsivity with high porosity, toughness, and hydrophilicity. The properties of the nanomat composites were highly dependent upon the amount of the superabsorber photochromic particles added. Stable, highly elastic composite nanomats with very high loading (up to ≈50 wt.-%), good water absorption capacity (4 000%) and relatively good tensile strength (3 MPa) were obtained. The photoresponsive behavior of the composites is demonstrated, which leads to relatively fast water desorption.

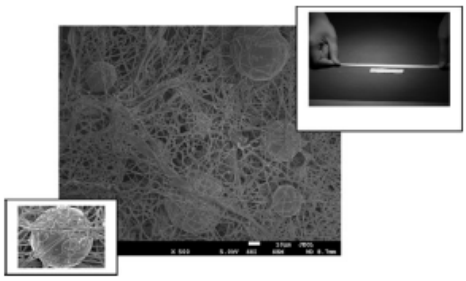

Introduction

Superabsorbers are crosslinked hydrophilic polymers with capability of absorbing and retaining water in large amounts.[1,2] The absorbing capacity is generally as high as 10–1 000 $g \cdot g^{-1}$. These are of interest both from academic and industrial point-of-view and have vast applications like sealants, soil additives and other agricultural applications, hygiene products and diapers, liquid filtration and drug delivery, wound dressing, tissue engineering, etc. The review by Zohuriaan-Mehr and Kabiri is a good reference for details regarding superabsorbent polymer materials and their various applications.[1] Chemically, the superabsorbers are based on both the natural and the synthetic polymers like crosslinked partially neutralized poly(acrylic acid).[3] For many applications, the important properties of a superabsorber are mainly the water absorption capacity and the strength. There are many different factors affecting these properties like basic polymer structure and its hydrophilicity, crosslink density, porosity, pore size, etc. Another important factor, common to all superabsorbers that restrict the water absorption capacity or rate of water absorption of superabsorbers is called "gel blocking" effect. This is due to the blocking of voids supplying liquid after some time of water absorption as the swollen particles can easily deform and glue together.[4,5]

Many efforts are made to improve the properties and performance of superabsorbers like by making particles more porous,[6,7] surface crosslinking is also applied to the particles giving them increased rigidity and absorbance capacity.[8] The combination of superabsorbent particles with nanofibers is another interesting variation since the nanofiber can serve as a substrate to separate and hold the particles besides providing large surface area and different pore sizes and improve mechanical strength. Smith and coworkers discussed the water absorption and mechanical properties of nanofibers with different amounts of superabsorber Waterlock particles[9] and the resulting nanomats are recommended for applications like wound care, drug delivery, and sanitary goods.

Keeping in view of our broad interest of developing new strategies and concepts for making use of polymeric nanomats for household use, an effort is made to make use of photoresponsive superabsorber particles for making fast water absorbing and desorbing nanomats for household cleaning purposes. Superabsorbers in general do not have only high water-absorbing capacity but also very high

F. Chen, A. Greiner, S. Agarwal
Philipps-University Marburg, Hans-Meerwein-Str., 35032 Marburg, Germany
E-mail: agarwal@staff.uni-marburg.de

DOI: 10.1002/mame.201000387

water-retaining capacity. For household cleaning purposes and many other applications making use of the same superabsorber nanomat for many times, it is desirable to have relatively fast water desorbing capacity of superabsorbing mats i.e., the requirement of a smart mat with high water absorbing and desorbing capacity. To the best of our knowledge there are no efforts in the literature in this direction. This work shows the proof-of-concept with formation and characterization of making responsive superabsorber nanomats. The composite nanomats of polymeric nanofibers and responsive superabsorbing particles are made by the technique of electrospinning. In the process of electrospinning,[10–13] a high electric field is applied to the droplet of a fluid (polymer solution or melt) coming out from the tip of a die, which acts as one of the electrodes and leads to the droplet deformation and finally to the ejection of an electrically charged jet from the tip of the cone accelerating toward the counter electrode leading to the formation of continuous fibers with diameters ranging from a few nanometers up to about 10 μm depending on the parameters and materials applied. These fibers form nonwovens with high porosities and high surface areas. Other advantages of this method are ease of processing, possibility of large scale production, easy functionalization, and availability of different variations of conventional electrospinning method like coaxial electrospinning, etc. Due to these unique properties, electrospun fiber would be favorable candidates for stabilizing photochromic superabsorbent particles to make superabsorbent nanofiber mats.

Two different substrates like polyurethane and polyamide were compared as matrix for making responsive superabsorbing nanomat composites with photochromic core/shell particles (photochromic superabsorbent polymers particles, PSAPs). The choice of substrate was based on their common hydrophilic nature but different elasticities. The maximum absorbency of superabsorbent nanomat composites in water, the absorption rate and the desorption rate, mechanical properties, and photoresponsive behavior are also reported.

Experimental Part

Materials

All the chemicals for synthesizing PSAP particles were purchased from Aldrich with the exception of 4,4′-azodianiline, which was purchased from Acros Organics. Reagents were purified using conventional literature methods. The surface crosslinker bis-(methacryloylamino)azobenzene (AC) was synthesized according to a procedure described previously.[14] The PSAP particles were synthesized following a method reported previously.[15] A total monomer concentration of 5 mol·L^{-1} [acrylic acid (AA) + acrylamide (AM)], an initiator (potassium persulfate) concentration of 1 wt.-% relative to total amount of monomers, a monomer molar ratio (AA/AM) of 4:1, a volume ratio of organic phase-(cyclohexane)/aqueous phase(water) of 2:1, a reaction temperature of 65 °C, and a reaction time of 2 h were used. Three different reactions were made using different amounts of crosslinker [bis(methacryloylamino)azobenzene] i.e., 5, 15, and 25 wt.-% with respect to the total monomers and the resulting particles are termed as PSAP1, PSAP2, and PSAP3, respectively.

The polyether-based thermoplastic polyurethane (TPU) block copolymer (Tecophilic SP-80A-150) was purchased from Thermedics, and polyamide 6 (PA6, Ultramid B24) was purchased from BASF company.

Preparation of Composite Polymeric Nanomats

A quantitative amount of TPU was added to dimethylformamide (DMF) and tetrahydrofuran (THF, 1:1) and subsequently stirred for 6 h at 60 °C and then cooled to room temperature to form 8 wt.-% homogeneous solutions. 20 wt.-% PA6 solution was made in $HCOOH/CH_3COOH$ (1:2). The next step was to suspend the PSAPs. Before mixing with TPU solution, the orange PSAPs were grounded and filtered through 100 mesh sieve (Sigma-Aldrich, 100 US standard testing sieve). The PSAPs particles in the respective polymer solutions (either TPU or PA) were suspended by mechanical stirring (100 rpm for 5 min) and electrospun. Various contents of PSAPs particles with respect to final fiber mats were prepared: 0, 8, 16, 32, and 50 wt.-%.

The electrospinning set-up was used as described previously.[16] A 0.65 mm diameter needle was used as an upper electrode where positive potential was provided by a high voltage power supply (0–30 kV). A counter electrode was placed 20 cm below the upper electrode. The negative potential was provided by a high voltage power supply (0–30 kV). A piece of Al foil was used as a collecting substrate. The flow rate of electrospinning of 1.2 mL·h^{-1} was controlled by a pump. Temperature and humidity in the electrospinning chamber were measured. Temperature was in the range 20–30 °C and humidity of 30–50%. During the electrospinning experiment all parameters were kept constant, except the PSAPs contents of electrospinning solution.

Characterization

0.08 g of dry sample was immersed in 250 mL distilled water for 24 h to attain equilibrium. After this time interval, the composite nanomat was collected, weighed, and used for water absorption and photoresponsive studies. The water absorption was calculated by taking the ratio of the mass of water absorbed as compared to the original nanomat. Since the composite nanomats have superabsorber particles physically entrapped in the polymer matrix, the particle residue test was conducted to determine the total amount of PSAPs particles lost from the nanofiber mats after it reached equilibrium absorption. Each sample taken from the fibrous mat was weighed and then was placed in a beaker with water and shaken in a Labquake shaker for 24 h. The sample was then removed, and the water from the beaker was transferred to an aluminum dish of known mass. The aluminum dish was placed in an oven until all of the water had evaporated. It was then weighed to determine the amount of residue that remained.

The morphology of composite nanofiber mats was evaluated using scanning electron microscopy (SEM, JSM-7500). Irradiation

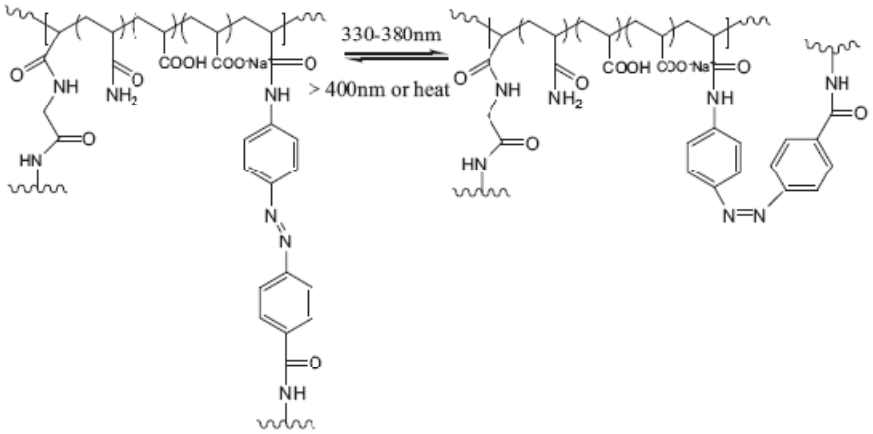

Scheme 1. Chemical structure of the photoresponsive superabsorber particles used for making superabsorber nanocomposites.

was carried out with spectrofluorophotometer (Shimadzu, RF-1502) with 350 nm wavelength. The mechanical strength of the fiber mats was measured in Zwick mechanical test machine (Zwick/Roell, type BT1-FRC.5TN.D14), the testing sample with dumbbell shape was cut from the fibrous mats, and the thickness of the fibrous mat was measured in three different positions by micrometer.

Results and Discussion

The photoresponsive superabsorber particles containing crosslinked hydrophilic core and hydrophobic azobenzene containing shell was used for making responsive polymeric nanomats. The chemical structure of the particles used in this work is given in Scheme 1 and the particles were synthesized by the known procedure.[15]

The well known trans-to-cis isomerization is known to change the distance between the 4 and 4′ carbons of the aromatic rings and thereby causes macroscopic volume change in the polymer on photo irradiation. This well known property has been combined with high porosity, toughness, and hydrophilicity of TPU nanofibers to produce photoresponsive superabsorber nanomats in this work. The photoresponsive particles of different AC crosslink density were made and water absorption capacity varied from about 138 (PSAP3) and 202 (PSAP2) to 220 (PSAP1) $g \cdot g^{-1}$. For

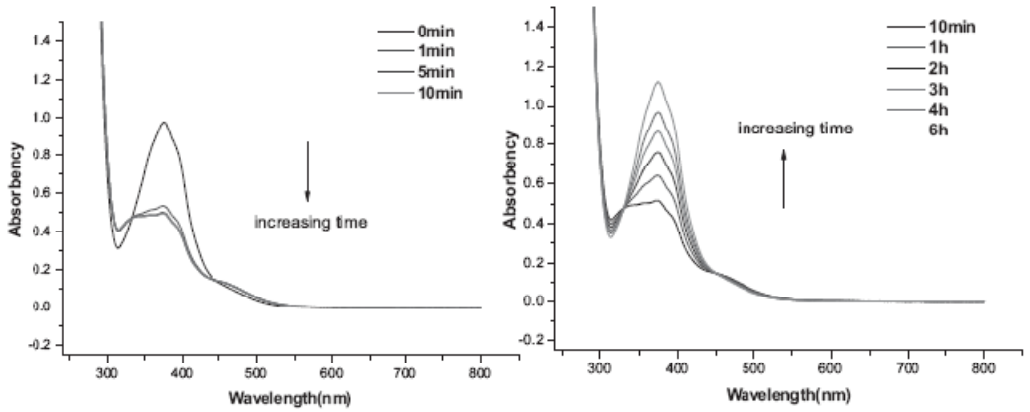

Figure 1. The absorption spectra of PSAPs in THF/water (30:70) irradiated at 350 nm (left) and cooling spectra of the irradiated PSAPs (right).

further experiments the particles with the highest water absorption capacity (PSAP1 with water absorbency of 220 $g \cdot g^{-1}$) were used.

Although the photoresponsive particles used in this work are already known and synthesized according to the procedure of Mudiyanselage and Neckers,[15] the photo induced isomerization was still investigated using the literature procedure before using them for composite formation. UV-Vis spectroscopy of the irradiated PSAP polymer (350 nm for time intervals of 0, 1, 5, and 10 min) and the cooling spectrum of the irradiated sample (for 30 min at 350 nm) for time intervals of 10 min and 1, 2, 3, 4, and 6 h are shown in Figure 1. The modulations of the absorption peak around 380 nm are due to the isomerization of the azo crosslinker in the polymer network (the UV-Vis spectra of AC crosslinker did not show here). Following storage in the dark, reappearance of the peak at 380 nm indicated that reverse isomerization of the azo crosslinker has taken place and this matched with the already reported results. These responsive particles were then used for making composite superabsorber nanomats.

Figure 2(A) shows the particle morphology and size. They have spherical shape with relatively broad size distribution, the diameter was around 50–100 μm. No attempts were made to get uniform size particles as this was not important for the present aim of the work. These particles were

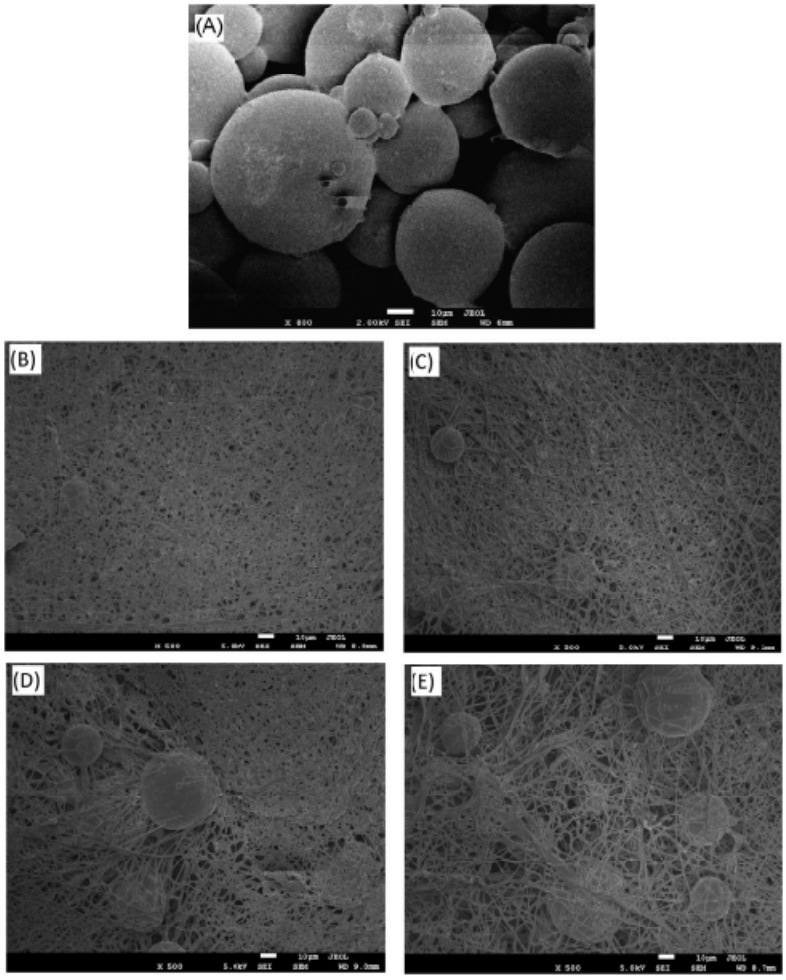

Figure 2. SEM images of (A) PSAP particles and (B) 8, (C)16, (D) 32, (E) 50% PSAPs in TPU nanofibers.

immobilized onto the hydrophilic TPU nanofibers by the process of electrospinning. The TPU polymer nanofiber served as a substrate for holding the particles and provided strength and elasticity to the hydrogel particles. Different amounts of particles were incorporated till about 50 wt.-% with respect to the matrix hydrophilic polyurethane. Electrospinning could not be performed for a composition with more than 50 wt.-% of the PSAPs because of frequent stoppage of the needle during electrospinning. The morphology of composite nanomats with different amounts of PSAP1 particles is shown in the Figure 2(B-E). Two important observations were made from these pictures: the particles were captured between the nanofibers of elastic TPU and they were separated and stabilized by nanofibers. The nanofiber diameter did not change much on changing the particles content in the composite, the average diameter of fiber is about 740 ± 35 nm, even with 50 wt.-% of particles in composite fiber. This morphology of particles trapped between the nanofibers could be very important to avoid "gel blocking" effect, a disadvantage in the conventional hydrogel particles.

The absorbency tests of nanomats were performed using water. Five samples of the PSAPs/TPU composite nanofiber were tested each time. Figure 3(A) shows a graph of the equilibrium absorbency of water containing 0–50 wt.-% PSAP1 particles at room temperature (around 22–23 °C). The absorption capacity increased with an increase in the amount of particles in the composite. The maximum absorbency capacity of water was 45 $g \cdot g^{-1}$ for composites with 50 wt.-% particles. Also, the composite superabsorbent nanomat had a much faster absorbency rate (60 s) to reach to equilibrium compared to the normal absorbent hydrogel particles (at least 5–10 min). The elastic characteristic of TPU fiber make it "capture" high amounts of particles separated by nanofibers and therefore allows all the absorbent particles to swell. The separation of particles by nanofibers in composites could prevent blocking of voids supplying liquid after some time of water absorption as swelling of individual particles in this case is not hindered by each other. Figure 4 shows the proposed model for fast absorbency rate of composite nanomats as compared to the normal gel materials which are subjected to "gel-blocking" effect as described above. The relatively hydrophobic outer shell made up of azo benzene containing crosslinker may have reduced the phenomenon of gel blocking by avoiding blocking of voids supplying liquid by preventing the deformation and sticking of particles together. This is only a supposition and could not be proven experimentally further.

To investigate the influence of substrate nanofiber on the water absorbency rate, PA6 nanomat with same amount of PSAPs particles was also prepared, the experiment showed that PA6/PSAPs composite nanofiber possessed fast absorbency rate as well because PA6 is a hydrophilic polymer, but the residue test showed after immersion in water for 24 h,

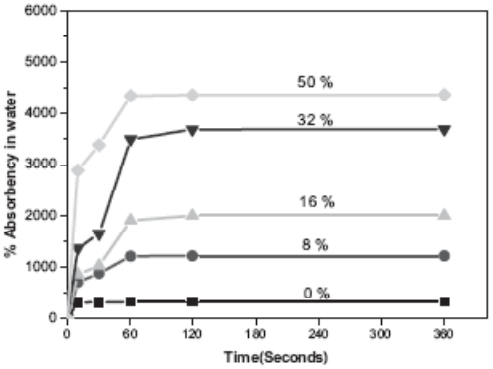

Figure 3. Rate of absorption of composite nanofiber with different contents of absorbent PSAP particles at room temperature in water.

most of PSAPs particles released from the fiber mats and the composite disintegrated. This shows the non-suitability of PA6 for such applications. While a very low residue of release free particles was seen in the case of TPU/PSAPs system (the residual percentage ranged from about 2 (for 8% particles in the mat) to about 7 wt.-% (for 50% particles in the mat). This was an acceptable amount of release of PSAPs particles from TPU nanofiber.

The absorbency test was repeated two more times on the same nanomat with about 50 wt.-% of PSAP particles and there was no loss in water absorbency. The loss of particles from nanomats after immersion in water for 24 h was about 7.2%. The loss of particles from the same mat after second and third immersion cycles in water were only slightly changed i.e., 10 and 12 wt.-%. This shows the stability and reusability of nanomats.

As discussed above, the TPU nanofiber served as a substrate for holding and stabilizing PSAPs particles in composite nanofiber, the mechanical properties were investigated with varied PSAPs particle contents (Figure 5). There was a decrease in the tensile strength of composites as compared to the matrix TPU nanomat and this decrease was more with increased amount of the particles. Interestingly the composites showed increased elongations at break as compared to TPU. The elongation at break showed a maxima with increase in the amount of particles and after that it decreased. This shows that at low contents (up to ≈16 wt.-%), the PSAP1 particles acted as a kind of crosslinker between the TPU nanofibers in composites and for high contents assumed the role of a mere filler. The composites with about 16 and 32 wt.-% of superabsorber particles, therefore, showed optimized properties in terms of stability in water (less disintegration, as determined by residue test), mechanical properties, and water absorbency.

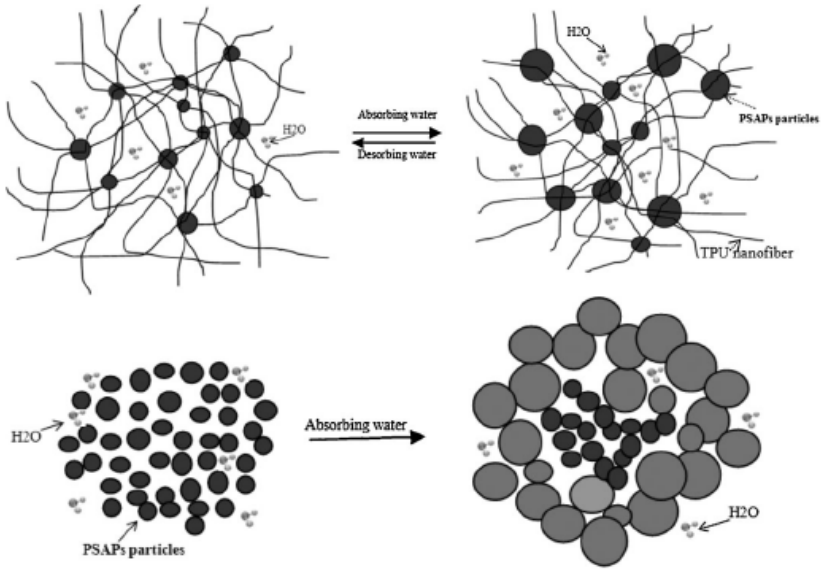

Figure 4. Schematic picture to explain the fast absorbency of the nanomat composites (up) and the "gel effect" for the normal absorbent polymer particles (bottom).

To further understand the absorbency properties of the composite TPU/PSAPs nanofiber, two series of composite fibers with 16 and 32 wt.-% PSAP particles were investigated at different temperatures in water (at room temperature, 50 and 80 °C) with different immersion times. Figure 6 and 7 show the composite nanofiber takes shorter time to reach to maximum absorbency when immersed in hot water (80 °C) compared to at room temperature, but the final absorbency is almost same after immersion for 24 h in hot water and cold water. This probably due to the diffusion of water molecules is much more intense in hot water which allow water molecules to flow freely to the particles for absorption, but for a long period, the water molecules finally penetrated into the network of composite nanofiber and reach to maximum absorbency.

For studying the photoresponsivity of the composite nanomats, weight loss of the equilibrated composites with water on irradiation at 350 nm was determined at 30 min

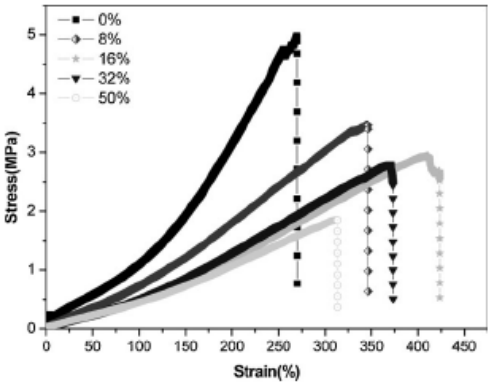

Figure 5. Stress/strain curve of the composite nanofiber mats with different contents of PSAP particles.

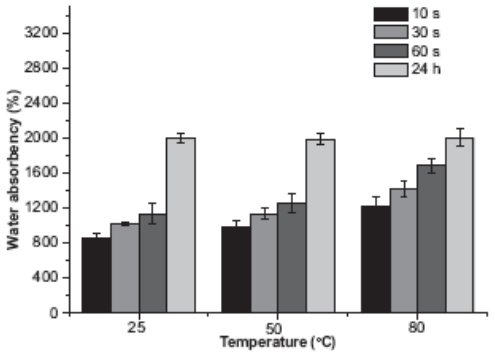

Figure 6. Rate of absorption of TPU/PSAP composite nanofiber with 16% PSAPs particles in water with different temperature.

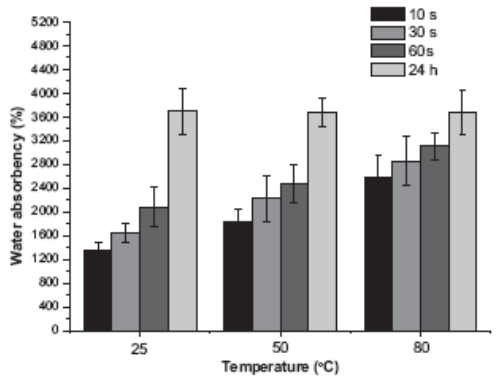

Figure 7. Rate of absorption of TPU/PSAP composite nanofiber with 32% PSAPs particles in water with different temperature.

time intervals (Figure 8). Two samples were prepared for weight loss test, a small amount of water loss could be observed even with no irradiation of the sample. This could probably because of some draining water trapped among the PSAPs particles. Irradiation of the samples made with TPU/PSAPs composite fiber showed higher weight loss due to the water expulsion from the PSAPs particles by isomerization of the crosslinker AC.

Conclusion

This work shows the success of making photoresponsive superabsorber nanomats. The properties of nanocomposites were highly dependent upon the amount of the superabsorber photochromic particles added. The maximum water absorption capacity obtained was about 4 000%. Also, the rate of water absorption was faster than the conventional particles. The substrate polymer in the composites also played an important role. The elastic polyurethanes were more suitable than polyamide and provided stable composites. Such nanocomposites could be of utility not only for house hold cleaning purposes but could be utilized for drug release or sensor applications. Although the desorption rate of water could be accelerated using light in the present study and is already a step forward in making a responsive superabsorber composite but further studies are required in terms of optimization of much faster desorption rate of water in the time scale of minutes rather than hours. They are in progress in our laboratory.

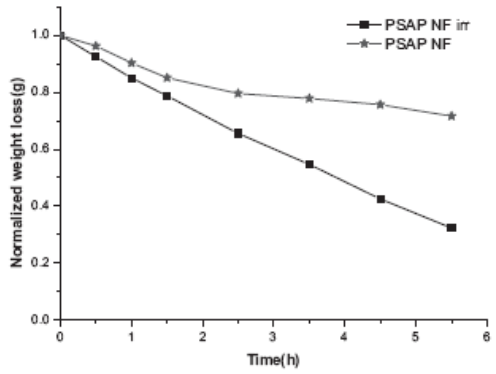

Figure 8. Weight loss of TPU/PSAP composite nanofiber with 32% of PSAPs particles on irradiation ("irr" means irradiation).

Acknowledgements: We would like to thank *Bundesministerium für Bildung und Forschun (BMBF)* (FKZ: 13N9877) for the financial support.

Received: October 28, 2010; Revised: December 12, 2010; Published online: DOI: 10.1002/mame.201000387

Keywords: composites; electrospinning; morphology; photoresponsivity; superabsorbers

[1] M. J. Zohuriaan-Mehr, K. Kabiri, *Iranian Polym. J.* 2008, *17*, 451.
[2] K. Kabiri, M. J. Zohuriaan-Mehr, *Polym. Adv. Technol.* 2003, *14*, 438.
[3] U. Dayal, S. K. Mehta, M. S. Choudhray, R. Jain, *J. Macromol. Sci. Rev. Macromol. Chem. Phys.* 1999, *C39*, 507.
[4] H. Wack, M. Ulbricht, *Proceedings of the First International Conference on Self Healing Materials*, 18–20 April 2007, The Netherlands.
[5] S. Kiatkamjornwong, *ScienceAsia* 2007, *33* (Suppl 1), 39.
[6] J. P. Zhang, L. Wang, A. Q. Wang, *Macromol. Mater. Eng.* 2006, *291*, 612.
[7] M. Antonietti, R. A. Caruso, C. G. Goltner, M. C. Weissenberger, *Macromolecules* 1999, *32*, 1383.
[8] B. Kusuktham, *J. Appl. Polym. Sci.* 2006, *102*, 1585.
[9] L. M. Hansen, D. J. Smith, D. H. Reneker, W. Kataphinan, *J. Appl. Polym. Sci.* 2005, *95*, 427.
[10] S. Agarwal, J. H. Wendorff, A. Greiner, *Chemie Ingenieur Technik* 2008, *80*, 1671.
[11] S. Agarwal, J. H. Wendorff, A. Greiner, *Polymer* 2008, *49*, 5603.
[12] S. Agarwal, A. Greiner, J. H. Wendorff, *Adv. Funct. Mater.* 2009, *19*, 2863.
[13] S. Agarwal, J. H. Wendorff, A. Greiner, *Adv. Mater.* 2009, *21*, 3343.
[14] H. Brondsted, J. Kopecek, *Biomaterials* 1991, *12*, 584.
[15] T. K. Mudiyanselage, D. C. Neckers, *Soft Matter* 2008, *4*, 768.
[16] M. Bognitzki, H. Hou, M. Ishaque, T. Frese, M. Hellwig, C. Schwarte, A. Schaper, J. H. Wendorff, A. Greiner, *Adv. Mater.* 2000, *12*, 637.

8.2 Manuscript "Multifunctional Polyurethane Aqueous Dispersions showing Thermo Responsivity with UCST and Antibacterial Properties"

Fei Chen, Judith Hehl, Yu Su, Claudia Mattheis, Seema Agarwal*, Multifunctional Polyurethane Aqueous Dispersions showing Thermo Responsivity with UCST and Antibacterial Properties, *Journal of Colloid and Interface Science*. **2011**, Submitted.

Multifunctional Polyurethane aqueous Dispersions showing Thermo Responsivity with UCST and Antibacterial Properties

Fei Chen, Judith Hehl, Yu Su, Claudia Mattheis, Seema Agarwal*

Philipps-Universität Marburg, Department of Chemistry and Scientific Center for Materials Science

Hans-Meerwein Strasse, D-35032, Marburg, Germany

*seema@chemie.uni-marburg.de

Abstract: Cationic segmented polyurethane dispersions with UCST behavior and antibacterial properties are highlighted in this article. The base polyurethanes were prepared by polyaddition reaction followed by quaternisation with methyl iodide. Aqueous dispersions were made by simple heating at high temperature and slow cooling. No additional emulsifiers / stabilizers or special procedures were required to obtain aqueous stable dispersions of solid contents of up to 10% wt/wt. The dispersions depending upon their composition showed high efficiency and fast time of action as antibacterial material. Particle size and UCST strongly depended on the solid content of the dispersions and the content of PEG segments in the copolymers. Such novel UCST, antibacterial dispersions have a big potential to be used for drug encapsulation and controlled release for various therapeutic applications besides general use as water stable coating at room temperature.

Keywords: polyurethane, antibacterial, dispersion, UCST

Introduction

Aqueous polyurethane dispersions are known since the late 1960s and have attracted both academia and the industry. The conventional PUs is water insoluble and requires strong shear forces and external emulsifiers for making water dispersion[1]. In the last few years modified PUs were made with an aim to provide self-dispersibility under mild conditions. This could be done by either introducing hydrophilic segments or ionic moieties in PU structure. For example, the introduction of a small amount of ionic charges into polyurethanes combine the properties of the parent polymers with those derived from the existence of ionic structures in the backbone, offering a big potential to form aqueous dispersions for different applications such as coating and hygiene products[2-4]. Different types of PUs depending on the nature of the charge (positive, negative or both) placed within the polymeric backbone, pendant or at the end of PU chains are already known [5-9]. The particle size of the dispersion is dependent to a large extent on the concentration of ionic groups[10]. Cationic PU dispersions show very high adhesion to various ionic substrates, especially anionic substrates such as leather and glass[11]. Also, besides the important application of cationic dispersions in synthetic leather industry, it has been reported that various polycations possess antibacterial properties in solution, presumably by interacting with and disrupting bacterial cell membranes[12]; due to this very general mode of action, these compounds can be used to kill a wide range of bacteria and the activity can potentially be recovered by removal of dead cells from the polymer surface[13].

The synthesis of PU dispersions is mainly carried out by stirring a solution of PU in organic solvent like acetone and methyl ethyl ketone with water i.e. solvent displacement method [14, 15]. Other highly used methods are: prepolymer mixing process and melt dispersion process. Landfester et al. showed the use of miniemulsion polymerizatiuon for making PU dispersions with diameters of about 200 nm[16].

The common drawback of these methods is that normally emulsifier is needed to stabilize the dispersion, or in the raw material stage of cationic polyurethane synthesis,

volatile organic solvents are necessary in the preparation and dissolution of prepolymers. Organic solvents are harmful for many reasons such as toxicity and flammability, and thereby cause severe concern in production with respect to environmental and safety issues. On the other hand, the hydrophilic modification of PUs for making it suitable as self-emulsifier leads to poor water resistance. This can be overcome by hydrophobic modifications or cross-linking of PU chains, but both of these strategies are time consuming and complicated synthetic route need to be adopted[17, 18].

Compared to hydrophobic modification or cross-linking of PU chains, employment of UCST (upper critical solution temperature) behavior would be another choice to improve the water resistance. The dissolved polymer chains undergo a change in conformation from coil to globule with temperature and thus undergo phase separation. Moreover such smart dispersions are always desirable for controlled release applications. Polymers exhibiting a sharp and reproducible change in physical properties upon a small change in the environment, e.g. temperature, ionic strength, pH, mechanical stimuli are classified as stimuli-responsive or also "smart" polymers[19]. A class of very prominent stimuli-responsive polymers are thermoresponsive polymers including the well-investigated and well-known poly(*N,N*-isopropylacrylamide) (PNiPAAm)[20]. Above 33 °C an aqueous solution of PNiPAAm shows a so called LCST behavior (lower critical solution temperature), i.e. phase separation[21]. UCST behavior (upper critical solution temperature) is much less well-known for polymeric materials than LCST. Only few examples can be found in literature [22-28]. Inverse emulsion polymerization of acrylamide and acrylic acid was used for making UCST microgels by Mijangos et al [29].

Here we report for the first time (to the best of our knowledge) a stable dispersion showing UCST based on the cationic polyurethanes. The proper choice of the alkylating group for quaternization and the use of poly(ethylene oxide) segments led to the self emulsification of cationic PUs. This facilitated the formation of a stable

dispersion without the use of external stabiliying agent. The facile preparation of cationic PU dispersions, the influence of copolymer composition on the dispersion formation and stability, antibacterial activity and UCST is reported here. The antibacterial nature of smart UCST dispersion could be promising for use in water stable coatings etc.

Experimental

Materials

2,4-toluenediisocyanate (TDI, Sigma-Aldrich, 95%) and diethanol-*N*-methylamine (DEMA, Acros, 99%+) were distilled under vacuum and stored under argon. 1,4-diazabicyclo[2.2.2]octane (DABCO, Sigma-Aldrich, 98%) was recrystallized from cyclohexane and stored under argon. Polyethylene glycol (PEG 2000) (Merck) was purified by dissolving in dichloromethane, precipitating in diethyl ether and drying in a vacuum oven. Tetrahydrofuran (THF, BASF, techn.) was pre-dried by distillation over potassium hydroxide, then dried over phosphorous pentoxide, distilled and stored under argon. Cyclohexane (BASF, techn.), hexane (BASF, techn.), methanol (BASF, techn.) and *N,N*-dimethyl formamide (DMF, BASF, techn.) were purified by distillation. Phosphorus pentoxide (Riedel-de Haën, 98.5 %), potassium hydroxide (Sigma-Aldrich, techn.), methyl iodide (Sigma-Aldrich, 99%), were used as received.

Characterization

Methods

The molecular weights and molecular weight distributions of the polymers (c = 1 g/L) were determined by size exclusion chromatography (SEC) using a PSS GRAM linear 50 mm · 8 mm column (10 µm) and two PSS GRAM linear 600 mm · 8 mm columns (100 Å and 3000 Å, respectively) at 25 °C and a refractive index detector (Knauer), using DMF or LiBr/DMF (5 g/L) as eluent at a flow rate of 1 mL/min. Polystyrene

standards were used for calibration with toluene as internal standard. The WinGPC Unity (5403) Software (PSS) was used for data recording and interpretation.

^{1}H and ^{13}C NMR spectra were recorded on Bruker Avance 300 A and Bruker DRX 500 spectrometers respectively, using deuterated dimethylsulfoxide (d_6-DMSO) as solvent. Topspin 3.0.b.7 (Bruker) was used for data interpretation. For calibration the residual signal of the deuterated DMSO was set to $\delta = 2.50$ ppm (^{1}H NMR) and $\delta = 39.5$ ppm (^{13}C NMR).

FTIR spectra were recorded on a Digilab Excalibur Series system using a Pike Miracle attenuated total reflection (ATR) unit. The samples were measured in powdered state without further preparation necessary. The Win-IR Pro 3.3 software (Digilab) was used for data recording and interpretation.

The particle size and morphology were characterized by scanning electron microscopy using a field emission scanning electron microscope JSM-7500F (JEOL) at acceleration voltages of 2-5 kV equipped with an ALTO-2500 LN_2-Cryo-transfer system (Gatan) and a YAG-BSE detector (Autrata) aso by Delsa™ Nano C particle analyzer.

UCST behavior of the dispersion was characterized by turbidity measurements using a TP1-D turbidity photometer from TEPPER-Analytic. The measurements were performed at a wavelength of 670 nm and a heating and cooling rate of 1°C/min in a temperature range from 90°C to 60°C. The cyclic temperature program was repeated 2 times. Measurements were carried out at constant stirring in a glass cuvette of 10 mm path length.

General synthesis of base polymer (PU-0)

A dry three-necked round bottom flask equipped with a dropping funnel and argon inlet was charged with TDI (71.17 g, 408.7 mmol, 1eq) and THF (500 ml). The resulting solution was cooled down to -50 °C by a dry-ice/isopropanol mixture. A solution of DEMA (48.7 g, 408.6 mmol, 0.99 eq) in THF (300 ml) was transferred

into the dropping funnel and added dropwise to the TDI solution at -50 °C. The DABCO catalyst (2.290 g, 20.42 mmol, 0.05 eq) was added to the reaction mixture which was subsequently warmed to room temperature and then 50 °C. After 3.5 h the polyaddition was stopped by cooling to room temperature and addition of methanol (50 ml). The polymer P(TDI-DEMA) (PU-0) was precipitated from hexane (6 l). Yield: 117 g (98%), $T_{5\%}$ = 220 °C. T_g = 77 °C, M_p = 30500 Da, ^{1}H-NMR (500 MHz, *d*$_6$-DMSO), δ/ppm: 9.57 (s, 1H, N8$_a$H), 8.82 (s, 1H, N8$_b$H), 7.51 (s, 1H, C3H), 7.17 (d, 1H, C5H, *J* = 8 Hz), 7.06 (d, 1H, C6H, *J* = 8.5 Hz), 4.14 (s, 4H, C10$_{a/b}$H$_2$), 2.68 (s, 4H, C11$_{a/b}$H$_2$), 2.30 (s, 3H, C12H$_3$), 2.11 (s, 3H, C7H$_3$). ^{13}C-NMR (125 MHz, *d*$_6$-DMSO), δ/ppm: 154.1 (C9$_{a/b}$=O), 153.7 (C9$_{a/b}$=O), 137.3 (C4H), 136.7 (C2H), 129.8 (C6H), 126.4 (C1H), 115.5 (C3H und C5H), 62.3 (C10$_{a/b}$H$_2$), 61.4 (C10$_{a/b}$H$_2$), 56.0 (C11$_{a/b}$H$_2$), 42.3 (C12H$_3$), 17.2 (C7H$_3$). FTIR (ATR), ν/cm^{-1}: 3298*w* (ν-NHCOO-), 2963*w*, 2804*w*, 1701*s* (ν(C=O), Amide-I), 1601*m*, 1531*s* (Amide-II), 1450*m*, 1223*s*, 1049*s*, 880*w*, 768*m* (Amide-V), 567*w*.

General synthesis of quaternized polymer (QPU-0)

P(TDI-DEMA) (15.03 g, 0.051 mol, 1.00 eq) was dissolved in DMF (300 ml) and the methyl iodide (6.5 ml, 0.104 mol, 2.03 eq) added. The reaction mixture was stirred at 70 °C for 48 h. The fully quaternized polymer QPU-0 was precipitated from THF (4.5 l). For further purification the crude, yellow product was extracted with THF (1.5 l) for 48 h. The product was obtained as white powder. Yield: 22g (99%) , $T_{5\%}$ = 217 °C, T_g = 165 °C, M_p = 10446 Da, ^{1}H-NMR (300 MHz, *d*$_6$-DMSO), δ/ppm: 9.72 (s, 1H, N8$_a$H), 9.01 (s, 1H, N8$_b$H), 7.57 (s, 1H, C3H), 7.21 (d, 1H, *J* = 8.5 Hz, C5H), 7.13 (d, 1H, *J* = 8.9 Hz, C6H), 4.55 (s, 4H, C10$_{a/b}$H$_2$), 3.81 (s, 4H, C11$_{a/b}$H$_2$), 3.24 (s, 6H, C12H$_3$ und C13H$_3$), 2.15 (s, 3H, C7H$_3$). ^{13}C-NMR (76 MHz, *d*$_6$-DMSO), δ/ppm: 153.3 (C9$_{a/b}$=O), 152.5 (C9$_{a/b}$=O), 136.7 (C4H), 136.0 (C2H), 130.5 (C6H), 126.2 (C1H), 115.1 (C3H und C5H), 63.0 (C10$_{a/b}$H$_2$), 57.8 (C11$_{a/b}$H$_2$), 51.5 (C12H$_3$, C13H$_3$), 17.1 (C7H$_3$). FTIR (ATR), ν/cm^{-1}: 3300*w* (ν-NHCOO-), 2884*m*, 1705*s*

(ν(C=O), Amide-I), 1602*m*, 1529*s* (Amide-II), 1450*m*, 1223*s*, 1056*s*, 878*w*, 762*m* (Amide-V).

General synthesis of co-polyurethane (PU-X)

The typical procedure for synthesis of co-polyurethane (PU-3) with 3 mol% of PEG2000 in the copolymer was described here. A dry three-necked round bottom flask equipped with a dropping funnel and argon inlet was charged with TDI (2.25 mL, 15.76 mmol, 1.00 eq) and THF (32 mL). The resulting solution was cooled down to -50 °C by a dry-ice/isopropanol mixture. A solution of DEMA (1.82 g, 15.27 mmol, 0.97 eq) in THF (300 mL) was transferred into the dropping funnel and added dropwise to the TDI solution at -50 °C. The DABCO catalyst (0.092 g, 0.79 mmol, 0.05 eq) and PEG 2000 (0.95g, 0.47 mmol, 0.03 eq) was added to the reaction mixture which was subsequently warmed to room temperature and then 50 °C. After 3.5 h the polyaddition was stopped by cooling to room temperature and addition of methanol (50 mL). The polymer PU-3 was precipitated from hexane, the product was heated at 45 °C under vacuum for two days.

General synthesis of quaternized polymer (QPU-X)

PU-3 (0.60g, mol, 1.00 eq) was dissolved in DMF (10 mL) and the methyl iodide (0.3 mL, mol, 2.03 eq) was added dropwise to the mixture. The reaction mixture was stirred at 70 °C for 48 h. The fully quaternized polymer QPU-3 was precipitated from THF (500 ml). For further purification, the crude yellow product was extracted with THF (1.0 l) for 48 h. The product was obtained as white powder. Yield: 22g (99%). Base homo-polyurethane and quaternized polyurethane were denoted as PU-0 and QPU-0, co-polyurethane and quaternized co-polyurethane were named as PU-X and QPU-X, with X referring to the molar ratio of PEG2000 in the copolymers.

Microbiological testing

By inoculation of a TSB (tryptic soy broth, Sigma Aldrich, aqueous solution c = 30 g/l) solution with a single colony of *E. coli* (DSM No. 1077, K12 strain 343/113),

incubation with shaking at 37 °C until the optical density at 578 nm had increased by 0.125 and dilution 1:99 with sterile liquid broth the *E. coli* inoculum was prepared. The exact cell density was determined by spreading serial tenfold dilution on nutrient agar plates, incubation for 24 h at 37 °C and colony counting.

The antibacterial activity of biocides is characterized by the minimum inhibition concentration (MIC), that is defined as the minimum amount of a substance which is required to inhibit bacteria growth, as well as the minimum bactericidal concentration (MBC), that gives the minimal concentration of a substance that kills 99.9% of the bacteria (4 log stages). For the determination of the MIC, a geometric dilution series of 1 % wt/wt dispersions in TSB was inoculated with an *E. coli* inoculum in a sterile 24 well plate and incubated for 24 h at 37 °C. The wells were visually evaluated for bacteria growth; the lowest dilution stage which did not show bacteria growth, i. e. did not become turbid, was taken as MIC; each test was done in duplicate. To determine the MBC, 100 µl of the dispersions which remained clear were spread on nutrient agar plates and incubated at 37 °C for 24 h. The lowest dilution stage which did not lead to colony formation was defined as MBC. The time-depending antibacterial activity was determined by spreading 100 µl specimens of the MIC dispersions after given time intervals on nutrient agar plates. After incubation at 37 °C for 24 h the colonies were counted; the reduction was calculated respective to the inoculum.

Results and Discussion

Quaternized polyuretnanes based on 2,4-toluenediisocyanate (TDI) and diethanol-*N*-methylamine (DEMA) were used for making functional dispersions. The polyurethanes were made by polyaddition reaction and were quaternized using methyl iodide (Scheme 1) by a simple S_N2 reaction. By using the low molecular weight DEMA which included the desired quaternizable amine unit as diol, a maximum amount of ionic groups in the final polymer could be facilitated. The resulting PUs were characterized using NMR and IR spectroscopy. To ensure full quaternisation excess alkylation agent and long reaction times were employed.

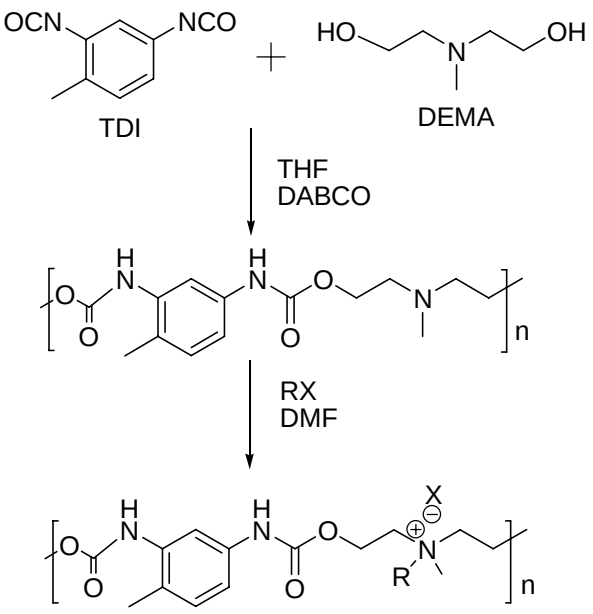

Scheme 1: Synthesis of the base polymer PU-0 and quaternized QPU-0 from 2,4-toluene diisocyanate (TDI) and diethanol-*N*-methylamine (DEMA).

The quaternized PU (QPU-0) showed upper-critical solution-temperature (UCST) behavior. The polymer was not soluble in water at room temperature but showed solubility in water on heating depending upon the polymer concentration at a very high temperature (98 °C). A polymer concentration of less than or equal to 5 wt% led to a clear solution of PUs in water at about 98 °C. The simple cooling of this solution to room temperature (20 °C) without stirring yielded opaque dispersions. The

dispersion was characterized by dynamic light scattering (DLS) and showed average particle size of about 130 nm. UCST was determined by turbidity measurements and found to be about 80^{o}C. Above this temperature the polymer made a clear solution and below it made a stable dispersion. The process was completely reversible. This process of using UCST behavior to obtain secondary dispersions is much easier compared to classic processes, e.g. the solvent displacement method[30]. In this process the material is dissolved in an organic water-miscible solvent of low boiling point and water added to the solution. The organic solvent is then subsequently evaporated from the dispersion[31]. Other means to produce secondary dispersions often employ special mixing techniques, e.g. sonification, high speed stirring or homogenization[32]. Typical procedures also often use additives, e.g. surfactants, to facilitate secondary dispersions. The dispersions made in this work using UCST behavior are surfactant free which is desirable for many different biomedical and agricultural applications. To further increase the solid content of the dispersion, we designed segmented PUs with PEG (polyethylene glycol) segments with increased hydrophilicity (Scheme 2).

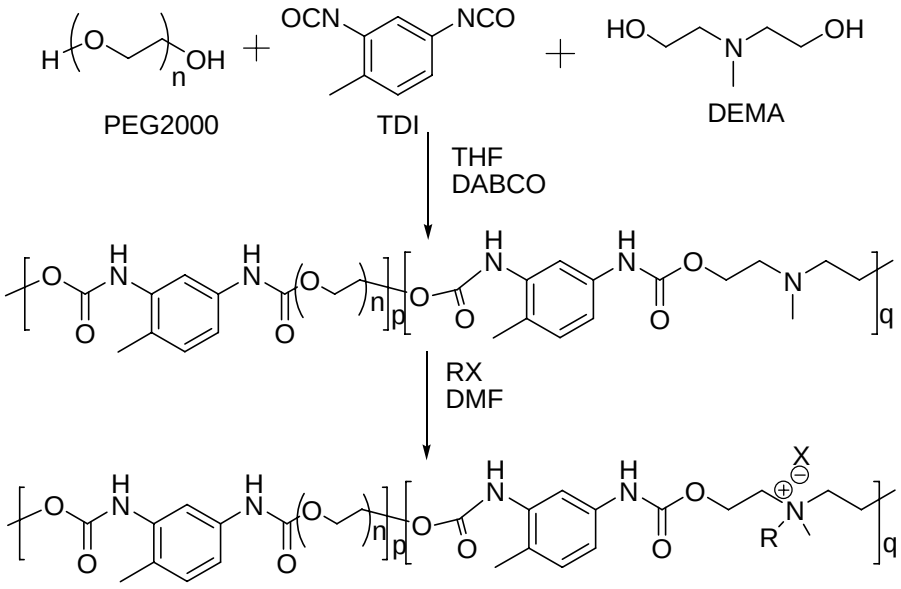

Scheme 2: Synthesis route of the base copolymer PU-X and quaternized co-polyurethanes QPU-X

The synthesis of the segmented block co-polyurethanes PU-X was accomplished by the same method as described above for PU-0 in **Scheme 2**. Compared with the homo-polyurethane PU-0 synthesis, additionally a PEG polyol with a number average molecular weight of 2000 g/mol was employed. By varying the ratio between DEMA and PEG2000, a series of segmented block co-polyurethanes were synthesized with PEG ranging from 0-10 mol%. The base copolymers PU-X were characterized by nuclear magnetic resonance (NMR), infrared spectroscopy (IR), size exclusion chromatography (SEC) and differential scanning calorimetry (DSC). **Figure 1** shows the ^{1}H-NMR spectrum of PU-X with 10 mol % PEG in the copolymer, as an example. A peak at 3.51ppm, which is assigned to CH_2 groups from PEG was observed which showed the successful incorporation of PEG in PUs. The copolymer composition was determined using the peak integrations of CH_2 protons of PEG (3.51 ppm) and -NCH_3 protons (2.3 ppm) of DEMA. In NMR, no signs of urea linkages, only urethane linkages were observed in the copolymers.

To introduce quaternary ammonium moieties into the copolymer, the tertiary amine groups were quaternized with methyl iodide according to **Scheme 2**. Again, excess methyl iodide and long reaction times (48 h) were employed to insure full quaternization for the whole series of copolyurethanes. **Figure 2** shows the ^{1}H-NMR spectrum of the copolymer QPU-X with 10 mol % of PEG. A significant shift of the protons 10a/b, 11a/b close to the quaternized nitrogen atom could be observed. No peaks were present at the original positions, thereby showing compelte quaternization. The weight average molecular weight of the copolyurethanes as determined by gel permeation chromatography in DMF with LiBr was about 22,600 but with broad polydispersity.

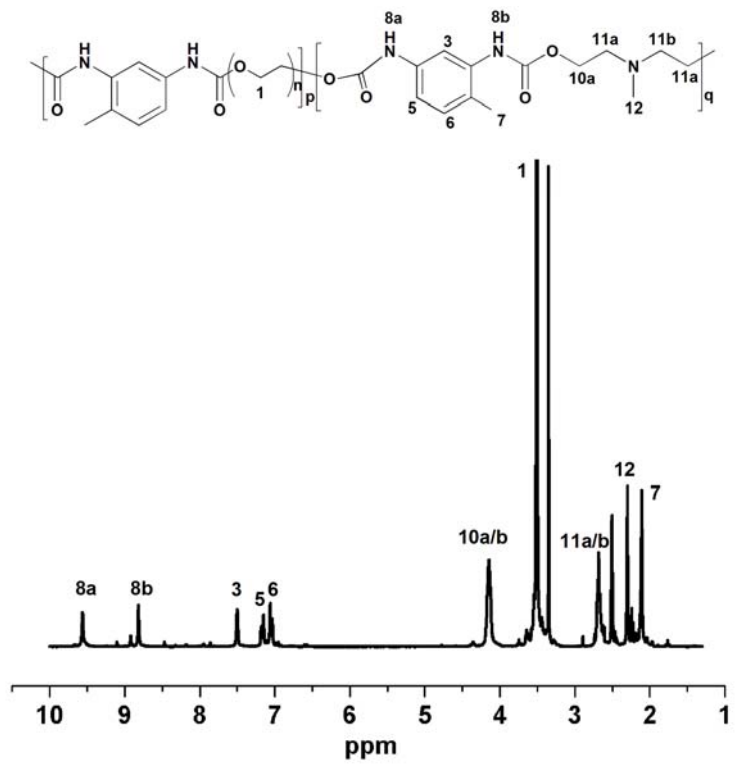

Figure 1: ^{1}H-NMR of PU-10 in d_6-DMSO.

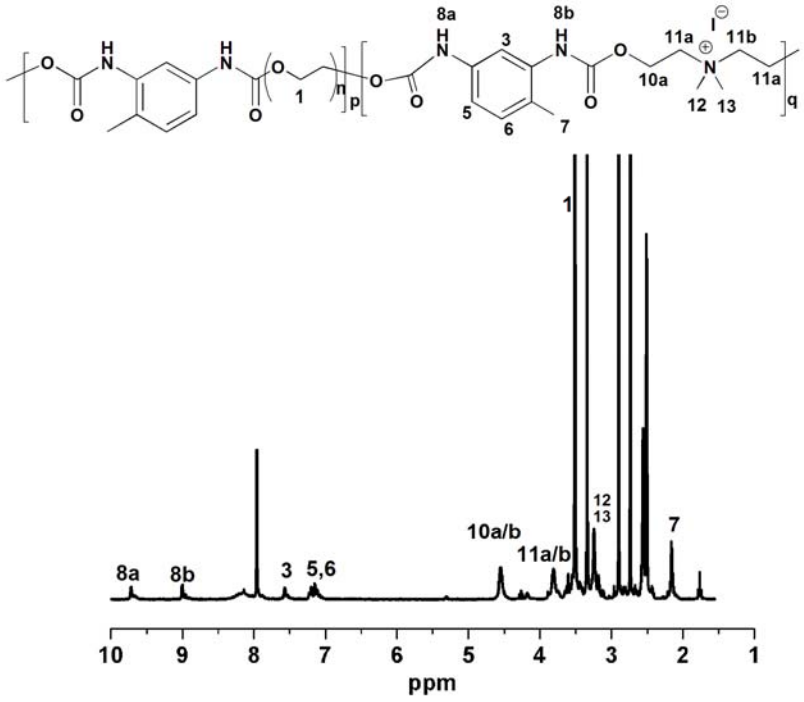

Figure 2: ^{1}H-NMR of QPU-10 in d_6-DMSO.

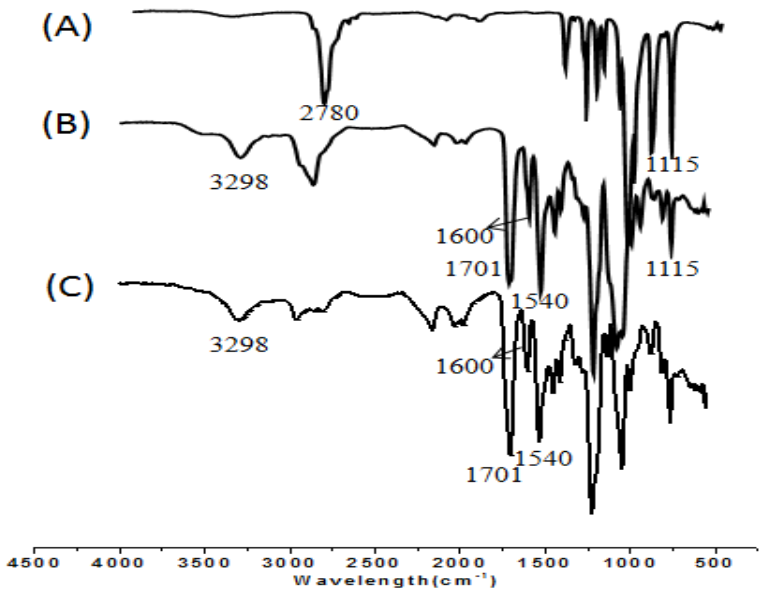

Figure 3 FT-IR spectra of (A) PEG 2000, (B) PU-10 and (C) PU-0.

Representative FT-IR spectra of PEG 2000, co-polyurethane and homo-polyurethane are shown in **Figure 3**. The spectra showed characteristic bands of urethane >NH at 3298 cm^{-1} and >C=O stretching of urethane linkage at 1701 cm^{-1}. The symmetric and asymmetric stretching of CH_2 and C-O-C stretching vibration at 1115 cm^{-1} of PEG was observed between 3000 and 2750 cm^{-1}. The aromatic >C=C< band of TDI was observed around 1600 cm^{-1}. The band at 1540 cm^{-1} is due to the C-N stretching and NH deformation. When the block copolymers were converted to their cationomers, the tertiary nitrogen atoms were converted to quaternary ammonium groups, which gave rise to peaks around 980–930 cm^{-1}, characteristic for aliphatic quaternary ammonium salts, see **Figure 4.**

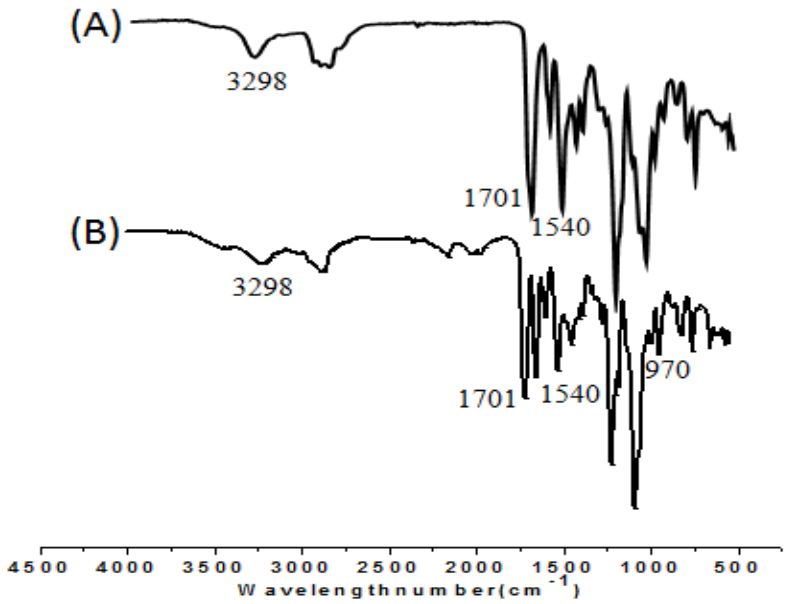

Figure 4. FT-IR spectra of PU-5 (A) before and (B) after quaternization with CH_3I.

It was interesting to investigate the influence of PEG on the solubility and stability of the dispersions compared with the quaternized homo-polyurethanes. Results indicated that the solubility of the copolymers increased with increase in the content of PEG in the copolymers (**Table 1**). When the content of PEG in the copolymers increased to 10 mol% (QPU-10), the copolymers could not form stable dispersions anymore. This is due to the high hydrophilicity of the copolymer and therefore remained in solution. Therefore, an optimum amount of PEG (about 5 wt %) was required in co-polyurethanes to make stable dispersions with high solid contents. The decrease in amount of PEG led to decreased solid content and an increase in its amount in co-polyurethanes led to disappearance of the UCST behavior.

Table 1: Dispersion experiments with the cationic polyurethanes.

+: soluble -: insoluble *: dispersion & gel like precipitate

QPU-X	**C(PU) /% wt/wt**	**Solubility**	**Dispersion**
QPU-0	≤5	+	*
	10	-	
QPU-1	>1≤8	+	*
QPU-3	>1≤10	+	*
QPU-5	>1≤12	+	*[a]
QPU-10	>1≤20	+	solution

a: quaternized co-polyurethane(QPU-5) could form dispersion only above 5wt%.

The dispersions were characterized by dynamic light scattering (DLS) and turbidity photometry. Particle sizes were determined as a function of the PEG content and concentration of the aqueous dispersions of quaternized co-polyurethanes by DLS (Table 2). An increase in particle size was observed with increasing dispersion concentration, for example, the particle size increased from 70 nm at 1wt % to around 1000 nm at 8 wt % for QPU-1 (Figure 5). This could be due to the repulsion between the ionic moieties.

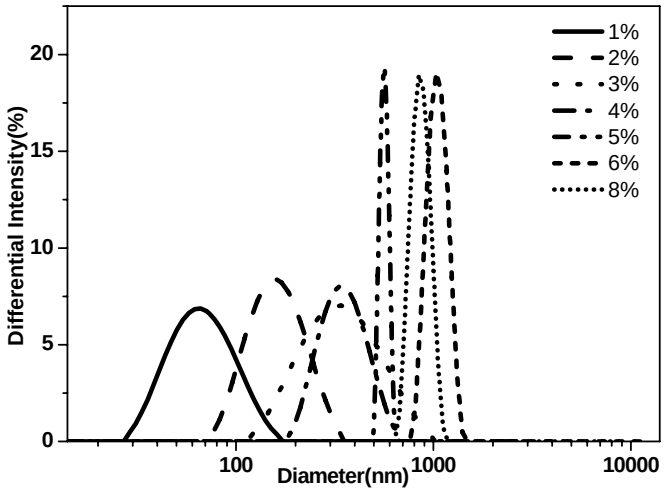

Figure 5. Effect of dispersion concentration for QPU-1 on Particle size.

The particles size measurement by DLS was also done for the same concentration of co-polyurethane with different PEG ratios. **Figure 6** showed that there is no big difference of particle size among all the samples, the only change was that by increasing the PEG content in the copolymer, the particle size distribution decreased but the particle size kept constant around 80 nm.

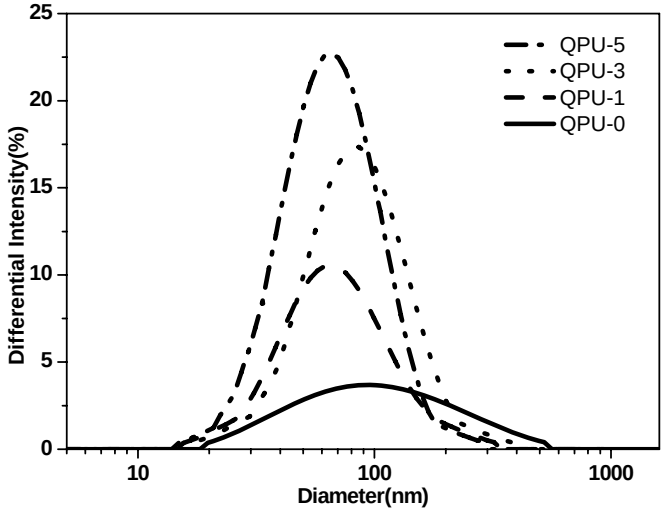

Figure 6. Effect of PEG (QPU-0, QPU-1, QPU-3 and QPU-5) content on particle size.

Table 2 Particles size of quaternized PU dispersions as measured by dynamic light scattering

QPU	Diameter /nm	QPU	Diameter /nm
1% QPU-0	128±97	1% QPU-1	71±26
1% QPU-1	71±26	2% QPU-1	167±53
1% QPU-3	100±35	3% QPU-1	369±164
1% QPU-5	136±58	4% QPU-1	358±94
		5% QPU-1	563±28
		6% QPU-1	1054±122
		8% QPU-1	863±93

The particle shape was characterized by scanning electron microscopy. **Figure 7** shows the morphology of 1 wt% of quaternized QPU-0 and QPU-1. Without dilution, the particles form a film; the diluted samples possessed almost spherical shape with some particles aggregation.

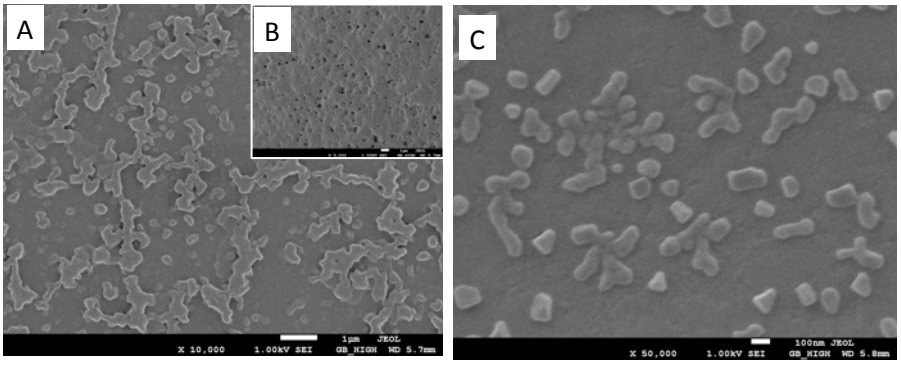

Figure 7: SEM images of a dried (A) diluted and (B) undiluted dispersion of QPU-0(1% wt/wt); (C) diluted QPU-1 dispersion.

The UCST behavior of the QPU dispersions was investigated using turbidity photometric measurements (Table 3). **Figure 8** shows the obtained turbidity curves for QPU-1 dispersions with different concentrations. At low concentration (1wt %)

the UCST was not sharp. Increase in the concentration led to significant and systematic increase in UCST (from 48 °C at 1 wt% to 81°C for 6 wt %) with sharp phase change. All dispersions showed good reproducibility of their respective UCST behavior over at 5 heating/cooling cycles (data not shown here). The UCST behavior of quaternized polyurethane dispersions with the same concentration but with different contents of PEG in the composition was also studied **(Figure 9)**. There was no significant influence of PEG in changing the UCST but led to stable dispersions with high solid contents.

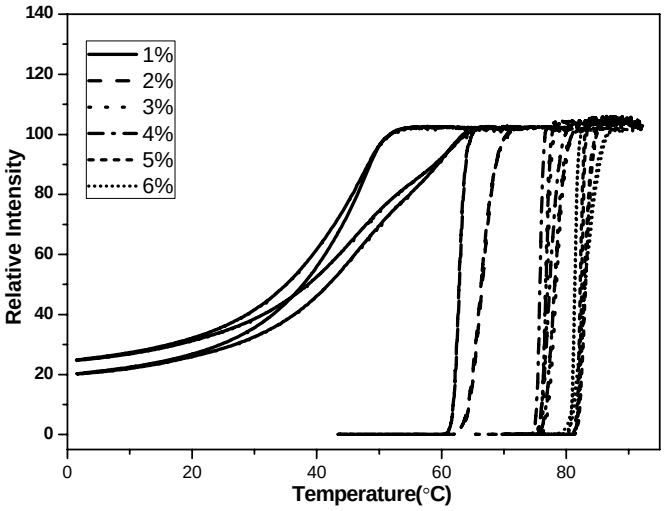

Figure 8: Turbidity measurements for the investigation of the UCST behavior of the iodide derivatives of the cationic QPU-1 with different concentrations.

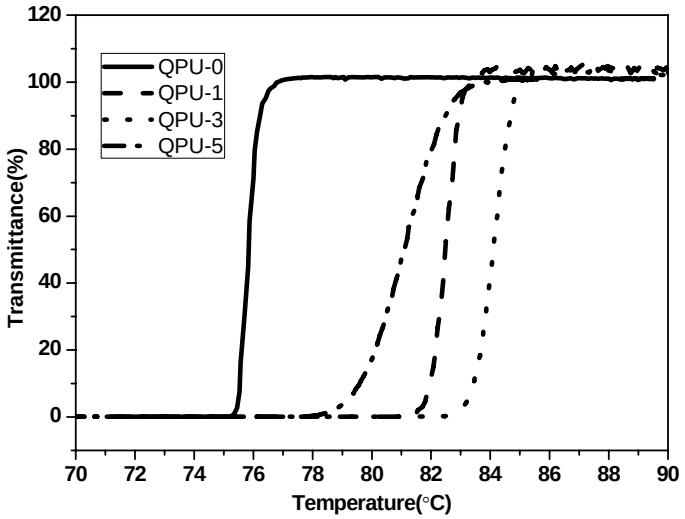

Figure 9. Turbidity measurements of 5 wt% quaternized PU with different PEG contents to investigate the influence of PEG on the UCST behavior of copolymers (first cooling cycle).

Table 3 Upper Critical Solution Temperature (UCST) of PU dispersions as measured by turbidity photometer.

QPU	**UCST / °C**	**QPU**	**UCST / °C**
5% QPU-0	76	1% QPU-1	48
5% QPU-1	83	2% QPU-1	63
5% QPU-3	84	3% QPU-1	77
5% QPU-5	82	4% QPU-1	78
		5% QPU-1	83
		6% QPU-1	81

The antibacterial properties of the dispersions were investigated by several standard methods. All dispersions proved to be active against *E. coli*; the determined MIC and MBC values do not differ among the tested dispersions (see **Table 4**) and are with

concentrations of 78 µg/ml as MIC and 156 µg/ml as MBC in a good range. When the focus comes to the speed of antibacterial action, the quaternized homo-polyurethane (QPU-0) dispersion showed to be the best: already after 10 minutes of contact, the solution with a concentration of 2.5 mg/ml and all higher concentrated samples killed > 99.9% of the bacteria, as shown in **Figure 10A**. After a longer contact time of 120 minutes also the other dispersions showed a total reduction of bacteria growth at concentrations of ≥ 625 µg/ml or even ≥ 313 µg/ml, when it comes to the QPU-0 dispersion, as depicted in **Figure 10B**.

Table 4. Minimum inhibition concentration (MIC) and minimum bactericidal concentration (MBC) of the dispersions towards a 10^5 cfu/ml suspension of *E. coli*.

Sample	MIC / µg ml^{-1}	MBC / µg ml^{-1}
QPU-0	78	156
QPU-1	78	156
QPU-3	78	156
QPU-5	78	156

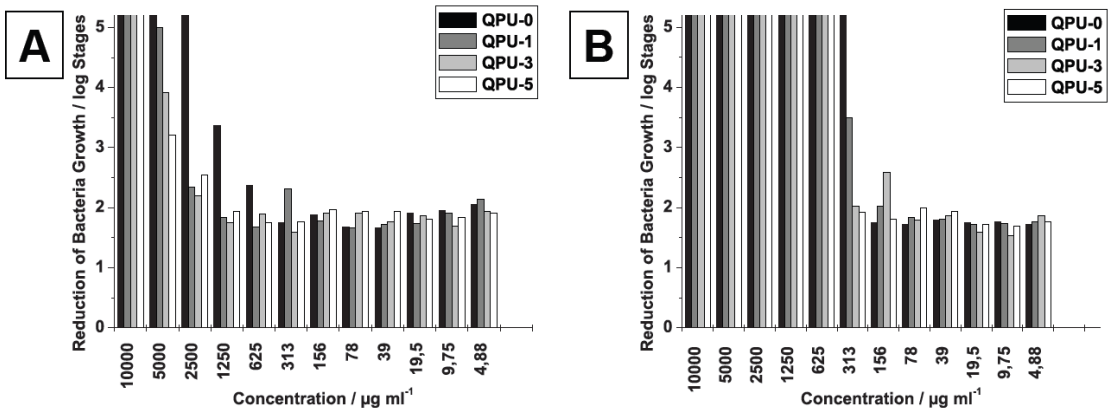

Figure 10. Reduction of bacteria growth for different concentration of the dispersions after (A) 10 minutes and (B) 120 minutes contact to *E. coli* (10^5 cfu/ml).

Conclusions

A simple and straightforward method of making UCST PU dispersions with high solid contents could be shown here. Cationic segmented polyurethanes having PEG segments with UCST behavior and antibacterial properties were successfully synthesized by polyaddition reaction followed by quaternization. The introduction of PEG into the system facilitated the formation of water stable dispersion with high solid contents up to 10 wt% without any additives. The dispersed particles are well below 1µm in size and comprise a low size distribution. Particle size and UCST could be easily controlled by the solid concentration and PEG content. More importantly, the introduction of PEG into the copolymer did not decrease the antibacterial activity. Low MIC and MBC against the gram-negative *Escherichia coli* suggest high suitability of the dispersions for functional coatings and antibacterial textile applications.

Acknowledgements: Financial support from department of Chemistry Phillips-University Marburg and BMBF, Germany is highly acknowledged.

References

[1] B. K. Kim, *Colloid and Polymer Science* **1996**, *274*, 599.

[2] C. L. Marx, Caulfiel.Df, S. L. Cooper, *Macromolecules* **1973**, *6*, 344.

[3] T. Buruiana, V. Melinte, E. C. Buruiana, A. Mihai, *Polymer International* **2009**, *58*, 1181.

[4] G. Radhakrishnan, S. Sundar, N. Vijayalakshmi, S. Gupta, R. Rajaram, *Progress in Organic Coatings* **2006**, *56*, 178.

[5] A. A. El-Sayed, F. A. Kantouch, A. Kantouch, *Journal of Applied Polymer Science* **2011**, *121*, 777.

[6] P. Krol, B. Krol, *Colloid and Polymer Science* **2009**, *287*, 189.

[7] S. Nomula, S. L. Cooper, *Journal of Colloid and Interface Science* **1998**, *205*, 331.

[8] K. Matsunaga, K. Nakagawa, S. Sawai, O. Sonoda, M. Tajima, Y. Yoshida, *Journal of Applied Polymer Science* **2005**, *98*, 2144.

[9] J. Y. Kim, C. Cohen, *Macromolecules* **1998**, *31*, 3542.

[10] J. C. Lee, B. K. Kim, *Journal of Polymer Science Part a-Polymer Chemistry* **1994**, *32*, 1983.

[11] M. A. Marchisio, P. Bianciardi, T. Longo, P. Ferruti, E. Ranucci, M. G. Neri, *Journal of Biomaterials Science-Polymer Edition* **1994**, *6*, 533.

[12] P. Gilbert, L. E. Moore, *Journal of Applied Microbiology* **2005**, *99*, 703.

[13] P. M. W. P.Broxton, P.Gilbert, *Journal of Applied Bacteriology* **1983**, *54*, 345.

[14] D. Dieterich, *Progress in Organic Coatings* **1981**, *9*, 281.

[15] B. K. Kim, J. C. Lee, *Polymer* **1996**, *37*, 469.

[16] F. Tiarks, K. Landfester, M. Antonietti, *Journal of Polymer Science Part a-Polymer Chemistry* **2001**, *39*, 2520.

[17] S. Sundar, P. Aruna, U. Venkateshwarlu, G. Radhakrishnan, *Colloid and Polymer Science* **2004**, *283*, 209.

[18] P. Krol, B. Krol, *Polimery* **2004**, *49*, 615.

[19] C. Alexander, K. M. Shakesheff, *Advanced Materials* **2006**, *18*, 3321.

[20] S. Agarwal, L. Q. Ren, *Macromolecular Chemistry and Physics* **2007**, *208*, 245.

[21] H. G. Schild, *Progress in Polymer Science* **1992**, *17*, 163.

[22] H. Katono, K. Sanui, N. Ogata, T. Okano, Y. Sakurai, *Polymer Journal* **1991**, *23*, 1179.

[23] T. Aoki, M. Kawashima, H. Katono, K. Sanui, N. Ogata, T. Okano, Y. Sakurai, *Macromolecules* **1994**, *27*, 947.

[24] H. Katono, A. Maruyama, K. Sanui, N. Ogata, T. Okano, Y. Sakurai, *Journal of Controlled Release* **1991**, *16*, 215.

[25] Z. Q. Jiang, Y. J. You, Q. Gu, J. Y. Hao, X. M. Deng, *Macromolecular Rapid Communications* **2008**, *29*, 1264.

[26] S. Y. Jiang, Z. Zhang, T. Chao, S. F. Chen, *Langmuir* **2006**, *22*, 10072.

[27] A. B. Lowe, C. L. McCormick, *Chemical Reviews* **2002**, *102*, 4177.

[28] M. Arotcarena, B. Heise, S. Ishaya, A. Laschewsky, *Journal of the American Chemical Society* **2002**, *124*, 3787.

[29] C. Mijangos, C. Echeverria, D. Lopez, *Macromolecules* **2009**, *42*, 9118.

[30] T. Kissel, M. Beck-Broichsitter, E. Rytting, T. Lebhardt, X. Y. Wang, *European Journal of Pharmaceutical Sciences* **2010**, *41*, 244.

[31] C. Hepburn, Elsevier Appl. Sci, London, **1993**.

[32] A. Koshio, M. Yudasaka, M. Zhang, S. Iijima, *Nano Letters* **2001**, *1*, 361.

8.3 Publication "A Fast Degrading Odd-Odd Aliphatic Polyester-5,7 made by Condensation Polymerization for Biomedical Applications"

Fei Chen, Jan Martin Nölle, Steffen Wietzke, Marco Reuter, Sangam Chatterjee, Martin Koch, Seema Agarwal*, A Fast Degrading Odd-Odd Aliphatic Polyester-5,7 made by Condensation Polymerization for Biomedical Applications, *Journal of Biomaterials Science: Polymer Edition*. **2011**, in press.

A Fast Degrading Odd-Odd Aliphatic Polyester-5,7 made by Condensation Polymerization for Biomedical Applications

Fei Chen[a], Jan Martin Nölle[a], Steffen Wietzke[b], Marco Reuter[b], Sangam Chatterjee[b], Martin Koch[b], Seema Agarwal[a*]

[a]Philipps-Universität Marburg, Fachbereich Chemie, Hans-Meerwein Strasse, D-35032, Marburg, Germany
[b]Philipps-Universität Marburg, Fachbereich Physics, Hans-Meerwein Strasse, D-35032 Marburg, Germany
agarwal@staff.uni-marburg.de

Abstract

A fast enzymatic degradable aliphatic biodegradable all-odd-polyester-5,7 based on 1,7-heptanedioicacid (pimelic acid) and 1,5-pentanediol was synthesized by polycondensation reaction. The structural characterization of the polyester was done using 1D and 2D NMR spectroscopic techniques. The properties of the resulting polyester like crystallization behavior, enzymatic degradation, thermal stability etc. were investigated by using differential scanning calorimetry (DSC), wide angle X-ray diffraction (WAXD), scanning electron microscopy (SEM) and gel permeation chromatography (GPC). Terahertz time-domain spectroscopy (THz TDS) was employed to determine the glass transition temperature, which could not be revealed reliably by conventional thermal analysis. The properties of all-odd-polyester-5,7 were compared with the well known enzymatic degradable polyester (polycaprolactone). The results indicated that polyester-5,7 has similar crystal structure like PCL but much faster degradation rate. The morphology of polyester-5,7 film during enzymatic degradation showed fibrillar structure and degradation began by surface erosion.

Key words: aliphatic polyester, condensation polymerization, degradable, enzymatic degradability

1. Introduction

Large number of commercially available degradable materials as environmental friendly materials or for medical and non-medical applications is based on aliphatic polyesters. They are generally made by ring-opening polymerization of cyclic esters [1-3] or polycondensation reaction between diols and diacids or diacid derivatives [4-5]. Both methods have their own advantages and disadvantages and can be chosen according to the application. Ring-opening polymerization of cyclic esters generally gives high molecular weight polyesters which is not possible by polycondensation reactions. On the other hand, polycondensation reaction provides more opportunities of tuning the properties of polyesters by using different combinations of diols and diacids. The use of polycondensation reactions for the synthesis of aliphatic polyesters (poly(alkylene dicarboxylates)) is known since 1930s from the work of Carothers [6]. In the recent times new catalysts and heat stabilizers are developed and researched with an aim to get the high molecular weight aliphatic polyesters by condensation polymerization. Poly(alkylene dicarboxylates like Poly(butylene succinate) (PBSu), poly(ethylene succinate) (PESu) and poly(ethylene adipate) (PEAd) are well characterized in terms of crystal structure and morphology [7-12]. Poly (propylene succinate) was the first degradable polyester from 1, 3-propanediol to be studied [13]. These aliphatic polyesters are enzymatic degradable due to their susceptibility to hydrolysis and are degraded by different enzymes like proteases [14], α-chymotrypsin [15], lipases and esterase [16].

From the materials point-of-view the properties and degradability rate, in general, depends upon the type of chemical linkage, molecular weight, hydrophilicity, crystallinity, flexibility, porosity and morphology of polyesters. The effect of these parameters on biodegradability of polyesters made by condensation polymerization can be seen in literature. For example, Mochizuki et al. [17] have studied the effect of structure upon enzymatic degradation of high molar mass poly (butylenes succinate-co-ethylene succinate). The hydrolysis rate of the copolymer was higher than the corresponding homopolymers due to decreased crystallinity. Most of the

examples in the literature made use of diols and diacids with even number of carbon atoms. Bhaumik et al. [18] have shown the effect of odd and even carbon atoms of diacid used on interchain packing and hence the properties like melting point of the resulting polyesters. There was zig-zag nature of melting point variation with number of carbon atoms (from 4 till 8) in diacid keeping ethylene glycol as the comonomer. Similar observations were made in 1954 for different combinations of alcohols and acids.[19] Cao et al.[20] checked degradability of poly(butylene succinate-co-caprolactone) (caprolactone with odd number of carbon atoms) in compost soil at 30 ^{o}C and 95% RH and showed higher degradability of copolymers as compared to the respective homopolymers due to increased flexibility and reduced crystallinity. Bikiaris et al. [21] have synthesized poly(alkylene succinates) from succinic acid and aliphatic diols with 2,3 and 4 methylene groups by melt polycondensation. These poly(alkylene succinates) are: poly(propylene succinate) (PPSu), poly(ethylene succinate) (PESu), poly(butylene succinate) (PBSu). Degradability studies of these polyesters with the same average molecular weight included enzymatic hydrolysis using *Rhizopus delemar* lipase at pH 7.2 and 30 °C. The degradation rates of the polymers decreased following the order PPSu > PESu ≥ PBSu i.e. odd diol enhanced the degradation as compared to the even ones. It was attributed to the lower crystallinity of PPSu compared to other polyesters, rather than to differences in chemical structure. Odd carbon atoms made packing of polymer chains difficult as compared to the even atoms and thereby led to reduced crystallinity and increased degradability as it depends to a large extent on polymer crystallinity.

With an aim to make and study a complete odd-polyester by polycondensation reaction, we synthesized polyester-5,7 starting from pentanediol and 1,7-heptanedioicacid. The properties of this aliphatic all-odd-polyester including enzymatic degradability are reported here. All-odd-polyester was found to be very fast enzymatic degradable as compared to the very well known biodegradable polyester-polycaprolactone (PCL). The possibility of measuring the glass transition temperature

by terahertz time-domain spectroscopy (THz TDS) is also highlighted. A variety of polymers is transparent to THz waves, which comprise the frequency range from 0.3 THz to 10 THz, tantamount to wave numbers of 10 cm^{-1} to 333 cm^{-1}. Due to the coherent detection scheme employed and the pulsed nature, THz TDS simultaneously provides access to the dielectric properties and the thickness of the sample, respectively, which sets it apart from techniques of the (far) infrared and the optical frequency regime. Details about the technique and the data extraction procedure can be found elsewhere [22].

2. Materials and Methods

2.1. Materials

1,5-pentanediol, 1,7-heptanedioicacid (Pimelic acid) were purchased from Alfa Aesar Co., Ltd. The reagents were used as received without further purification. The Titanium (IV) butoxide catalyst ($Ti(OBu)_4$) was purchased from Acros and the lipase of Pseudomonas Cepacia (50 U/mg) was purchased from Sigma-Aldrich. 0.05 M phosphate buffer solution with pH 7.0 was prepared in the laboratory. All the other chemicals and solvents of analytical grade were used as received without further purification.

2.2. Synthesis of poly (pentylene heptanoate) (polyester-5,7)

The aliphatic all-odd-polyester-5,7 was synthesized by the two-stage melt polycondensation between 1, 5-pentanediol and 1,7-heptanedioicacid (Scheme 1**)**. The molar ratio of 1,5-pentanediol to heptanedioicacid was 1.05:1, and the $Ti(OBu)_4$ catalyst was 0.05 mol% of the total monomers. A representative polymerization procedure is as follows: in a 100 ml round-bottom flask equipped with a nitrogen inlet, a stir bar, was charged 16.0 g (100 mmol) of 1,7 heptanedioicacid (pimelic acid), 11.0 ml of 1,5-pentanediol (105 mmol) and 10.0µl (0.03 mmol) of the catalyst. After charging into the flask, the mixture was heated to 190 °C and reacted for 2 h under nitrogen with vigorous stirring. After this time, the calculated amount of water was collected and then, the pressure of the mixture was gradually reduced to 0.2 mPa for

30 min to avoid excessive foaming and minimize oligomer sublimation. 5mg (0.05mmol) PPA (polyphosphoric cid) was added to the mixture and the mixture was slowly heated to 230 °C and reacted for 6 h to obtain the polyester-5,7. After the polycondensation reaction was complete, the polymer was cooled to room temperature and dissolved in 50 mL of chloroform, followed by the precipitation into 800 mL of methanol. The pale-white polymer powder was collected and dried under vacuum at 40 °C for 24 h.

^{1}H-NMR (500 MHz, $CDCl_3$): δ = 1.30-1.42 ppm (m, 4H,); δ = 1.62 ppm (dt, 8H, $^{3}J_{H,H}$ = 7,5 Hz,); δ = 2.28 ppm (t, 4H, $^{3}J_{H,H}$ = 7.5 Hz); δ = 4,05 ppm (t, 4H, $^{3}J_{H,H}$ = 6.5)

2.3. Instruments

^{1}H, ^{13}C and 2D nuclear magnetic resonance (NMR) spectra were recorded using a Bruker spectrometer operating at 300 MHz, the original polyester sample was measured in $CDCl_3$ while the degradation products were dissolved and measured in D_2O. Chemical shifts (δ) were given in ppm using tetramethylsilane(TMS) as internal reference.

The molecular weights of the polymers were determined by GPC using a Knauer system equipped with one column, PSS-SDV (linear XL, 5 µm, 8.0 x 300 mm), a differential refractive index detector, $CHCl_3$ as eluent at a flow rate of 0.5 mL/min. All the measurements were done against the standard calibration with PMMA. Toluene was used as internal standard. Molecular weight distributions (MWDs) of the polymers after degradation (the water soluble portion) were determined by gel permeation chromatography (GPC) in a setup comprising a Knauer pump equipped with two NOVEMA column (particle size 10 µm, dimension 8.00mm × 300.00 mm, porosity 1000 Å and 3000 Å) calibrated with poly (2-vinylpyridine)-(P2VP) standards and a differential refractive index detector using 0.3 N formic acid as eluent with a flow rate of 1 $mL \cdot min^{-1}$.

The surface morphology of the films were observed using JSM-7500F SEM with a voltage of 5 kv, the dry film was directly stuck on conductive sample holder, before

measurement, all the samples were coated with a layer of gold to increase conductivity. The samples were observed at 5 Torr and 7 °C.

Mettler thermal analyzers having 851^e TG and 821^e DSC modules were utilized for the thermal characterization of the polymers. DSC scans were recorded under a nitrogen atmosphere (flow rate =80 mL/min) at a heating rate of 10°C $\cdot min^{-1}$. The sample amount was about 10mg and an aluminum crucible (40mL) was used. The thermal stability was determined by recording thermogravimetric (TG) traces in a dry air atmosphere (flow rate = 50 mL/ min) using powdered samples in open aluminum oxide crucibles (70mL). A heating rate of 10 °C $\cdot min^{-1}$ and a sample size of 10-12mg were used in each experiment. The STAReSW 9.20 software (Mettler) was used for data recording and interpretation.

X-ray diffraction pattern of the polymer films (100 mm thick) was recorded with a Siemens goniometer D5000 using Cu Ka-radiation, of λ=1.54 Å.

A Zwick/Roell BT1-Fr0.5TN-D14 machine equipped with a 200 N KAF-TC load sensor was used to determine the mechanical properties of the polymer films. Bone-like specimens were punched out of the polymer with an average length of 1.4 cm and a width of 0.20 cm. The thickness of the films was measured by micrometer in different position. A preload of 0.1 MPa and a subsequent traction speed of 50 mm/min were applied. 5 samples were measured for each composition. DMTA measurements were performed on a "Dynamic Mechanical Thermal Analyzer" by PL Thermal Sciences. The acquired data were evaluated with the associated software Plus5 5.2 by PL Thermal Sciences; vibration frequencies of 10, 1 and 0.1 Hz were applied for analysis.

For degradability studies, weight loss was calculated by the following equation,

$$\text{Weight loss } \% = (W_0 - W_t) / W_0$$

Where W_0 and W_t represent respectively the dry weights of the films before and after degradation.

2.4. Enzymatic degradation

Enzymatic degradation experiments were carried out at 37 °C in a 0.05 M, pH 7.0 phosphate buffer. Square samples with dimensions of 10×10×0.2mm were cut from the films of polyester and placed in vials containing 5ml of buffer solution with 1 mg of pseudomonas lipase and 1 mg of sodium azide. At predetermined time intervals, the degradation medium was filtered by disposable filter (pore size 0.5 μm). The filtered solid was washed with distilled water, and then vacuum-dried at room temperature for 2 days before analysis (GPC and NMR). The filtrate (solution) was evaporated by freeze-drying and the residue was analysed by GPC and ^{1}H NMR.

3. Results and Discussion

An all-odd aliphatic polyester-5,7 (*poly(pentylene heptanoate)*) was made by condensation polymerization of 1,5-Pentanediol and 1,7-heptandioicacid (pimelic acid) in the presence of titanium tetrabutoxide (TBT) catalyst. The reaction was carried out in two steps and polyphosphoric acid was used as heat stabiliser (Scheme 1). The weight average molecular weight of the polyester-5,7 as determined by gel permeation chromatography in THF was about 23,000 with polydisperisty of 1.8. The structural characterization of the resulting polymer was done using NMR spectroscopy. The representative ^{1}H NMR spectrum of the resulting polymer with peak assignments is shown in the Fig. 1. The peak appearing at δ=2.24 ppm (proton 4) was assigned to –C(O)C$\boldsymbol{H}_2$- protons of pimelic acid part and the peak at δ=4.0 ppm (proton 1) originated from -OC$\boldsymbol{H}_2$- protons of di alcohol part. Other peaks from methylene protons of diacid and diols parts were observed as overlapping peaks centered at δ=1.59 ppm and δ=1.34 ppm in ^{1}H NMR but were splitted into well resolved peaks in ^{13}C NMR spectrum. To further confirm the structure of the polyester and for the correct peak assignments in ^{1}H and ^{13}C NMR spectra, the 2D NMR techniques like HMQC (Heteronuclear Multiple Quantum Correlation) and HMBC (Heteronuclear Multiple Bond Correlation) were used. HMQC (Not shown here) helped in unambiguous assignment of carbons 1 and 4 and in correlating other

methylene peaks in ^{1}H NMR to ^{13}C NMR peaks. The correct and unambiguous peak assignments of other peaks were done by seeing corresponding correlations in HMBC NMR spectrum (Fig. 2). Proton 1 as expected showed 3 cross-peaks (2 and 3 bond correlations with carbons 2,3 and the carbonyl carbon 7 respectively). Further, methylene protons in the lower ppm region were also distinguished by seeing expected correlations in HMBC NMR spectrum as shown in the Fig. 2.

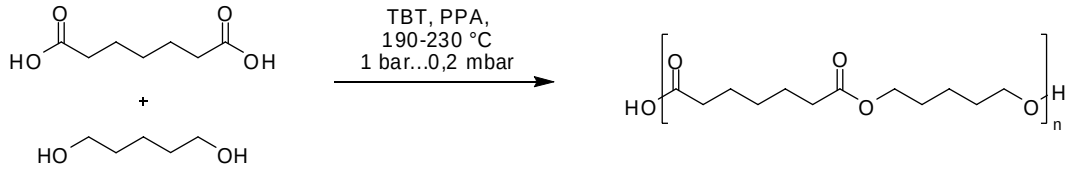

Scheme 1. Synthetic scheme for the formation of polyester-5,7 by polycondensation of 1,7-heptanedioicacid and 1,5-pentanediol.

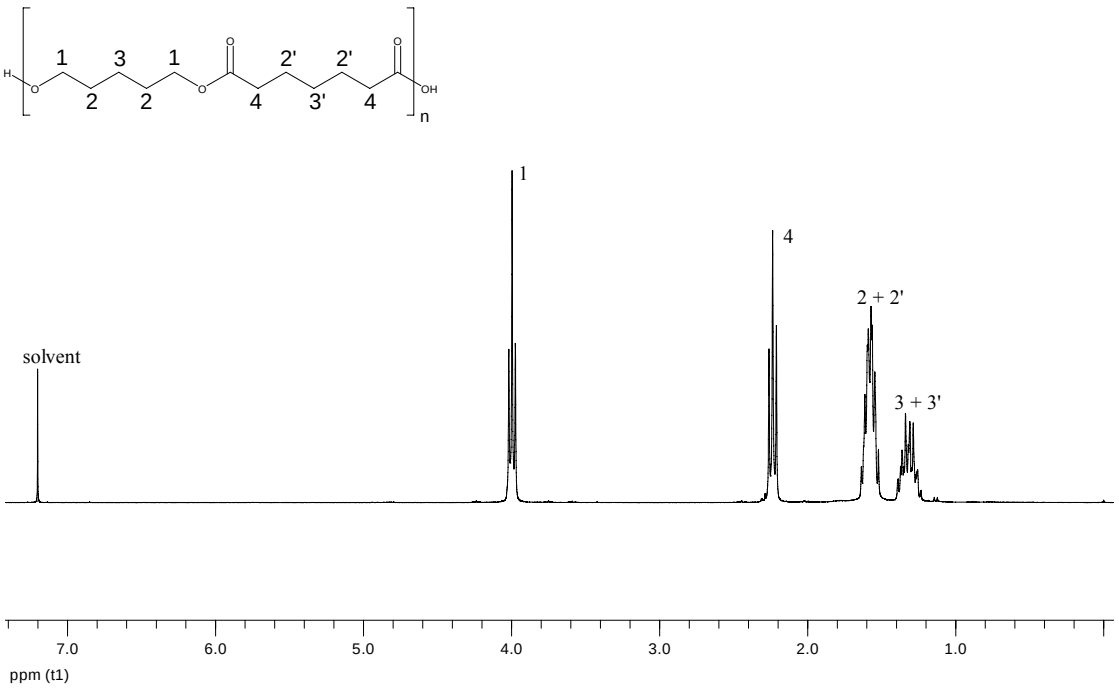

Figure 1. ^{1}H NMR spectrum of polyester-5,7 in $CDCl_3$.

The thermal stability of the polyester as checked using thermogravimetric analyzer and was found to be well above 300 ^{o}C. One of the measures of thermal stability, $T_{5\%}$ (temperature at which 5% weight loss takes place) was very high, of about 360 ^{o}C.

Differential scanning calorimetry was used for determining the phase transitions like glass transition and melting. A single melting peak was seen at about 43 ^{o}C. No clear glass transition could be seen in DSC. In an attempt to observe glass transition temperature, different DSC scans were run by changing the amount of the sample and heating rates but still no clear DSC was seen. Further dynamic mechanical thermal analysis (DMTA) on polyester films were carried out for seeing the glass transition at different frequencies. The DMTA curves are shown in the Fig. 3. DMTA showed very broad transitions and therefore could not give accurate glass transition temperature of the polyester. Hence, a new tool for determining the glass transition temperature was employed: non-contact, non-destructive THz TDS [23].

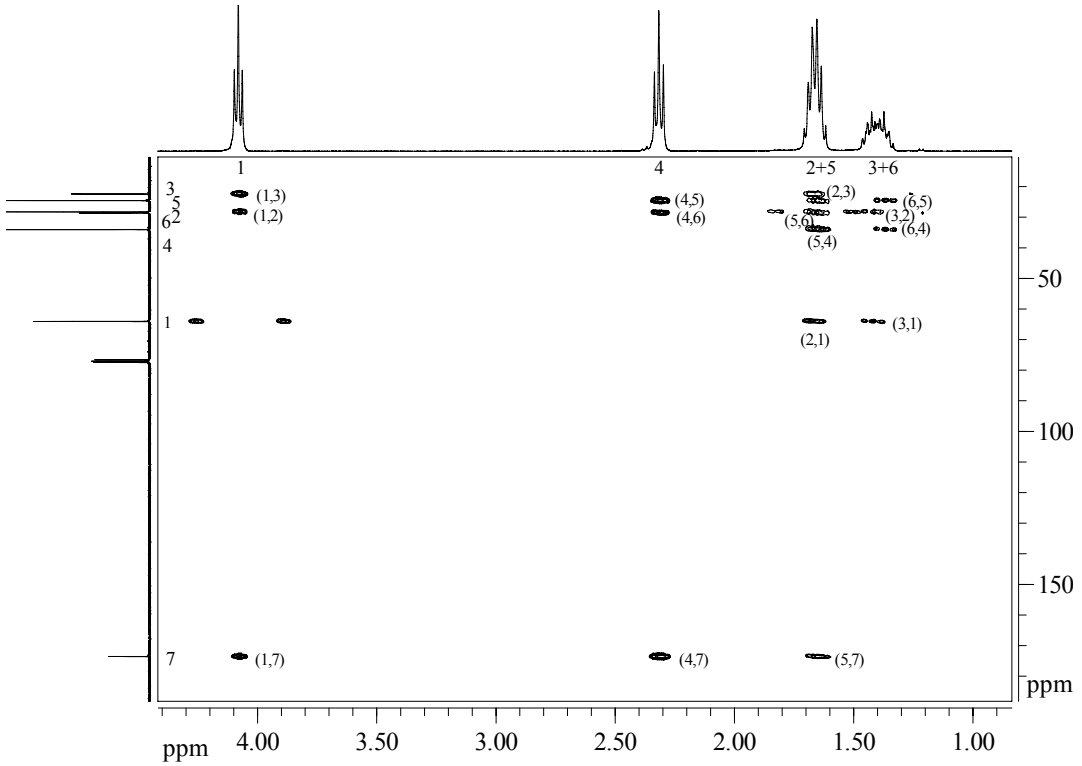

Figure 2. 2D ^{1}H-^{13}C HMBC (Heteronuclear Multiple Bond Correlation) of polyester-5,7.

Temperature-dependent THz TDS measurements reveal the glass transition by a change in the thermal gradient of the THz refractive index. This step marks the beginning of the translational motion of backbone chain segments in the amorphous domains. Due to the model of the free volume, there is a decrease in density with

increasing temperature that is higher at temperatures above the glass transition than below. This two regime behavior is reflected by the refractive index according to the Lorentz-Lorenz law [24]. Figure 4 depicts the temperature-dependent refractive index of the biodegradable polyester-5,7 at 1.0 THz (33 cm^{-1}). Both temperature regimes can be fitted by a linear regression. The intersection yields the glass transition temperature T_g in the vicinity of -53 °C. This novel method still succeeds when conventional techniques, such as differential scanning calorimetry or dynamic-mechanical analysis, fail, e. g. in case of highly-crystalline samples [25].

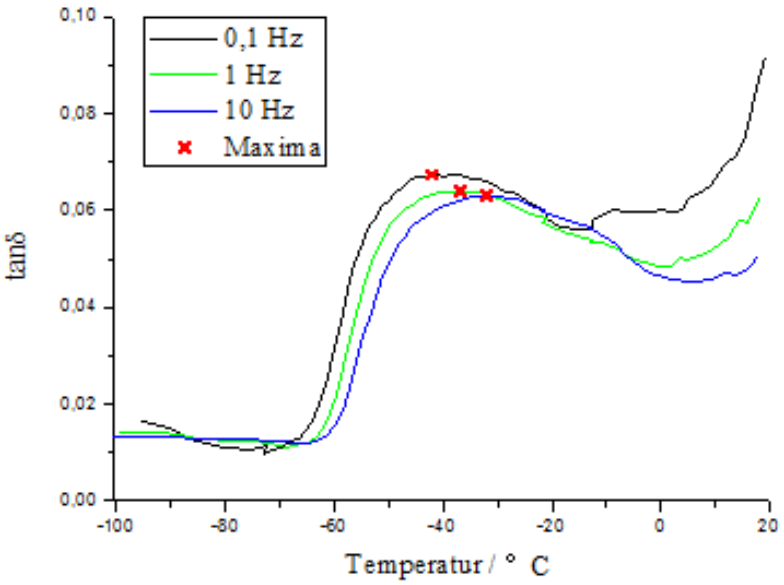

Figure 3. Dynamic mechanical thermal analysis of polyester-5,7 at different frequencies showing broad transitions.

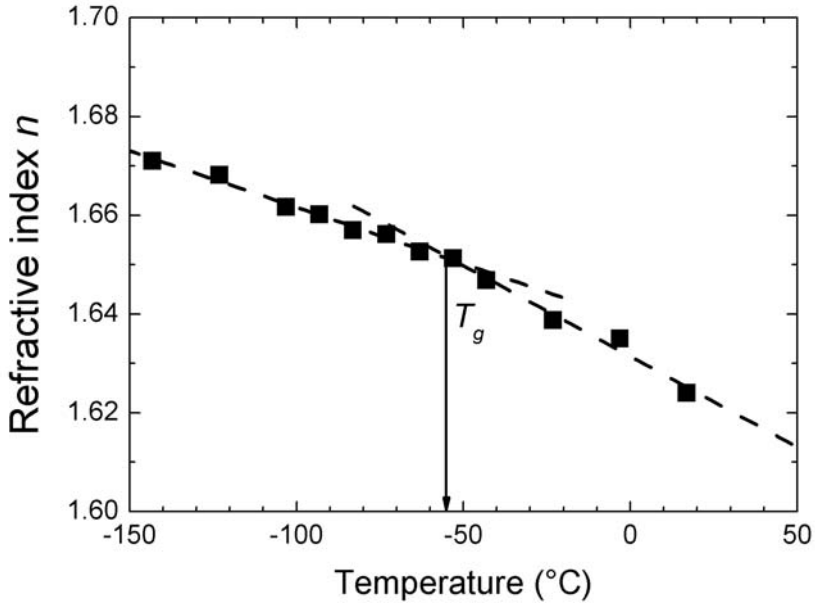

Figure 4. THz refractometry reveals the glass transition temperature at the intersection of two linear fits representing the two temperature regimes of the refractive index at 1.0 THz (33 cm^{-1}).

Mechanical testing showed very low elongation at break of around 1.5%, moderate tensile strength of about 4 MPa and E modulus of 0.36 GPa for polyester-5,7. The known degradable polyester PCL shows tensile strength in the range 4-28 MPa depending upon molecular weight. PCL of Mn = about 42,500 (Aldrich) showed a tensile strength of about 13 MPa as tested by us. Although, the XRD study (Fig. 5) of the polyester-5,7 revealed no additional diffraction profile distinct from those coming from the semi-crystalline PCL (the strong diffraction rings derived from the (110) and (200) planes were observed at 2θ = 21.4° and 23.8° respectively), a significant difference in elongation behavior between PCL and polyester-5,7 showed difficult crystallizability tendency of polyester-5,7 on stretching because of odd-odd carbon atoms.

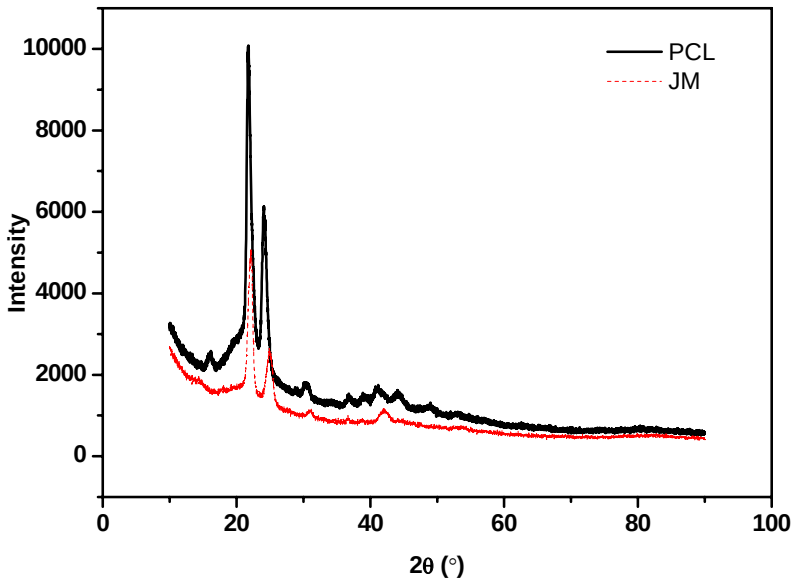

Figure 5. XRD reflexes of PCL (Aldrich) due to the planes (110) and (200) at 2θ = 21.4" and 23.8" in comparison to the polyester-5,7.

The degradability of the polyester-5,7 was evaluated using lipase from *P. Cepacia* at 37 ^{o}C. The weight loss profile of polyester-5,7 at different time intervals in presence of lipase enzyme is shown in the Fig. 6. A very fast degradation of polyester can be seen from this data in comparison to the biodegradable PCL; after 8h in 0.2 mg/ml *pseudomonas lipase* buffer solution, weight loss was already about 53%, after 22 h more than 90 wt% of samples degraded to water soluble products which were further analyzed by ^{1}H NMR and GPC. The GPC of the degradation products in water after different time intervals showed the presence of only low molecular weight fractions (Fig.7a). Accurate molecular weights could not be determined as this range falls below the calibration limit of the used GPC instrument. The ^{1}H NMR spectrum of the degradation products of polyester in water after 8 h of degradation is shown in the Fig.8. The two new distinct peaks appeared at ppm 2.1 and 3.5 ppm which could be attributed to the HOOC-C$\boldsymbol{H}_2$- and OH-C$\boldsymbol{H}_2$- end group protons and some new overlapping peaks in the lower ppm region of the degradation products. The degradation of the polyester is expected to give water soluble products like

1,5-pentanedio, 1,7-heptanedioicacid and oligomeric polyesters with HO-CH_2- and HOOC-CH_2- end groups. These end groups and 1,5-pentanedio, 1,7-heptandioicacid were clearly seen in the NMR of the degradation product. The ^{1}H NMR of 1,5-pentanedio, 1,7-heptanedioicacid is shown for comparison.

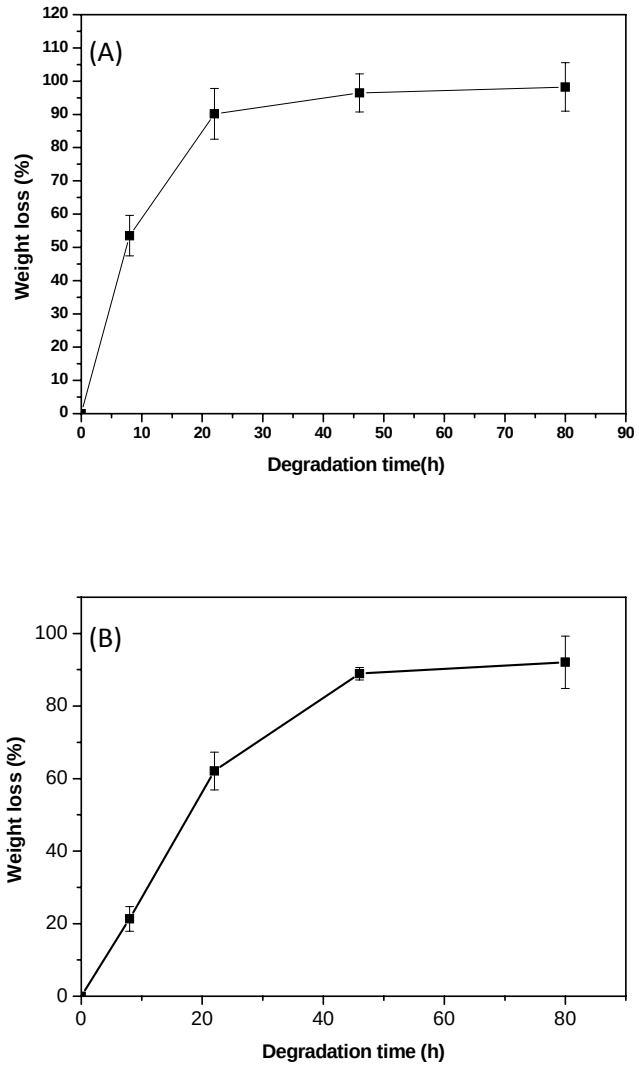

Figure 6. Weight loss profiles of A) polyester-5,7 and B) PCL; degradation in phosphate buffer (pH 7.0) in presence of Pseudomonas lipase (0.2mg/ml).

The molecular weight of the solid product left after different time intervals of enzymatic degradation is also followed by GPC and is shown in the figure 7b. There was no significant change in the molecular weight and polydispersity index till about 22 h of enzymatic degradation. This gives a hint about the surface degradation

mechanism which was further confirmed by monitoring the surface morphology as described below. In comparison to the fast enzymatic degradation, the hydrolytic degradation under physiological conditions did not show any weight loss within 3 weeks. This behavior is similar to polycaprolactone.

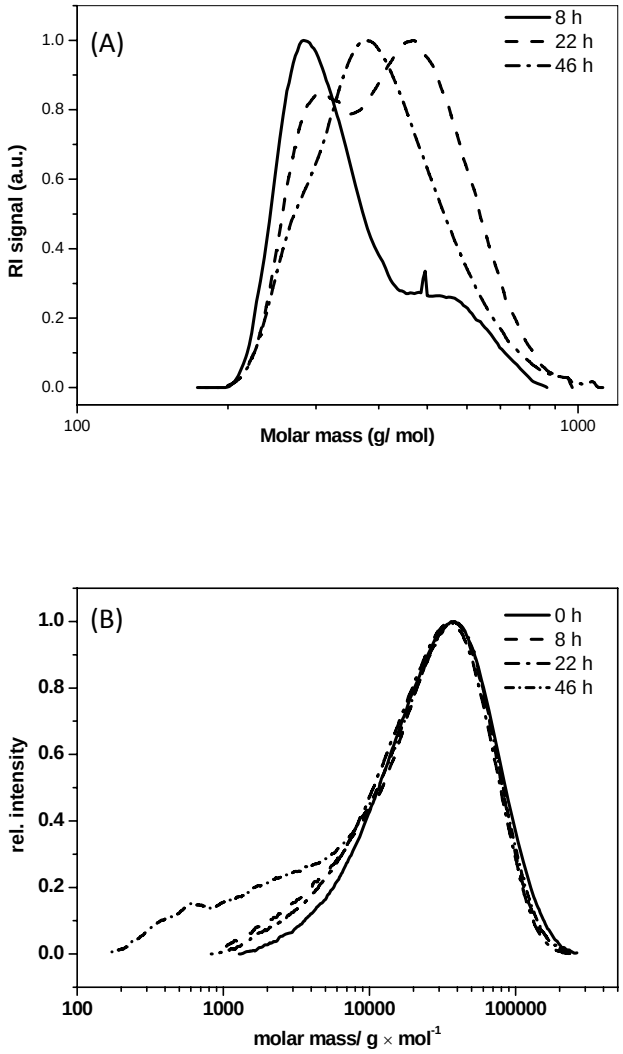

Figure 7. (a) GPC curves for degradation products of polyester-5,7 at different time intervals; degradation was done at 37 °C in pH 7.0 with Pseudomonas lipases (0.2 mg/ml).(b) Gel permeation chromatographic profiles of polyester-5,7 residues after degradation at different time in pseudomonas lipase (0.2 mg/ ml).

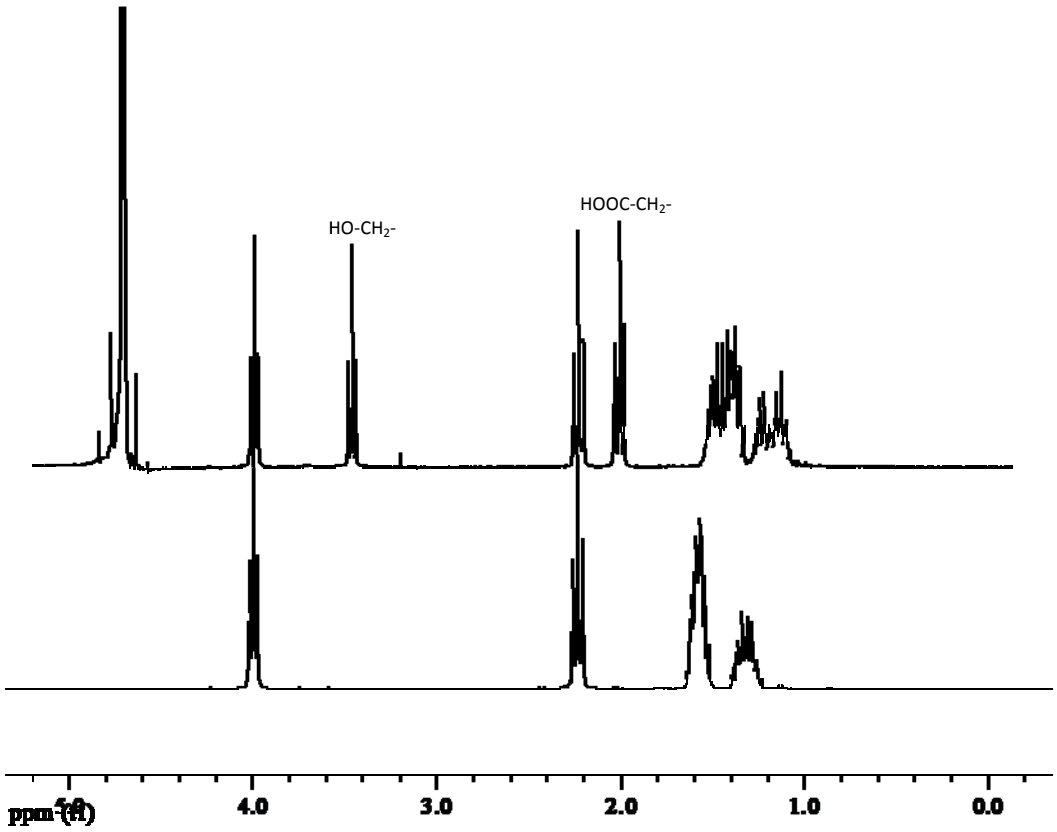

Figure 8. ^{1}H NMR of polyesert-5,7 after 8h of degradation; degradation was done at 37 °C in pH 7.0 with Pseudomonas lipases (0.2 mg/ ml).

Polyester-5,7 before degradation was semicrystalline with about 50% crystallinity calculated based on the heat of fusion observed in the first heating cycle from DSC and the bigger spherulites as observed by optical microscope. The % crystallinity calculated for PCL was about 60% (Melting enthalpy of 136 J/g for 100% crystalline PCL is taken from the literature) and smaller spherulites (Fig. 9). After degradation for about 8 h, the % crystallinity increased in the left over samples of polyester-5,7 and PCL to about 67-68% but with smaller spherulites for PCL. This could be due to the degradation in the amorphous region thereby increasing the % crystallinity of the degraded sample.

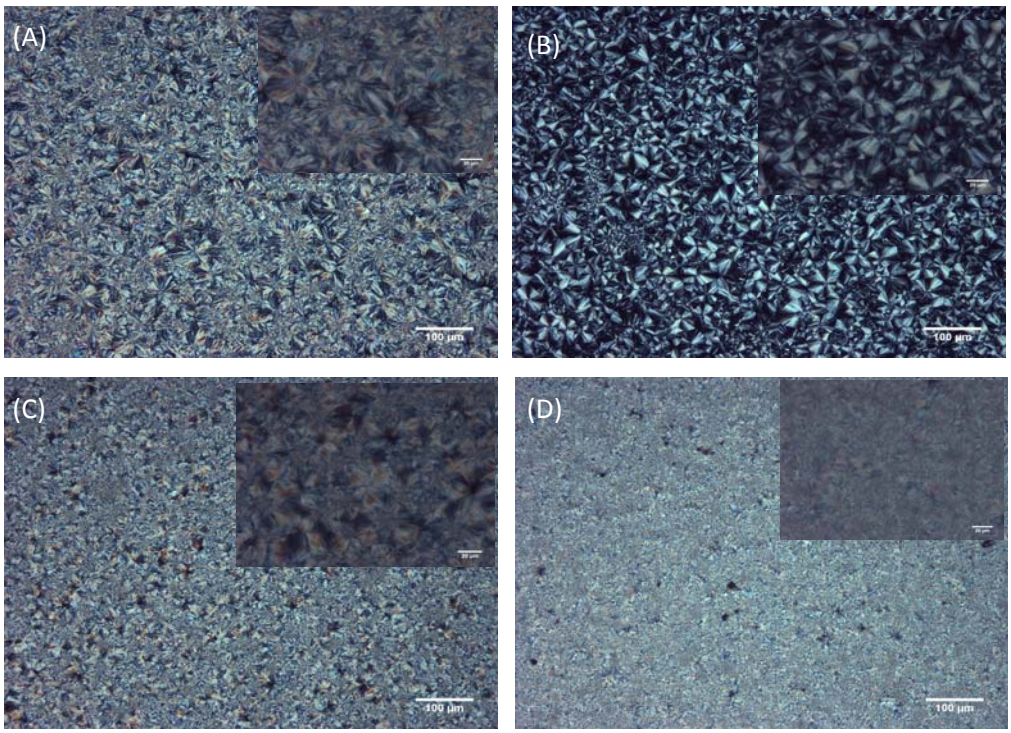

Figure 9. Optical microscope pictures of polyester-5,7 (A) before degradation (B) after degradation (8h) (C) polycaprolactone (PCL) before degradation and (D) PCL after degradation (8h).

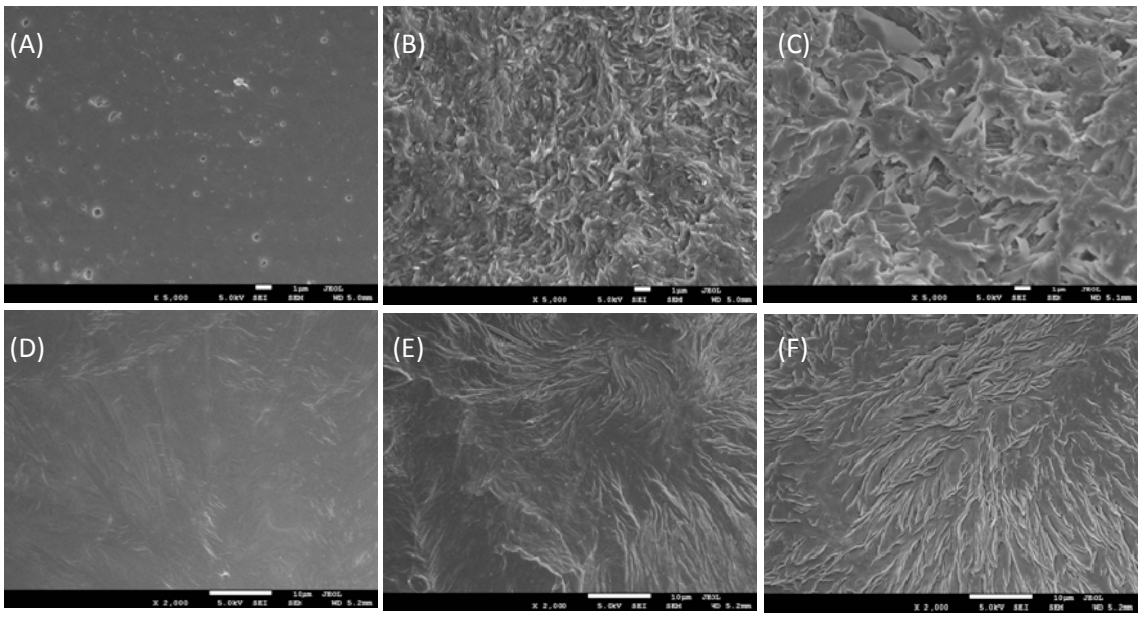

Figure 10. SEM pictures of polyester-5,7 and PCL films during degradation; (A) Polyester-5,7 before degradation (B) after 8h (C) after 22h of degradation; (D) PCL before degradation (E) after 8h (F) after 22 h of degradation.

SEM was used to investigate the surface morphological changes during degradation. The scanning electron micrographs of polyester before and after degradation are shown in the Fig. 10. Degradation led to the surface erosion and fibrillar and sponge like structures were observed. The SEM characterization of cross section of the polyester film before and after 22 h degradation in lipase was also done. The morphology after 22 h degradation remained same as before degradation, which showed degradation was by surface erosion. The degradation behavior observed for polyesters was almost same as observed for polycaprolactone except its fast rate of enzymatic degradation.

4. Conclusions

Enzymatic polyester-5,7 based on pimelic acid and 1,5-pentanediol was successfully synthesized by polycondensation in the melt. The chemical structure and composition of the polyester was confirmed by 1D and 2D NMR techniques like ^{1}H, ^{13}C, HMQC and HMBC. The polyester-5,7 was found to have similar crystal structure and degradation mechanism as PCL but with fast degradation rate. The enzymatic degradation products are mainly composed of low molecular weight oligomers and diols and diacids. The degradation was started in the amorphous region and on the surface with change in surface morphology. Initial studies regarding hydrolytic degradation under physiological conditions showed similar trend like PCL and detailed studies at different pH values are in progress. Such aliphatic polyesters are highly promising for various applications where PCL is currently being used with the advantage of having fast enzymatic degradation rate like degradable glue, packaging etc. The degradation under conditions closer to animal organisms will come up later on. Once the time of hydrolytic degradation under physiological conditions is also established, it would be another addition to the class of degradable aliphatic polyesters having its own profile for different biomedical applications.

References

1. S. Agarwal, M. Puchner, A. Greiner and J. H. Wendorff, *Polym. International* **54 (10)**, 1422 (2005).
2. S. Agarwal and X. Xie, *Macromolecules* **36(10)**, 3545 (2003).
3. K. Ito, Y. Hashizuka and Y. Yamashita, *Macromolecules* **10**, 821 (1977).
4. G. Z. Papageorgiou, D. S. Achilias and D. N. Bikiaris, *Macromol. Chem. Phys.* **210**, 90 (2009).
5. J. Su, A. Y. Chen and L. Tan, *J. Biomat. Sci.* **20**, 99 (2009).
6. W. H. Carotehrs, *J. Am. Chem. Soc.* 51, 2548 (1929).
7. J. J. Ihn, E. S. Yoo and S. S. Im, *Macromolecules* **28**, 2460 (1995).
8. T. Miyata and T. Masuko, *Polymer* **39**, 1399 (1998).
9. Z. Gan, H. Abe and Y. Doi, *Biomacromolecules* **1**, 704 (2000).
10. Z. Qiu,T. Ikehara and T. Nishi, *Polymer* **44**, 5429 (2003)**.**
11. Z. George and D. N. Bikiaris, Polymer **46**, 12081 (2005).
12. D. Bhaumik and J. E. Mark, Makromol. Chem. **187**,1329 (1986).
13. G. Z. Papageorgios and D. N. Bikiaris, Polymer **46**, 12081 (2005).
14. J. P. Bell, S. J. Huang and J. R. Knox, U.S. NTIS, AD-A Rep No 009577 (1974).
15. I. Tabushi, H. Yamada, H. Matsuzaki and J. Furukawa, J.Polym. Sci. Polym. Lett. Ed. **13**, 447 (**1975)**
16. T. Yutaka and T. Suzuki, Nature **270(3)** ,76 (1977)**.**
17. M. Mochizuki, K. Mukai, K. Yamada, N. Ichsi, S. Murase and Y. Iwaya, Macromolecuels **30**, 7403 (1997).
18. D. Bhaumik and J. E. Mark, *Makromol. Chem.* **187**, 1329 **(1986)**.
19. V. V. K0rshak, S. V, Vinogradova, and E. S. Vlasova, *Russian Chem. Bull.* **3(6),** 957 (1954).
20. A. Cao, T. Okamur, C. Ishiguro, K. Nakayama, Y. Inoue and T. Masuda, Polymer **43**, 671 (**2002)**,

21. D. N. Bikiaris, G. Z. Papageorgiou and D. S. Achilias, *Polymer Deg. Stability* **91(1)**, 31 (**2006).**

22. S. Wietzke, C. Jansen, T. Jung, M. Reuter, B. Baudrit, M. Bastian, S. Chatterjee and M. Koch, *Optics Express* **17(21)**, 19006 (2009).

23. J. P. Laib and D. M. Mittleman, *J. Infrared Milli. Terahz. Waves* **31(9)**, 1015 **(2010)**.

24. R. B. Beevers, *J. Polym. Sci.: Polym. Phy. Ed.* **12(7)**, 1407 (1974).

25. S. Wietzke, C. Jansen, C,M. Reuter, T. Jung, T, J. Hehl, D.Kraft, S. Chatterjee, A. Greiner and M. Koch, *Applied Physics Letters* **97(2)**, 022901 (2010).

8.4 Publication "Nanofibers by Green Electrospinning of Aqueous Suspensions of Biodegradable BlockCopolyesters for Application in Medicine, Pharmacy and Agriculture"

Jinyuan Sun, Kathrin Bubel, ***Fei Chen***, Thomas Kissel, Seema Agarwal, Andreas Greiner*, Nanofibers by Green Electrospinning of Aqueous Suspensions of Biodegradable Block Copolyesters for Applications in Medicine, Pharmacy and Agriculture, *Macromol. Rapid Commun*. 2010, 31, 2077–2083

Macromolecular Journals

Macromolecular Rapid Communications

Nanofibers by Green Electrospinning of Aqueous Suspensions of Biodegradable Block Copolyesters for Applications in Medicine, Pharmacy and Agriculture

Jinyuan Sun, Kathrin Bubel, Fei Chen, Thomas Kissel, Seema Agarwal, Andreas Greiner*

Poly(hexamethylene adipate)-PEO block copolymers (PHA-*b*-PEO) with different PEO contents were synthesized and processed to aqueous suspensions with high solid contents by a solvent displacement method followed by dialysis. The best suspension displayed a solid content of 16 wt.-% and an average particle size of 108 nm. This suspension was mixed with a small amount of high molecular weight PEO and Brij78 and electrospun into corresponding nanofibers. After extraction with water, nanofibers of PHA-*b*-PEO were obtained. Electrospinning of aqueous suspensions of biodegradable polyesters alleviates concerns regarding safety, toxicology and environmental problems, which are associated with spinning of such polyesters from harmful organic solvents and thereby offers novel perspectives for applications in medicine, pharmacy and agriculture. Electrospinning of polymers from aqueous suspensions avoiding harmful organic solvents is suggested to be "green electrospinning".

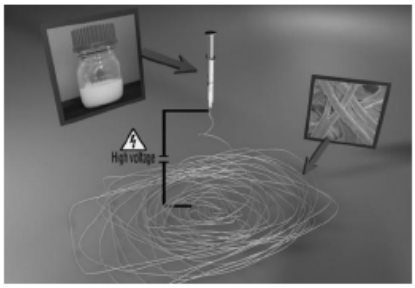

Introduction

Electrospinning has matured into a highly versatile method for the preparation of polymer nanofiber-based non-wovens.[1–6] Nanofiber non-wovens from biodegradable polymers are of particular interest for potential applications in medicine, drug delivery and agriculture. Biomedical applications of such non-wovens comprise scaffolds for tissue engineering[7–13] and drug eluting wound dressings.[14–16] Applications of nanofibers in agriculture could include biotechnical plant protection by release of insect pheromones.[17] Among other polymers, mainly aliphatic polyesters have been used as biodegradable polymers for nanofiber preparation by electrospinning. Poly(ε-caprolactone) (PCL),[18–19] polylactide (PLA)[20] and block copolymers of polyester-poly(ethylene oxide)[21–23] are representative examples of biodegradable aliphatic polyester which have been processed into nanofibers by electrospinning. All these polymers have the fact that they are soluble in harmful organic solvents only in

J. Sun, K. Bubel, F. Chen, S. Agarwal, A. Greiner
Philipps-Universität Marburg, Department of Chemistry and Scientific Centre for Materials Science, Hans-Meerwein-Strasse, Geb. H, D-35032 Marburg, Germany
E-mail: greiner@mailer.uni-marburg.de
T. Kissel
Philipps-Universität Marburg, Department of Pharmacy, Institute of Pharmaceutics and Biopharmacy, Ketzerbach 63, D-35032 Marburg, Germany

Macromol. Rapid Commun. 2010, *31*, 000–000

DOI: 10.1002/marc.201000379

common, limiting their utility for actual biomedical and agricultural applications. The high viscosities of the polymer solutions, even for low weight % polymer solutions, prevent high polymer concentrations and thereby limits the productivity of the electrospinning process (generally, for conventional electrospinning, a maximum of 10 – 15 wt.-% polymer solution has to be used). Recently, it has been demonstrated by some of us that polystyrene and polyacrylates can be processed from water by latex suspension (solid content about 25%) electrospinning in the presence of a small amount of a water soluble polymer.[25,26] Extraction of the resulting nanofibers with water yields stable nanofibers of polystyrene or polyacrylates. "Green electrospinning",[24] which could be defined as an approach which would alleviate concerns regarding safety, toxicology and environmental problems, could be accomplished by electrospinning from aqueous suspensions. In addition, "green electrospinning" would also overcome the restrictions of too high polymer concentrations of polymer solutions as aqueous suspensions, as mentioned above, allowing higher polymer concentrations (solid content) for the electrospinning process. Therefore, "green electrospinning" of biodegradable polyesters from aqueous suspensions could be a promising approach to overcoming the concerns about electrospinning from organic solvents.

Aqueous suspensions of biodegradable polyesters, e.g., PLA nanoparticles, are well known.[27,28] Suspensions of PLA nanoparticles are obtained as secondary suspensions, for example, by solvent displacement methods and emulsion, double emulsion and salting out methods.[29,30] The method selected is dependent on the size and loading efficiency required for different biomedical applications. These secondary suspensions generally have a very low solid content; for example, previously some of us reported a 1% solid content of sulfobutylated poly[(vinyl alcohol)-*co*-glycolide] made by the solvent displacement method.[31] To the best of our knowledge, there are no efforts in the literature to increase the solid content of aqueous secondary suspensions of biodegradable polymers, although this could be of interest for the processing of such polymers. Recently, secondary aqueous suspensions of dye loaded PLA nanoparticles were electrospun along with poly(vinyl alcohol) (PVA) or poly(ethylene oxide) (PEO) to yield "nano in nano" composite fibers, which are of interest as a novel drug eluting system with retarded release profiles.[32] However, later attempts to remove PVA and PEO by extraction of such composite fibers with water to obtain PLA nanofibers failed as the complete disintegration of the fibers occurred. This was most likely due to the fact that the interaction between PLA nanoparticles and their overall concentration in the composite fibers was too low. Therefore, there is a need to develop a novel concept that will allow processing of biodegradable polyester by "green electrospinning" from water yielding water stable polyester nanofibers. This in turn requires the development of a high solid content polyester suspension in water where the melting point of the polyester blocks should be relatively low. Our concept is that the polyester should be well dispersible in water by having hydrophilic segments and that the melting point of the polyester blocks should be relatively low. Nanofibers consisting of spherical polyester suspension particles with low melting points should result in blending of the particles and thereby mechanical stabilization of the nanofibers as has been observed before for polyacrylate nanofibers.[26] It is well known that the hydrophilicity of polyester can be increased by block copolymerization with PEO, which has been shown, e.g., for PLA-PEO or PCL block copolymers.[21,34] Due to the high melting point and the above mentioned trials with PLA nanoparticles, PLA-containing block copolymers are not suitable for our goals. Polyesters like PCL or polyadipates show melting points typically below 70 °C. Therefore, we selected poly(hexamethylene adipate)-PEO block copolymers (PHA-*b*-PEO) as suitable candidates for suspension electrospinning.

In this contribution we present the synthesis of PHA-*b*-PEO diblock copolymer, the preparation of high solid content aqueous suspensions of PHA-*b*-PEO by secondary suspension, and their processing into water stable polyester nanofibers by the electrospinning of these suspensions, which is claimed here to be "green electrospinning".

Table 1. Educts and yields for the synthesis of poly[(hexamethylene adipate)-*block*-(methoxypolyethylene oxide)] (PHA-*b*-PEO).

Substance	PHA-PEO-1	PHA-PEO-2	PHA-PEO-3
Adipic acid g ($\times 10^{-3}$ mol)	2.503 (17.1)	2.501 (17.1)	2.505 (17.1)
1,6-hexanediol g ($\times 10^{-3}$ mol)	2.028 (17.2)	2.023 (17.1)	2.027 (17.2)
α-hydroxy-ω-methoxy-PEO g	0.384	0.763	1.523
Polyphosphoric acid Mg	8.5	6.5	6.7
Molar ratio in feed (PEO: PHA)	1:2	1:1	2:1
Yield (related to adipic acid) %	85	87	88

Macromol. Rapid Commun. **2010**, *31*, 000–000

Macromolecular Journals
DOI: 10.1002/marc.201000379

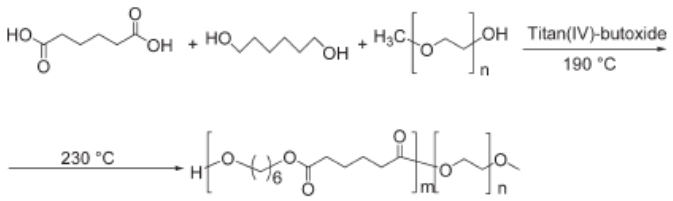

Scheme 1. Synthesis of poly[(hexylene adipate)-*block*-(methoxypolyethylene oxide)] (PHA-*b*-PEO).

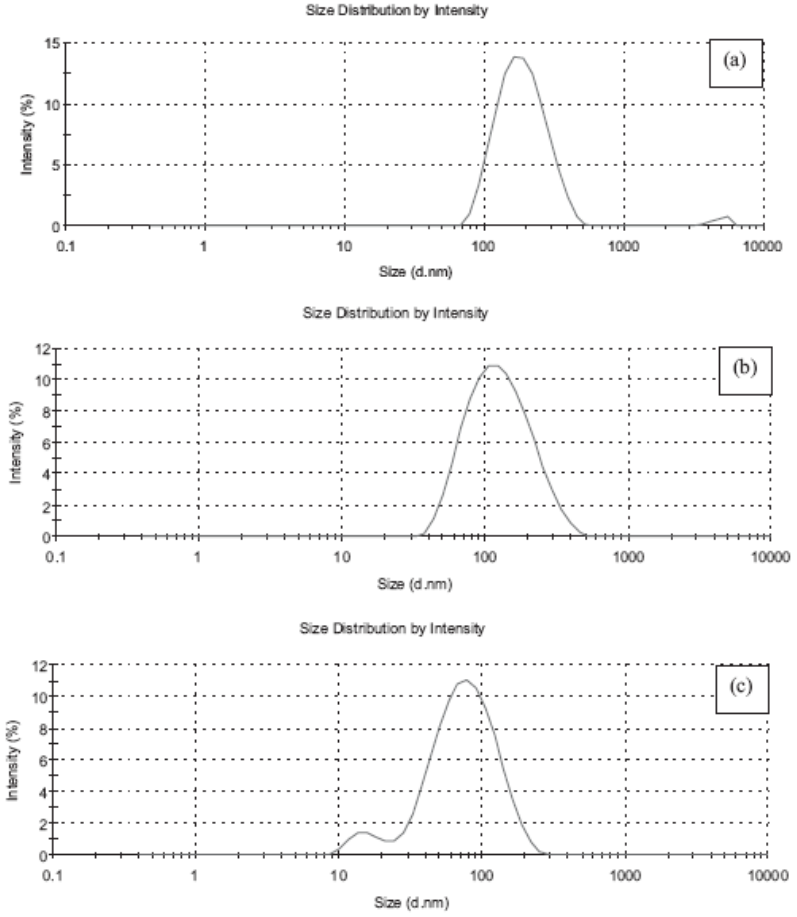

Figure 1. Particle size versus intensity (%) by dynamic light scattering of aqueous suspensions of 2.32 wt.-% (PHA-*b*-PEO-1) (a), 2.94 wt.-% (PHA-*b*-PEO-2) (b), and 2.96 wt.-% (PHA-*b*-PEO-3) (c).

Experimental Part

Materials

Adipic acid (Aldrich) was purified by recrystallization. 1,6-hexandiol (Aldrich) was purified by vacuum distillation. α-Hydroxy, ω-methoxy-PEO ($\overline{M}_w = 5\,000$), titanium (IV) butoxide, Brij78 and poly(vinyl alcohol) (PVA) were used as received (Aldrich). Acetone was distilled prior use. Deionized water was used for suspensions.

Measurements and Equipment

Infrared spectroscopy (IR) was performed by means of a Digilab (Excalibur series) instrument with ATR crystal ZnSe and WinIRPro software version 3.3. ^{1}H and ^{13}C NMR spectroscopy was carried out using a Bruker ARX300 spectrometer in $CDCl_3$ solution and the software MestRec version 4.9.9.6. Gel permeation chromatography (GPC) was completed in THF using a PSS-SDV pre-column (10 μm) and 2 PSS SDV linear columns at 20 °C at a flow rate of 0.8 mL · min^{-1} and Win GPC software. Differential scanning calorimetry (DSC) was carried out on a Mettler Toledo DSC 821c using heating/cooling rates of 10 K · min^{-1} under an N_2 atmosphere. Evaluation was done with 2 heating runs and STARe software. Dynamic light scattering for particle size analysis was carried out on a Malvern Zetasizer from Malvern. Ultrasound treatment was performed with an ultrasonic device (Bandelin electronic UW 60, Bandelin Sonoplus HD 60 adapter, power 30 W). For dialysis, Spectra Por dialysis tubes, MWCO = 10 000 (Roth) were used. The dialysis tubes were pre-cleaned by treatment with deionized water for 20 min. Electrospinning was completed using a previously described set-up.[35]

Synthesis of Poly[(hexamethylene adipate)-*block*-(methoxypolyethylene oxide)] (PHA-*b*-PEO)

Adipic acid, 1,6-hexanediol and α-hydroxy-ω-methoxy-PEO were filled under an argon atmosphere in the given amounts (Table 1) into a flame-dried 3-necked flask equipped with a distilling head, a Stutz-bubbler, a septum and a stirring bar. 5 μL of titanium butoxide (catalyst) were injected using a syringe through the septum. The mixture was heated to 190 °C for 3 h until most of the water was distilled off. Subsequently, polyphosphoric acid (which prevents side reactions and thermal decomposition) was added and the mixture was heated to 230 °C and subjected to a vacuum (0.4 mbar) for 40 h. After cooling to room temperature, the mixture was dissolved in 100 mL of THF, precipitated in 1 L of *n*-hexane and dried in a vacuum at 20 °C until the weight remained constant.

PHA-*b*-PEO-1

^{1}H NMR ($CDCl_3$): $\delta = 1.34 - 1.39$ (m), 1.60 – 1.67 (m), 2.31 (t), 3.64 (s), 4.05 (t). ^{13}C NMR ($CDCl_3$): $\delta = 24.39$, 25.57, 28.5, 33.89, 64.27 70.55 (Ce-PEG), 173.37. IR: 2 938, 2 866, 1 726, 1 258, 1 161 cm^{-1}. GPC: $\overline{M}_n = 13\,400$ g · mol^{-1}, $\overline{M}_w = 25\,000$ g · mol^{-1}, $\overline{M}_w/\overline{M}_n = 1.9$. DSC: $T_m = 56$ °C, $T_g = -56$ °C.

PHA-*b*-PEO-2

^{1}H NMR ($CDCl_3$): $\delta = 1.34 - 1.39$ (m), 1.60 – 1.67 (m), 2.31 (t), 3.64 (s), 4.05 (t). ^{13}C NMR ($CDCl_3$): $\delta = 24.39$, 25.57, 28.5, 33.89, 64.27,

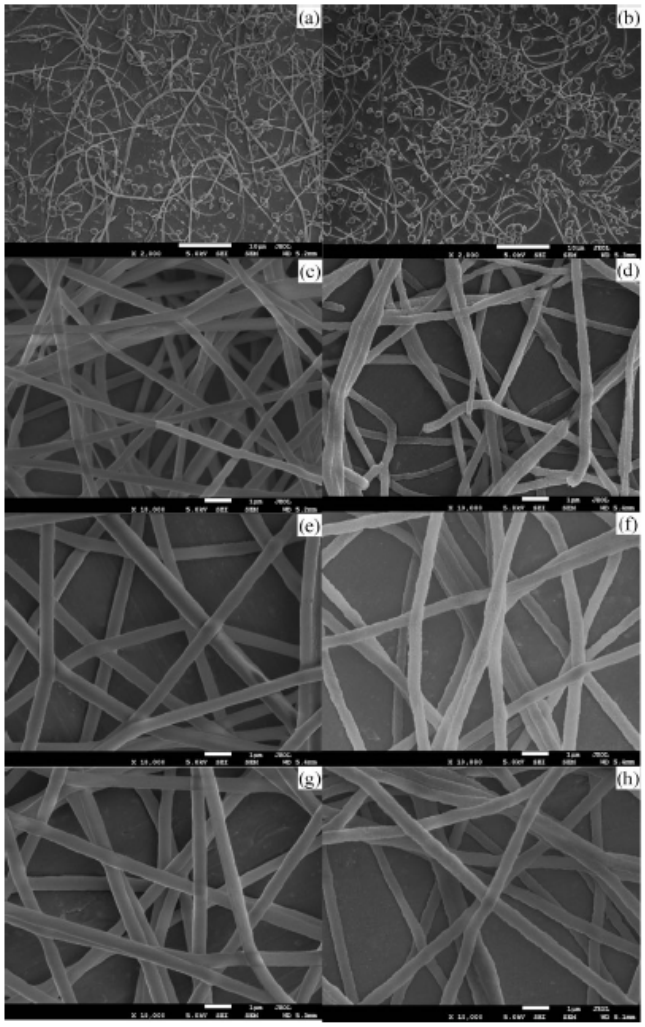

Figure 2. SEM of electrospun fibers of PHA-*b*-PEO-2b with PEO, before water treatment 1% PEO (a), 2% PEO (c), 3% PEO (e), 4% PEO (f)) and the corresponding fibers after water treatment for 2 d at 25 °C (b, d, f, h).

Macromol. Rapid Commun. **2010**, *31*, 000–000

Macromolecular Journals
DOI: 10.1002/marc.201000379

70.55, 173.37. IR: 2938, 2867, 1727, 1258,1161 cm^{-1}. GPC: $\overline{M}_n = 10\,800$ g·mol^{-1}, $\overline{M}_w = 26\,500$ g·mol^{-1}, $\overline{M}_w/\overline{M}_n = 2.4$. DSC: $T_m = 52$ °C, $T_g = -57$ °C.

PHA-PEO-3

^{1}H NMR ($CDCl_3$): $\delta = 1.35 - 1,39$ (m), 1.62 – 1.65 (m), 2.31 (t), 3.63 (s), 4.04 (t). ^{13}C NMR ($CDCl_3$): $\delta = 24.38, 25.56, 28.49, 33.87, 64.26, 70.54, 173.35$. IR : 2937, 2867, 1727, 1258,1161,1107. GPC: $\overline{M}_n = 6100$ g·mol^{-1}, $\overline{M}_w = 12\,600$ g·mol^{-1}, $\overline{M}_w/\overline{M}_n = 2.1$. DSC: $T_m = 54$ °C, $T_g = -61$ °C.

Suspension of PHA-*b*-PEO in Water

0.5 g of PHA-*b*-PEO-2 was dissolved in 12.5 mL of acetone. After addition of a solution of 20 mL of water and 0.05 g Brij78, the mixture was subjected to ultrasound for 4 min. The resulting suspension was purged under a mild air stream at 20 °C to remove the acetone. Complete removal of acetone was verified by ^{13}C NMR analysis.

Preparation of PHA-*b*-PEO-2b by Up-concentration via Dialysis of PHA-*b*-PEO-2

A larger batch of a new aqueous suspension of PHA-*b*-PEO (2.5 wt.-% of PHA-*b*-PEO-2, $\overline{M}_n = 6\,400$, $\overline{M}_n/\overline{M}_w = 2.1$, particle size 108 nm) was used for the up-concentration by dialysis. 500 mL of the suspension were filled in a dialysis tube with a length of 15 cm and placed in 6 L of an aqueous solution of PVA (15 wt.-%). After 100 h, the tube was removed from the PVA solution and rinsed with water and dried. The solid content of PHA-*b*-PEO-2b was obtained by freeze drying and weighing.

Electrospinning of PHA-*b*-PEO with Varying Amounts of PEO

PHA-*b*-PEO-2b was mixed with different amounts of PEO (see Figure 2) and electrospun, applying a feed of 0.05 mL·min^{-1}, an electrode distance of 15 cm and a voltage of 15 kV. Aluminum foil was used a substrate for collecting the electrospun fibers.

Results and Discussion

Polyester Synthesis

Based on some initial attempts with di- and triblock copolyesters and polyethylene oxides of different molecular weights and the above mentioned hypothetical considerations, we selected diblock copolyesters consisting of PHA and α-hydroxy-ω-methoxy-PEO as a candidate for water-based suspension. The synthesis of the diblock copolyesters was performed by melt polycondensation, as shown in Scheme 1.

The theoretical amounts of PEO and PHA were varied between molar ratios of 1:2 (PHA-*b*-PEO-1), 1:1 (PEO-*b*-PHA 2) and 2:1 (PEO *b* PHA 3). The expected chemical structure of PHA-*b*-PEO was confirmed by ^{1}H NMR, ^{13}C NMR and IR spectroscopy. The experimental ratios of PHA and PEO were analyzed by ^{1}H NMR spectroscopy by comparing the integration of $-OCH_2$ protons of PEO at 3.55 ppm and $-OCH_2$ protons of PHA at 4.0 ppm, and were in good agreement with the theoretical ratios. Molecular weights, as obtained by THF-GPC, ranged from $\overline{M}_n = 13\,400$ ($\overline{M}_w/\overline{M}_n = 1.9$) for PHA-*b*-PEO-1, to $\overline{M}_n = 10\,800$ ($\overline{M}_w/\overline{M}_n = 2.4$) for PHA-*b*-PEO-2, and $\overline{M}_n = 6\,100$ ($\overline{M}_w/\overline{M}_n = 2.1$)) for PHA-*b*-PEO-3. The melting point of the block copolyester PHA-*b*-PEO-2 was found at 58 °C. No signals were found in the DSC for pure α-hydroxy-ω-methoxy-PEO ($T_m = 66$ °C).

Preparation and Characterization of Suspensions

The PHA-*b*-PEO was dissolved in acetone. After addition of a solution of water and Brij78, ultrasound was applied. Finally, acetone was removed by slow evaporation under a mild air stream at 20 °C. Following this procedure, milky aqueous suspensions without any precipitation were obtained with contents of 2.92 wt.-% (PHA-*b*-PEO-1), 2.94 wt.-% (PHA-*b*-PEO-2) and 2.96 wt.-% (PHA-*b*-PEO-3) which was stable at room temperature for at least

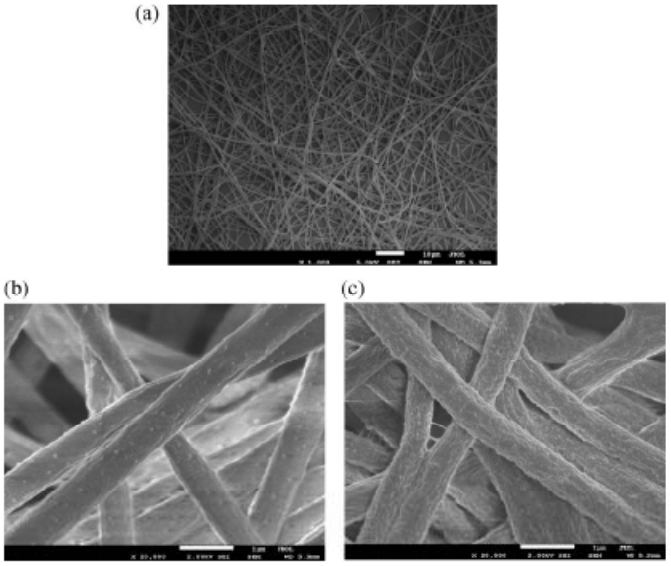

Figure 3. SEM of electrospun fibers of PHA-*b*-PEO-2b with 4% PEO, after (a) water treatment (b) and (c) are before and after water treatment for 2 d at 25 °C at higher magnification.

10 d. Analysis of the particle diameter by dynamic light scattering showed average particle diameters of 177 nm for PHA-*b*-PEO-1, 112 nm for PHA-*b*-PEO-2 and 61 nm for PHA-*b*-PEO-3, and bimodal particle size distributions for PHA-*b*-PEO-1 and PHA-*b*-PEO-3 but a monomodal distribution for PHA-*b*-PEO-2 (Figure 1).

All of the suspensions were of too low a solid content to be useful for nanofiber preparation by suspension electrospinning. However, suspensions of PHA-*b*-PEO-2 were selected as a promising candidate (due to their monomodal particle size distribution) for achieving higher concentrated suspensions using dialysis in analogy to ref. [36] PVA (15 wt.-% in water) was used instead of dextrane and a larger batch of PHA-*b*-PEO-2 ($\overline{M}_n = 6\,400$, $\overline{M}_w/\overline{M}_n = 2.1$, 2.5 wt.-%, aqueous suspension with Brij78, average particle size = 108 nm, monomodal). Due to the osmotic pressure difference, a constant weight loss of the original suspension in the dialysis tubes was measured within 100 h, resulting in a corresponding aqueous suspension of 16 wt.-% PHA-*b*-PEO-2 (PHA-*b*-PEO-2b). This milky suspension did not show visible precipitation and displayed an average particle diameter of 108 nm by dynamic light scattering.

Electrospinning Experiments

As mentioned before, water soluble polymers are required as template polymers for suspension electrospinning. Electrospinning of PHA-*b*-PEO-2b with poly(vinylpyrrolidone), PVA and PEO showed the best results in terms of spinnability and fiber shape with high molecular weight PEO ($\overline{M}_w = 900\,000$). Therefore, electrospinning of PHA-*b*-PEO-2b was completed with different amounts of PEO relative to PHA-*b*-PEO-2b. After electrospinning, the composite fibers were treated with water in order to test the water stability of the fibers. Fiber diameters of the as spun fibers ranged from 350 to 550 nm (Figure 2(a), 2(c), 2(e) and 2(g)). After treatment with water at 20 °C for 24 h, the fibers with 3% and 4% PEO showed no sign of swelling or disintegration (Figure 2(b), 2(d), 2(f), 2(h)). The fiber surfaces of the as spun fibers (Figure 3(b)) appeared to be somewhat smoother than the corresponding fibers after water treatment (Figure 3(c)). However, no particles resulting from the suspension could be identified after water treatment. Obviously, the suspension particles of PHA-*b*-PEO-2b were smoothened during fiber formation, which was also reported for polyacrylate fibers upon suspension electrospinning.[26]

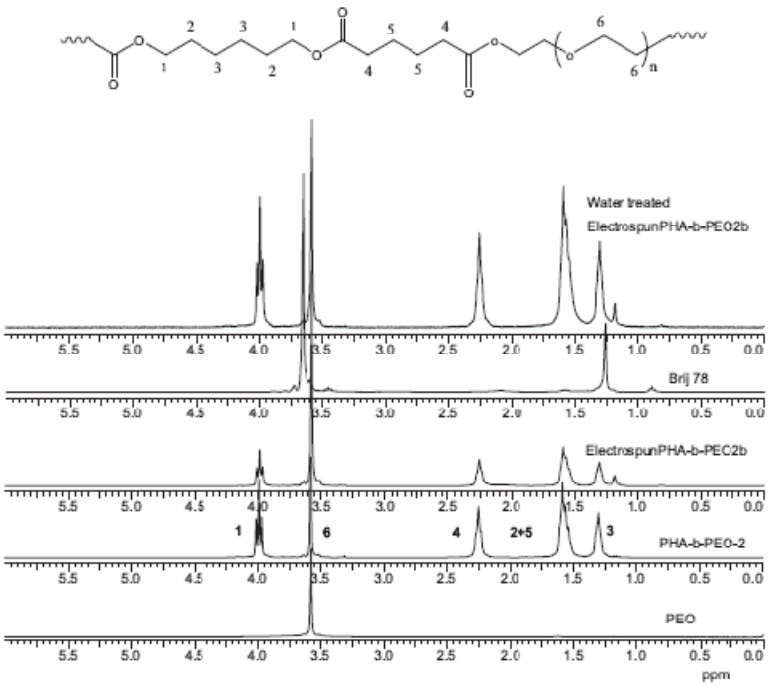

Figure 4. ^{1}H NMR spectra of PEO, PHA-*b*-PEO-2, electrospun PHA-b-PEO2b, Brij78 and water treated fibers of PHA-*b*-PEO2b in $CDCl_3$.

Macromol. Rapid Commun. **2010**, *31*, 000–000

DOI: 10.1002/marc.201000379

As spun fibers and water treated fibers were also analyzed with ^{1}H NMR spectroscopy (Figure 4). The presence of PHA-*b*-PEO-2 was clearly proven by ^{1}H NMR spectroscopy in as spun fibers and water treated fibers (Figure 4). PEO 900 000 and Brij78 were identified in the as spun fibers in the expected amounts but no trace of this PEO and Brij78 were found in the water treated fibers, thereby showing the complete removal of PEO and the surfactant. This also proved the success of the concept of making stable biodegradable nanofiber non-wovens from secondary water suspensions free of additives like surfactants and additional template polymers.

Conclusion

Biodegradable block copolyester with PEO blocks can be dispersed in water to concentrations of about 2 wt-%. Solid contents of suspensions up to 16% were realized by dialysis. However, this could be optimised, which is the topic of present work. These high solid content suspensions can be processed into corresponding block copolyester nanofibers when a small amount of PEO is added. The resulting fibers do not show any short term disintegration upon contact with water and are free of additives like surfactants and additional template polymers. This type of aqueous polyester formulation will open up many perspectives for water-based electrospinning, coined as "green electrospinning", resulting in water stable non-wovens. Surely this type of formulation could also be useful for other processing techniques as well, e.g., film preparation and coatings. With this new aqueous formulation, progress in applications in medicine, pharmacy and agriculture can be pushed further.

Acknowledgements: The authors are indebted to *T. Lebhardt* for support with dynamic light scattering, to *R. Agarwal* for technical support (and preparation of the Table of Contents figure) and to *BMBF (project Nanofatex)* and *DFG* for financial support.

Received: June 22, 2010; Revised: August 9, 2010; Published online: DOI: 10.1002/marc.201000379

Keywords: biodegradable; block copolymers; fibers; nanotechnology; polyesters

[1] D. H. Reneker, I. Chun, *Nanotechnology* 1996, *7*, 216.
[2] A. Greiner, J. H. Wendorff, *Angew. Chem., Int. Ed.* 2007, *46*, 5670.
[3] W. E. Teo, S. Ramakrishna, *Nanotechnology* 2006, *17*, R89.
[4] D. Li, Y. Xia, *Adv. Mater.* 2004, *16*, 1151.
[5] D. H. Reneker, A. L. Yarin, *Polymer* 2008, *49*, 2387.
[6] S. Agarwal, A. Greiner, J. H. Wendorff, *Adv. Funct. Mater.* 2009, *19*, 2863.
[7] P. Zhao, H. Jiang, H. Pan, K. Zhu, W. Chen, *J. Biomed. Mater. Res., Part A* 2007, *83*, 372.
[8] J. Ji, K. Ghosh, B. Li, J. C. Sokolov, R. A. F. Clark, M. H. Rafailovich, *Macromol. Biosci.* 2006, *6*, 811.
[9] N. Ashammakhi, A. Ndreu, A. M. Piras, L. Nikkola, T. Sindelar, H. Ylikauppila, A. Harlin, M. E. Gomes, N. M. Neves, F. Chiellini, V. Hasirci, H. Redl, R. L. Reis, *J. Nanosci. Nanotechnol.* 2007, *7*, 862.
[10] A. S. Scott, G. L. Bowlin, *J. Mater. Chem.* 2008, *18*, 260.
[11] S. Agarwal, J. H. Wendorff, A. Greiner, *Adv. Mater.* 2009, *21/32*, 3343.
[12] S. Agarwal, J. H. Wendorff, A. Greiner, *Polymer* 2008, *49*, 5603.
[13] U. Boudriot, R. Dersch, A. Greiner, J. H. Wendorff, *Artificial Organ.* 2006, *30*, 785.
[14] E. R. Kenawy, G. L. Bowlin, K. Mansfield, J. Layman, D. G. Simpson, E. H. Sanders, G. E. Wnek, *J. Controlled Release* 2002, *81*, 57.
[15] X. H. Zong, K. Kim, D. F. Fang, S. F. Ran, B. S. Hsiao, B. Chu, *Polymer* 2002, *43*, 4403.
[16] P. Sikareepaisan, A. Suksamrarn, P. Supaphol, *Nanotechn.* 2008, *19*, 1.
[17] C. Hellmann, A. Greiner, J. H. Wendorff, *Polym. Adv. Techn.* 2010, in press DOI: 10.1002/pat.1532.
[18] D. H. Reneker, W. Kataphinan, A. Theron, E. Zussman, A. L. Yarin, *Polymer* 2001, *43*, 6785.
[19] K. H. Lee, H. Y. Kim, M. S. Khil, Y. M. Raand, D. R. Lee, *Polymer* 2003, *44*, 1287.
[20] J. P. Jeum, Y. H. Kim, Y. M. Lim, J. H. Choi, C. H. Jung, P. H. Kang, Y. C. Nho, *J. Ind. Eng. Chem.* 2007, *13*, 592.
[21] K. Kim, M. Yu, X. Zong, J. Chiu, D. Fang, Y.-S. Seo, B. S. Hsiao, B. Chu, M. Hadjiargyrou, *Biomaterials* 2003, *24*, 4977.
[22] D.-J. Yang, L.-F. Zhang, X. Liang, C.-D. Xiong, D. Jing, Y.-Z. Wang, *J. Biomed. Mater. Res., Part A* 2007, *82*, 680.
[23] P. D. Dalton, J. L. Calvet, K. Ahmed, M. Moeller, *Biotechn. J.* 2006, *1*, 998.
[24] The term "Green Electrospinning" was first used, to the best of our knowledge, in: R. Krishnan, J. Venugopal, S. Sundarrajan, S. Ramakrishna, *14th European Conference on Composite Materials*, ECCM14, 7-10 June, 2010, Budapest, Hungary
[25] A. Stoiljkovic, M. Ishaque, U. Justus, L. Hamel, E. Klimov, W. Heckmann, B. Eckhardt, J. H. Wendorff, A. Greiner, *Polymer* 2007, *48*, 3974.
[26] A. Stoiljkovic, R. Venkatesh, E. Klimov, V. Raman, J. H. Wendorff, A. Greiner, *Macromolecules* 2009, *42*, 6147.
[27] Z. Hou, H. Wei, Q. Wang, Q. Sun, C. Zhou, C. Zhan, X. Tang, Q. Zhang, *Nanoscale Res. Lett.* 2009, *4*, 732.
[28] T. H. Thi, M. Matsusaki, M. Akashi, *Langmuir* 2009, *25*, 10567.
[29] I. Bala, S. Hariharan, M. Kumar, *Crit. Rev. Ther. Drug Carrier* 2004, *21*, 387.
[30] O. A. O. Abbas, M. D. Donovan, K. Salem, *J. Pharmaceutical Sci.* 2008, *97*, 2448.
[31] T. Jung, A. Breitenbach, T. Kissel, *J. Controlled Release* 2000, *67*, 157.
[32] M. Beck-Broichsitter, M. Thieme, J. Nguyen, T. Schmehl, T. Gessler, W. Seeger, S. Agarwal, A. Greiner, T. Kissel, *Macromol. Bioscience*, 2010, DOI: 10.1002/mabi.201000100.
[33] D. Cohn, H. Younes, *J. Biomed. Mater. Res.* 1988, *22*, 993.
[34] J. Kang, K. J. Beers, *Biomacromolecules* 2006, *7*, 453.
[35] M. Bognitzki, H. Hou, M. Ishaque, T. Frese, M. Hellwig, C. Schwarte, A. Schaper, J. H. Wendorff, A. Greiner, *Adv. Mater.* 2000, *12*, 637.
[36] C. Vauthier, B. Cabane, D. Labarre, *European J. Pharma. Biopharma* 2008, *69*, 466.

8.5 Publication "Low dielectric constant polyimide nanomats by electrospinning"

Fei Chen, Debaditya Bera, Susanta Banerjee*, Seema Agarwal*, Low dielectric constant polyimide nanomats by electrospinning, *Polymers for Advanced Technologies*, **2011**, early view online.

Research Article

polymers advanced technologies

Received: 09 February 2011, Revised: 25 March 2011, Accepted: 26 March 2011, Published online in Wiley Online Library: 2011

(wileyonlinelibrary.com) DOI 10.1002/pat.1997

Low dielectric constant polyimide nanomats by electrospinning

Fei Chen[a], Debaditya Bera[b], Susanta Banerjee[b]* and Seema Agarwal[a]**

The proper combination of material (i.e. fluorinated polyimides) and processing technique (electrospinning) could lead to the formation of polyimides with low dielectric constant, high thermo-oxidative stability and glass transition temperature, and high hydrophobicity. The polyimides in this work were based on 4, 4-bis [3′-trifluoromethyl-4′ (4′-amino benzoxy) benzyl] biphenyl (O) and various fluorinated and non-fluorinated dianhydrides namely benzene-1,2,4,5-tetracarboxylic dianhydride, 3,3′,4,4′-biphenyltetracarboxylic dianhydride, benzophenone-3,3′,4,4′-tetracarboxylic dianhydride, and 4,4′-(hexafluoroisopropylidene)diphthalic anhydride (6FDA). Processing of the polyimides was carried out in poly[amic acid) stage by two different methods—electrospinning and solution casting for comparison purposes. The processing of polyimides by electrospinning led to enhancement in mechanical properties (dianhydride-structure dependent) and hydrophobicity without sacrificing thermo-oxidative stability and glass transition temperatures significantly. Also, low dielectric constants (as low as 1.43) could be attained by suitable combination of dianhydride (6FDA) with 4, 4-bis [3′-trifluoromethyl-4′ (4′-amino benzoxy) benzyl] biphenyl diamine.

Keywords: fluorinated polyimide; electrospinning; nanomats

INTRODUCTION

Polyimides (PIs) are an important class of materials for diversified applications like composites, insulators, dielectrics, coatings, and adhesives.[1–3] This class of polymers is known for their high glass transition temperature, high strength, and chemical resistance. The properties of PIs can be significantly altered by a small change in the structure of the dianhydride and diamine components.[4,5] For the use of PIs in microelectronic devices, the low dielectric constant is one of the important prerequisite. The dielectric constant of commercially available PIs like Kapton H (Dupont, Circleville, USA), Upilex-S (UBE Europe GmBH, Düsseldrof, Germany), ULTEM 1000 (GE plastics, North America) is around 3.1–3.5, which is at the higher side of the requirement. Also, the processing of these class of polymers, in general, is a problem. For example, both Kapton and Upilex are available as thermoset films. ULTEM 1000, a PI, is a melt-processable engineering resin with T_g = 218°C. However, its higher moisture absorption and lower continuous-use temperature limits its use for microelectronic industry. Therefore, there is a continuous search for low dielectric constant PIs having higher thermal and hydrolytic stability and better processability. In the recent years, several modifications in the molecular level by designing new monomers made processing of PIs possible in solution and in the melt.[6,7] PIs bearing trifluoromethyl or hexafluoroisopropylidine groups have been a subject of considerable interest to material chemists because the presence of these groups in the PI structure have been shown to cause significant improvements in their properties like thermal and hydrolytic stability over the corresponding non-fluorinated PIs.[8–12] The recent review article by one of us highlights the importance, synthesis, and properties of fluorinated PIs.[10] Haider *et al.*[13] and Chung *et al.*[11] studied the properties of fluorinated PIs for getting a low dielectric constant polymer. They showed that the incorporation of fluorine-containing monomers lowers the dielectric constant, but still the values were relatively high (around 3.0).

Recently, the use of electrospinning has been shown to make ultra-low dielectric constant (1.53–1.56) PI fibers based on pyromellitic dianhydride and diaminodiphenyl ether (Kapton).[14] There is no mention of hydrolytic and thermal stability of these fibers. Polymeric nanofibers can be processed by a number of techniques such as drawing, template synthesis, phase separation, self-assembly, and electrospinning. Among these techniques, electrospinning (continuous nanofibers) is of great interest because of its potentiality for industrial-scale processing and repeatability in control of fiber dimension. It is an enabling technology with applications in medical, pharmaceutical, chemical, textile, and electronic industries. The technique produces very fine, nanometer to micrometer diameter fibers.[15] Electrospinning of PIs was also used by Hou *et al.*[16–18] to make high-strength fibers. They used rod-like PIs poly(*p*-phenylene biphenyltetracarboximide), and the electrospun nonwoven fabric mats showed a tensile strength of more than 650 MPa and a tensile modulus of more than 15 GPa.

* *Correspondence to: S. Banerjee, Materials Science Centre, Indian Institute of Technology, Kharagpur 721302, India. E-mail: susanta@matsc.iitkgp.ernet.in*

** *Correspondence to: S. Agarwal, Fb. Chemie, Philipps-Universität Marburg, Hans-Meerwein Strasse, 35032, Marburg, Germany. Materials Science Centre, Indian Institute of Technology, Kharagpur 721302, India. E-mail: agarwal@staff.uni-marburg.de*

a *F. Chen, S. Agarwal*
Fb. Chemie, Philipps-Universität Marburg, Hans-Meerwein Strasse, 35032 Marburg, Germany

b *D. Bera, S. Banerjee*
Materials Science Centre, Indian Institute of Technology, Kharagpur 721302, India

With an aim to provide low dielectric constant PI membranes with good processability, high thermal stability, and low water absorption, we chose fluorinated PIs and used electrospinning for processing into nanomats. The PIs in this work were based on 4, 4-bis [3′-trifluoromethyl-4′ (4′-amino benzoxy) benzyl] biphenyl (Q) and various fluorinated and non-fluorinated dianhydrides (Scheme 1). The detailed characterization in terms of thermal stability, dielectric constant, and hydrophobicity is also reported. The combination of suitable materials and processing technique in this work provided highly stable, hydrophobic, and low dielectric constant PI mats.

EXPERIMENTAL PART

Materials

Benzene-1,2,4,5-tetracarboxylic dianhydride (PMDA) and benzophenone-3,3′,4,4′-tetracarboxylic dianhydride (BTDA) (Fluka, Germany) were purified by sublimation under reduced pressure. 4,4′-(Hexafluoroisopropylidene)diphthalic anhydride (6FDA) (99%) and 3,3′,4,4′ biphenyltetracarboxylic dianhydride (BPDA) (97%) were purchased from Aldrich chemical company and were heated at 180°C prior to use. Dimethylformamide (DMF) (Merck, Darmstadt, Germany) was purified by stirring with NaOH and distilled twice from P_2O_5 under reduced pressure. The monomer 4, 4-bis [3′-trifluoromethyl-4′ (4′-amino benzoxy) benzyl] biphenyl (Q) was synthesized as previously reported.[19] The compound was purified by column chromatography using dichloromethane as eluent.

Polymerization

The PIs were made in two steps. In the first step, an equimolar amount of diamine and dianhydride monomers was reacted under nitrogen atmosphere. A representative polymerization procedure is as follows: in a 100-ml round-bottomed flask equipped with a nitrogen inlet, a stirring bar was charged 2.23 g (3.396 mmol) of the diamine monomer (Q) and 21.2 ml of DMF. The solution was stirred until the diamine dissolved completely. After this, 0.741 g (3.396 mmol) of PMDA was added slowly to form 14 w/v % of solution. The resulting highly viscous solution was stirred slowly and continuously for 3 h at room temperature. The resulting poly(amic acid) solution was kept in freezer for later use. Using similar procedure, other poly(amic acid)s were also synthesized just by taking different dianhydrides. The resulting poly(amic acid)s were designated as Q-PMDA, Q-BPDA, Q-BTDA, and Q-6FDA. The second stage of PI formation, i.e. thermal imidization, of poly(amic acid) was carried out after electrospinning. This is described in the later part.

Fabrication of aligned nanofiber mats

The aligned nanofiber mats were made by the process of electrospinning in DMF using the poly(amic acid) synthesized earlier. The properties of the electrospinning solution are listed in Table 1. The average electrical field was 1 kV cm^{-1}, which was carried out by introducing a 15-kV electrical potential into a 15-cm gap from the spinneret to a drum-shaped collector (with diameter around 0.28 m), which rotated at a shear rate of 1000 s^{-1}. The as-electrospun nanofibers were collected as a mat of aligned nanofibers on the rotating drum.

Imidization of nanofiber mats

Imidization of the nanofiber mats was implemented within a tubular glass reactor at temperatures ranging from room

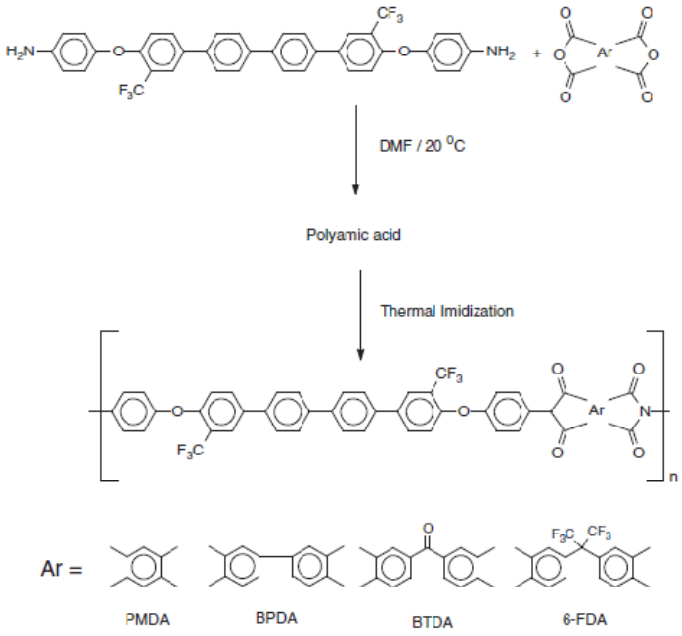

Scheme 1. Reaction scheme for the synthesis of poly(ether imide)s.

Table 1. Properties of poly(amic acid) solutions in dimethylformamide for electrospinning

Sample	Electrospinning solution concentration (w/v %)	Viscosity ($Pa\,s^{-1}$)	Electrical conductivity ($\mu s\,cm^{-1}$)
Q-PMDA	8	2.54	0.28
Q-BPDA	5	2.23	0.17
Q-BTDA	14	2.18	0.43
Q-6FDA	13	4.66	0.08

temperature to 300°C, with N_2 gas at a flow rate of 1 $ml\,min^{-1}$. This process follows the protocol: (i) heating up to 100°C at a rate of 2°C min^{-1} and holding at this temperature for 1 h to remove the residual solvent; (ii) heating up to 150°C at a rate of 2°C min^{-1} and annealing for 30 min; (iii) heating up to 200°C at a rate of 1°C min^{-1} and annealing for 30 min; (iv) heating up to 250°C at a rate of 1°C min^{-1} and annealing for 30 min; (v) heating up to 300°C at a rate of 1°C min^{-1} and annealing for 15 min to complete the imidization process and then cooling down to room temperature. The samples after imidization were designated as Q-PMDA-i, Q-BPDA-i, Q-BTDA-i and Q-6FDA-i.

Characterization

Infrared spectra of the poly(amic acid) and PI nanofiber mats samples were recorded by using a Digilab UMA 600 spectrophotometer (Krefeld, Germany) in the attenuated total reflectance mode. Images of the nanofiber mats were measured by using a JSM-7500 F scanning electron microscope (SEM) (JEOL GmbH, Eching, Germany) with a voltage of 5 kV, the dry mat was directly stuck on a conductive sample holder, and before measurement, all the samples were coated with a layer of platinum to increase conductivity. The mechanical properties of the PI nanofiber mats were measured using uniaxial tension tests on an electromechanical universal testing machine (model: Zwick/Roell (Ulm, Germany), type BT1-FRO.5TN.D14). All the tension tests were performed under the displacement-control mode at the constant cross-head speed of 20 $mm\,min^{-1}$. The samples for tensile testing were 8 mm in width and 60 mm in length. The thickness of the sample was calculated based on the sample weight and density of corresponding PI. For example, the weight of a piece of the PI nanofiber mat of $60 \times 10 \times 2\,mm^3$ was 12.8 mg, and the density of the PI was 1.35 $g\,cm^{-3}$, which was determined from the weight and volume of the corresponding film. The thickness of the aligned 6F-PI nanofiber mat was 15.3 µm. Thermal stability analysis of the nanofibers was carried out on a thermogravimetric analyzer (Mettler Toledo (Giessen, Germany), TGA/SDTA 851) at a heating rate of 10°C min^{-1} in air. Differential scanning calorimetric (DSC) measurement was conducted on the nanofiber mat samples using a Mettler Toledo DSC 821 in standard aluminum pans with a heating and cooling rate of 10°C min^{-1}, and the glass transition temperature was determined from the second heating cycle. The capacitance of the aligned nanofiber mats and the films were measured by using an Impedance analyzer from Wayne-Kerr (London, UK) (UM), model no. 1Z6505B. Silver paint was used to get better contact. The contact angle of the PI films was measured by G10 contact angle analysis system (KRÜSS, Hamburg, Germany).Water droplets (about 2 µl) were dropped onto the samples. The average contact angle of each sample was calculated by measuring five positions on the same sample.

RESULTS AND DISCUSSION

Preparation of polyimide films and polyimide nanomats

The syntheses of poly(ether imide)s were carried out via poly (amic acid) intermediate (Scheme 1) using our previous literature procedure.[16] The diamine monomer 4, 4-bis [3′-trifluoromethyl-4′ (4′-amino benzoxy) benzyl] biphenyl (Q) was reacted with equimolar amounts of PMDA, BPDA, BTDA or 6FDA in DMF at room temperature (22 ± 1°C). The diamine monomer was dissolved in measured amount of dry DMF, and the dianhydride monomers were added slowly. In all cases, the reaction mixture became highly viscous within 10–15 min. The reactions were continued for 3 h. The highly viscous poly(amic acid) solutions were diluted to different solid contents and electrospun (Table 1). The nanofibers were collected on a rotating drum-shaped roller. The nanofiber mats of poly(amic acid)s were imidized in a tubular glass furnace under programmed heating up to 300°C. For comparison purposes, the same heating program was used to obtain poly(ether imide) films from the poly(amic acid) solutions cast on flat Petri dishes.

Spectroscopy

Both the poly(ether imide) films and nanofiber mats showed infrared spectra with similar pattern; absorption band at about 1760–1785 cm^{-1} (C=O asymmetric stretching), 1725–1745 cm^{-1} (C=O symmetric stretching), 1360–1385 cm^{-1} (C—N stretching band), 740–745 cm^{-1} (ring deformation), and 680–720 cm^{-1} (C=O bending) corresponding to the characteristic of the imide band. No absorption bands were found between 3400 and 3600 cm^{-1} for (—OH) stretching, 1720 cm^{-1} corresponding to C=O stretching of carboxylic acid, and 1660 cm^{-1} corresponding to C=O amide stretching, indicating complete conversion of poly (amic acid) to poly(ether imide)s during imidization. The representative attenuated total reflectance—infrared spectra of the poly(amic acid) and the aligned nanofiber mat of poly(ether imide) prepared from PMDA as representative example are shown in Fig. 1.

Morphology of polyimide nanomats

The fiber morphology and dimensions of the nanofiber mats was investigated using SEM. It was observed that the nanofibers

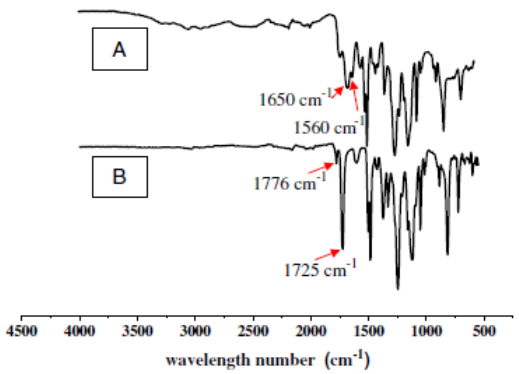

Figure 1. Fourier transform infrared spectra of (A) Q-PMDA [poly(amic acid)] and (B) Q-PMDA-i [poly(ether imide)] mat.

were aligned longitudinally and the fiber dimension varies from 100 to 200 nm. The SEM images of the imidized fiber mats prepared from different dianhydrides are shown in Fig. 2.

Thermal properties

Thermal properties of aligned PI nanofiber mats and the PI films were studied using thermogravimetric analysis and DSC and are summarized in Table 2. PI mats showed a single-step degradation and very high thermal stability in air. The temperature at which 5 wt% loss took place was more than 500°C for all the samples. Although there was a slight decrease in the thermal stability of mats as compared with the corresponding films (Table 1; Fig. 3), this difference was not very significant. This small difference could be attributed to the different sample forms. The mats were porous as compared with the dense films. The glass transition temperatures (T_g) of the poly(ether imide) mats and films were evaluated by DSC. All the polymers showed amorphous morphology without any melting or crystallization transitions. The PI mats had very high glass transition temperatures, which varied with dianhydride structure. The glass transition temperature of the polymers depends on many factors such as polymer symmetry, intermolecular force, and rigidity of polymer backbone. The PMDA based PIs (both film and mat) showed highest T_g values than other dianhydride based polymers, which can be explained on the basis of rigid PMDA moieties in the PI backbone. The higher T_g values of 6FDA-based polymers in comparison with BTDA-based polymers were expected because of the presence of bulky 6F unit in the polymer backbone, and the same trend was observed. The PIs, which were derived from BTDA, showed the lowest T_g in the series. In general, the effect of dianhydride structure was not very significant on the thermal properties of the resulting polyimide mats. All had high thermal stability (more than 500°C) and high glass transition temperatures (more than 275°C).

Mechanical properties

Further, electrospun PI mats were evaluated for their mechanical properties (Table 3). Stress–strain plots of the PI mats and the films are shown in Fig. 4(A and B), respectively. The PI mat prepared from BPDA showed highest tensile strength at break. The value is much higher than the PI film prepared from BPDA. Although the tensile strength of the PI mat prepared from BPDA and PMDA were reasonably higher than that of the analogous PI films, the reverse trend was observed for Q-6FDA and Q-BTDA polymers. These results are in accordance with the published literature of Hou *et al.*[15] in which they showed the importance

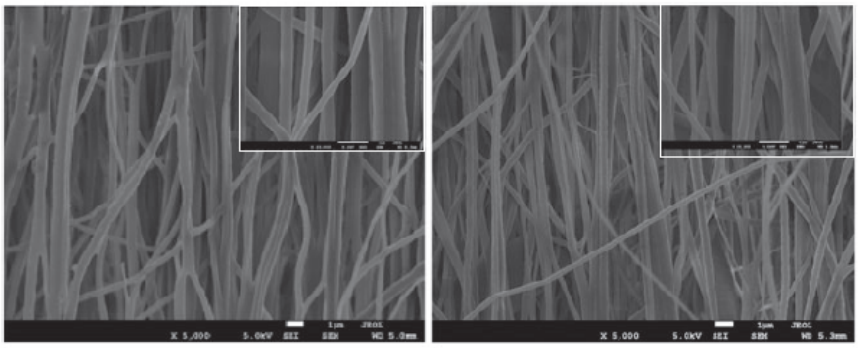

Q-BPDA-i Q-6FDA-i

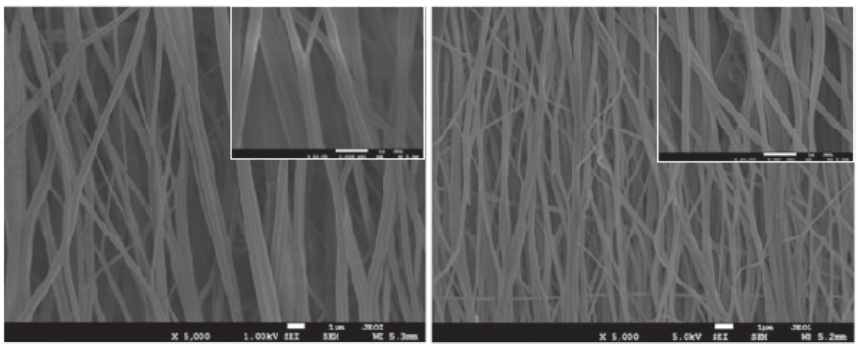

Q-BTDA-i Q-PMDA-i

Figure 2. Scanning electron microscope images of the aligned nanofiber mats prepared from different dianhydrides.

Table 2. Thermal properties of the imidized aligned nanofiber mats

Sample	Aligned nanofiber mats		Polyimide films	
	Glass transition temp. (°C)	5% weight loss temp. (°C)	Glass transition temp. (°C)	5% weight loss temp. (°C)
Q-PMDA-i	324	532	310 (316)[a]	550 (519)[a]
Q-BPDA-i	288	564	292	574
Q-BTDA-i	275	528	280 (262)[a]	561 (531)[a]
Q-6FDA-i	301	519	299 (273)[a]	528 (526)[a]

[a]Values taken from Chen *et al.*[16]

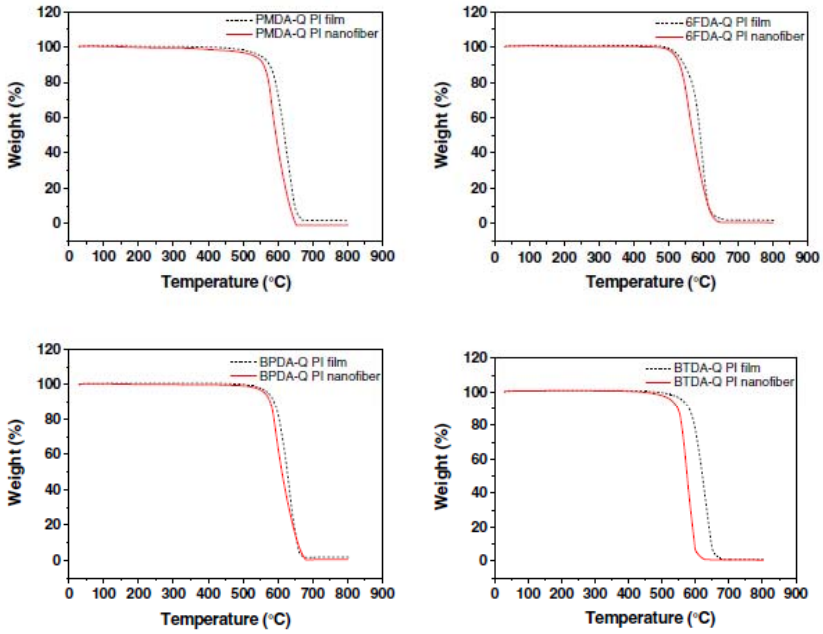

Figure 3. Thermal gravimetric analysis of polyimide (PI) mats in air in comparison with the corresponding films.

Table 3. Mechanical properties of the imidized aligned nanofiber mats and the polyimide films

Sample	Aligned nanofiber mats			Polyimide films		
	Tensile strength (MPa)	Tensile modulus (GPa)	Elongation (%)	Tensile strength (MPa)	Tensile modulus (GPa)	Elongation (%)
Q-PMDA-i	180.31 ± 8.18	1.54 ± 0.05	22.7 ± 2.4	95.80 ± 13.59	1.20 ± 0.18	25.3 ± 5.2
Q-BPDA-i	280.68 ± 38	2.1 ± 0.04	39.2 ± 2.3	119.33 ± 4.10	1.63 ± 0.07	52.0 ± 3.6
Q-BTDA-i	71.33 ± 3.95	0.9 ± 0.01	26.8 ± 2.8	106.93 ± 6.33	0.94 ± 0.5	36.9 ± 16.4
Q-6FDA-i	38.59 ± 1.96	0.75 ± 0.02	14.6 ± 2.7	96.81 ± 0.84	0.93 ± 0.16	28.6 ± 3.0

of rod-rigid structure of PI in getting high-strength and high-modulus fibers. Q-6FDA and Q-BTDA, because of the presence of carbonyl and trifluoromethyl groups, could not form rod and rigid PI structure, and therefore, low degree of compactness prevented polymer interchain interaction.

Water contact angle

There was an improvement in the water contact angle of PI mats made by electrospinning as compared with the corresponding films (Table 4). All PI mats showed hydrophobic nature with the

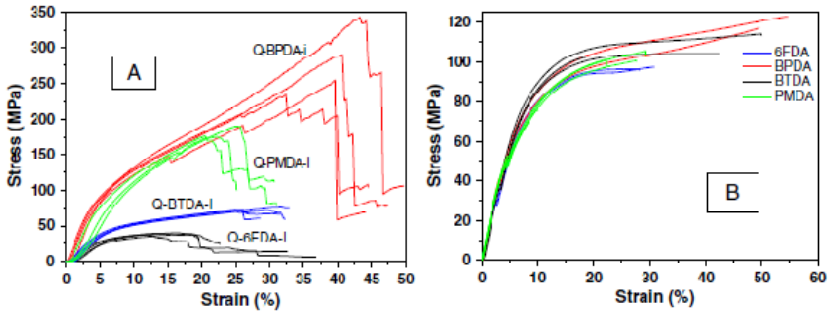

Figure 4. Stress–strain curves of (A) polyimide mats and (B) films.

Table 4. Water contact angle and dielectric constant of the imidized aligned nanofiber mats and the polyimide films

Sample	Aligned polyimide mats		Polyimide films	
	Contact angle (°)	Dielectric constant at 1 MHz	Contact angle (°)	Dielectric constant at 1 MHz
Q-PMDA-i	114 ± 5	1.739	84 ± 5	2.901
Q-BPDA-i	118 ± 4	1.607	77 ± 2	2.861
Q-BTDA-i	120 ± 3	1.765	75 ± 2	2.957
Q-6FDA-i	125 ± 4	1.430	83 ± 3	2.787

Figure 5. Different wetting behaviors of (A) polyimide Q-6FDA-i polyimide mat (contact angle 125 ±4°) and (B) Q-6FDA-i film (contact angle 83 ± 3°).

highest value of contact angle about 125° for fluorinated PI mat Q-6FDA-i (Fig. 5). By now, it is very well known that porous rough nanostructures generated by electrospinning enhance the hydrophobicity of any polymer. We have previously shown the increase in hydrophobicity for different polymer surfaces made by electrospinning.[20] The combination of low-energy material (fluorinated PIs) and the processing technique, i.e. electrospinning in our case, led to the enhancement of the hydrophobicity of the mat surfaces. The highest contact angle value of Q-6FDA nanomat sheet could be due to the highest fluorine content in the base polymer; however, the same trend was not found in the case of the polymer films.

Dielectric properties

The dielectric constant of the PI mats and the films was calculated from their corresponding capacitance values at 1 MHz. The dielectric constant values are summarized in Table 4. It was observed that the dielectric constant of the aligned nanofiber mats was considerably lower than that of their analogous film samples. The values are much lower than those of the commercially available poly(etherimide) ULTEM 1000 and PI Kapton H at 1 kHz. In fact, ultra low dielectric constant was obtained from the PI mats. The lower dielectric constant of these materials was due to the large pores in electrospun nanofiber and high surface to volume ratio of the mats.

CONCLUSIONS

Polyimide nanofiber mats and films have been prepared by the reaction of a fluorinated diamine monomer 4, 4-bis [3′-trifluoromethyl-4′ (4′-amino benzoxy) benzyl] biphenyl (Q) with different commercially available fluorinated and non-fluorinated dianhydrides in two steps. Processing of the polymers was carried out in poly(amic acid) stage by two different methods—electrospinning and solution casting. The processing technique had significant influence on some of the properties like dielectric constant, mechanical properties, and hydrophobicity. The mechanical properties of the aligned mats prepared from PMDA and BPDA (rigid structures) showed considerably higher tensile strength than their corresponding films. However, there was not much difference in the mechanical properties when BTDA and 6-FDA were used as dianhydrides. This showed the importance

of dianhydride structures giving rigid and compact alignment of polymer chains in getting high mechanical properties. The amorphous poly(ether imide)s containing bis-trifluoromethyl groups (Q-6FDA) exhibited not only low dielectric constants—lower than those of the commercially available poly(ether imide) Ul TEM 1000 and PI Kapton H at 1 kHz—but also excellent long-term thermo-oxidative stability and enhanced hydrophobicity relative to non-fluorinated dianhydride-based PIs. By the use of proper material and processing technique, it was possible to make low dielectric constant PIs with high thermo-oxidative stability, high glass transition temperatures, and high hydrophobicity. Such materials could be of high use as insulating material in interlayer dielectrics besides their use in filter and composite industry.

Acknowledgements

S.B. acknowledges the financial support received from the Alexander von Humboldt Foundation. The authors would also like to thank Professor Andreas Greiner for his kind support in many ways during the course of this work.

REFERENCES

[1] C. E. Sroog, *Prog. Polym. Sci.* **1991**, *16*, 561. doi:10.1016/0079-6700(91)90010-I
[2] K. L. Mittal, Ed., *Polyimides and Other High Temperature Polymers*, Vol. 5, VSP/Brill, Leiden, The Netherlands, **2009**.
[3] M. Hasegawa, K. Horie, *Prog. Polym. Sci.* **2001**, *26*, 259. doi:10.1016/S0079-6700(00)00042-3
[4] S. Tamai, A. Yamaguchi, M. Ohta, *Polymer* **1996**, *37*, 3683. doi:10.1016/0032-3861(96)00178-4
[5] T. Takasaki, Y. Kuwana, T. Takahashi, S. Hayashida, *J. Polym. Sci. A Polym. Chem.* **2000**, *38*, 4832. doi:10.1002/1099-0518(200012)38:1
[6] M. Ghaemy, S. Mojtaba Amini Nasab, *Polym. J.* **2010**, *42*, 648. doi:10.1038/pj.2010.57
[7] S. Zhang, Y. Li, T. Ma, J. Zhao, X. Xu, F. Yang, X. Xiang, *Polym. Chem.* **2010**, *1*, 485. doi:10.1039/b9py00339h
[8] G. Maier, *Prog. Polym. Sci.* **2001**, *26*, 3. doi:10.1016/S0079-6700(00)00043-5
[9] C. P. Yang, Y. Y. Su, M. Y. Hsu, *Polym. J.* **2006**, *38*, 132. doi:10.1295/polymj.38132
[10] M. Dhara, S. Banerjee, *Prog. Polym. Sci.*, **2010**, *35*, 1022. doi:10.1016/j.progpolymsci2010.04.003
[11] R. H. Vora, P. S. G. Krishnan, S. H. Goh, T.-S. Chung, *Adv. Funct. Mater.* **2001**, *11*, 361. doi:10.1002/1616-3028(200110)11:5
[12] K. R. Carter, R. A. DiPietro, M. I. Sanchez, S. A. Swanson, *Chem. Mater.* **2001**, *13*, 213. doi:10.1021/cm990707o
[13] M. Haider, E. Chenevey, R. H. Vora, W. Cooper, M. Glick, M. Jaffe, *MRS Symp. Proc.* **1991**, *27*, 279.
[14] J. Liu, Y. Min, J. Chen, H. Zhou, C. Wang, *Macromol. Rapid Commun.* **2007**, *28*, 215. doi:10.1002/marc.200600607
[15] A. Greiner, J. H. Wendorff, *Angew. Chem. Int. Ed.* **2007**, *46*, 5670. doi:10.1002/anie.200504646
[16] S. Chen, P. Hu, A. Greiner, C. Cheng, H. Cheng, F. Chen, H. Hou, *Nanotechnology* **2008**, *19*, 015604. doi:10.1088/0957-4484/19/01/015604
[17] C. B. Huang, S. L. Chen, D. H. Reneker, C. L. Lai, H. Q. Hou, *Adv. Mater.* **2006**, *18*, 668. doi:10.1002/adma.200501806
[18] C. B. Huang, S. Q. Wang, H. A. Zhang, T. T. Li, S. L. Chen, C. L. Lai, H. Q. Hou, *Eur. Polym. J.* **2006**, *42*, 1099. doi:10.1016/j.eurpolymj.2005.11.005
[19] S. Banerjee, M. K. Madhra, A. K. Salunke, D. K. Jaiswal, *Polymer* **2003**, *44*, 613. doi:10.1016/S0032-3861(02)00801-7
[20] S. Agarwal, S. Horst, M. Bognitzki, *Macromol. Mater. Eng.* **2006**, *291*, 592. doi:10.1002/mame.200600076

